CREDENTIALING IGF1R PATHWAY ACTIVATION AS A NOVEL THERAPEUTIC TARGET IN E-CADHERIN DEFICIENT BREAST CANCER

by

Alison Mary Nagle

B.S., Biology, University of North Carolina Wilmington, 2012

Submitted to the Graduate Faculty of

School of Medicine in partial fulfillment

of the requirements for the degree of

PhD in Molecular Pharmacology

University of Pittsburgh

2018

UNIVERSITY OF PITTSBURGH

SCHOOL OF MEDICINE

This dissertation was presented

by

Alison Mary Nagle

It was defended on

March 14, 2018

and approved by

Committee Chair: Satdarshan (Paul) Singh Monga, MD, Professor, Pathology

Steffi Oesterreich, PhD, Professor, Pharmacology & Chemical Biology

Shivendra Singh, PhD, Professor, Pharmacology & Chemical Biology

Rachel C. Jankowitz, MD, Professor, Medicine

Dissertation Advisor: Adrian V. Lee, PhD, Professor, Pharmacology & Chemical Biology

CREDENTIALING IGF1R PATHWAY ACTIVATION AS A NOVEL THERAPEUTIC TARGET IN E-CADHERIN DEFICIENT BREAST CANCER

Alison Mary Nagle, PhD

University of Pittsburgh, 2018

Insulin-like growth factor 1 (IGF1) plays an important role in breast cancer initiation and progression due to its regulation of cell proliferation, migration, and invasion. Our laboratory previously demonstrated that overexpression of constitutively activated IGF1 receptor (IGF1R) transformed human mammary epithelial cells and induced epithelial to mesenchymal transition. These characteristics make IGF1R an attractive therapeutic target, however, only subsets of patients have shown beneficial response to anti-IGF1R therapy in clinical trials, likely due to crosstalk with the insulin signaling pathway and lack of predictive biomarkers. To identify biomarkers of response to activated IGF1 and insulin signaling, we performed a proteomic screen in 21 breast cancer cell lines stimulated with IGF1 and insulin. We identified E-cadherin (*CDH1*), a major component of the adherens junction, as a repressor of IGF1 and insulin signaling. We further provide evidence that loss of E-cadherin hyperactivates the IGF1R pathway and increases sensitivity to IGF1R targeted therapy, thus highlighting the IGF1R pathway as a potential target in E-cadherin deficient breast cancer. Knockdown or antibody-mediated inhibition of E-cadherin increased IGF1-induced activation of IGF1R signaling and cell cycle progression. IGF1R and E-cadherin co-localized at points of cell-cell contact and a direct endogenous interaction using *in situ* proximity ligation assay indicated a physical regulation of E-cadherin on IGF1R signaling. Importantly, the E-cadherin gene (*CDH1*) is genetically lost in invasive lobular breast carcinoma (ILC), a subtype of breast cancer accounting for ~10-15% of total cases. We found increased expression of IGF1 ligand and levels of IGF1R

phosphorylation in E-cadherin deficient estrogen receptor positive (ER+) ILC in TCGA compared to ER+ invasive ductal carcinomas (IDC). We demonstrated that IGF1R and PI3K/Akt pathway inhibitors were effective in inhibiting growth in ER+ ILC cell lines and synergized with endocrine therapy. Additionally, we showed efficacy of IGF1R inhibition in ILC xenografts cultured *ex vivo.* Our data supports the use of IGF1R pathway inhibition as a potential novel therapeutic strategy for the treatment of ILC.

TABLE OF CONTENTS

LIST OF TABLES

LIST OF FIGURES

PREFACE

Without the guidance and support of others, I would not be where I am today. I want to first thank my thesis advisor, Adrian, for his unwavering support and trust in my scientific abilities—thus allowing me to build confidence and belief in myself. I value the mentorship you have provided and your willingness to allow me to grow as both a scientist and a person. I also want to thank my co-mentor, Steffi, for challenging me to be the best version of myself. I admire your strength as a dedicated, driven female scientist and aspire to always self-advocate in the way that you do. I want to thank the other members of my thesis committee—Paul, Shivendra, and Rachel—for providing helpful and insightful feedback during the development of my project and helping to guide me down a successful path. I am also appreciative that Rachel has helped me to gain critical clinical research and oncology experience during the remaining few months of my dissertation, allowing me to bring my research experience full circle from bench to bedside. I want to thank the Department of Pharmacology and Chemical Biology and the Molecular Pharmacology training program—especially Bruce, Patrick, and Shannon—for their endless support for the development and success of the graduate students in our program.

Finally, I want to thank my family and friends (and my kitten, Lucy) for continuing on this journey with me. My lab-mates past and present (these are in no particular order, so no hard feelings)—Courtney, Beth, Emily, Kevin, Nolan, David, Ryan, Amir, Susan, Jenny, Tiffany, Matt, Hannah, Maddie, Rekha, Jian, Ahmed, Nilgun, Nadine, Renee, Vaciry, Lan, Peilu, Jingci, Becky, Julie, and Sreeja—thank you for being the very best lab family and making coming to lab everyday so easy and enjoyable. You are all wonderful humans and I wish you the absolute best

in everything you do. I want to thank my sister for her love and friendship—always dream big and never let anyone tell you otherwise. I want to thank my parents—mom and dad—your selflessness and love has allowed me to pursue my every dream. I can never thank you enough for your love and support. Finally, I want to thank my partner, for his unconditional love and dedication. You have been my unwavering rock and I cannot imagine completing this journey with anyone else by my side.

1.0 INTRODUCTION

1.1 BREAST CANCER

Breast cancer is the second most common malignancy in women in the United States, behind cutaneous melanoma, accounting for an estimated 246,000 new diagnoses and over 40,000 deaths per year[1]. The incidence of breast cancer has increased over the last four decades, likely due to enhanced detection methodology, heightened awareness of the importance of regular screening, and trends in female parity that alter inherent risk for breast cancer development[1,2]. Despite the high incidence of breast cancer, survival outcomes are remarkable, with five-year overall survival hovering around 90%. However, the five-year survival rate for patients with advanced metastatic disease has remained stagnant at approximately 25%, highlighting the importance of understanding the biology underlying metastatic disease and developing new therapeutic targets[1,3,4].

1.1.1 Molecular subtypes of breast cancer

Breast cancer is stratified into distinct molecular and histological subtypes, which serve to guide treatment strategy and guidelines. Tumors are classified by expression of estrogen receptor (ER), progesterone receptor (PR), and epidermal growth factor-2 receptor (Her2). ER-positive disease is primarily treated with endocrine therapy to block estrogen signaling, including selective

estrogen receptor modulators (e.g. tamoxifen, raloxifene [SERM]) that compete with estrogen for binding to ER, selective estrogen receptor downregulators (e.g. fulvestrant/ICI [SERD]) that bind and induce degradation of ER, and aromatase inhibitors (e.g. exemestane) that block the conversion of androgens to estrogen in postmenopausal women[5,6]. Similarly, Her2-positive tumors are treated with targeted therapy to inhibit Her2-mediated signaling, including antibody biologics (e.g. trastuzumab, pertuzumab, TDM-1) and receptor tyrosine kinase inhibitors (e.g. Neratinib)[7–9]. Both types of treatment modalities are typically used in ER- and Her2-positive tumors. Tumors that lack expression of all three receptors, and regarded as the most aggressive, are referred to as the triple negative breast cancer (TNBC) subtype[10]. Unfortunately, there are less therapeutic options for patients with TNBC, and patients mainly receive chemotherapy as standard of care. Recent advances in TNBC treatment have been made, including the FDA approval of PARP inhibitor (e.g. Olaparib) for the treatment of advanced disease harboring BRCA1/2 mutations, and the initiation of clinical trials investigating the use of immunotherapy[10–13]. Further research is required to identify targeted therapy for this subtype of the disease.

In addition to receptor expression, breast tumors are molecularly classified based on their gene expression profiles. Not surprisingly, unsupervised hierarchical clustering segregated ER-positive from ER-negative tumors, but additionally identified five unappreciated intrinsic subtypes (LumA, LumB, Her2, Basal, Normal-like). These subtypes are routinely determined using gene expression from a concise 50-gene set known as PAM50. Because of the prognostic significance associated with each PAM50 subtype, clinical versions of the panel (e.g. Prosigna, MammaPrint, Oncotype DX) are now used to identify risk for distant recurrence and aid in treatment decisions, mainly whether a patient would gain potential benefit from chemotherapy.

1.1.2 Histological subtypes of breast cancer

Breast cancer is divided into two major histological subtypes. Invasive ductal carcinoma (IDC) is the most common subtype, accounting for 70% of total breast cancer cases diagnosed per year. This subtype grows as the typical mass in the breast, usually identified by mammography or self-breast exam. In contrast, invasive lobular carcinoma (ILC) accounts for 10-15% of total cases, approximately 30,000 cases per year in the United States[14,15]. This subtype of disease is molecularly defined by the loss of functional E-cadherin (*CDH1*), a major component of the adherens junction, leading to a discohesive linear growth pattern throughout the breast tissue (Figure 1)[14,16,17]. ILC tumors are often clinically diagnosed using an E-cadherin/p120 dual immunohistochemistry stain—IDC tumors display brown membranous E-cadherin staining whereas ILC tumors display a lack of brown membranous E-cadherin staining coupled with pink cytoplasmic p120 staining[17,18].

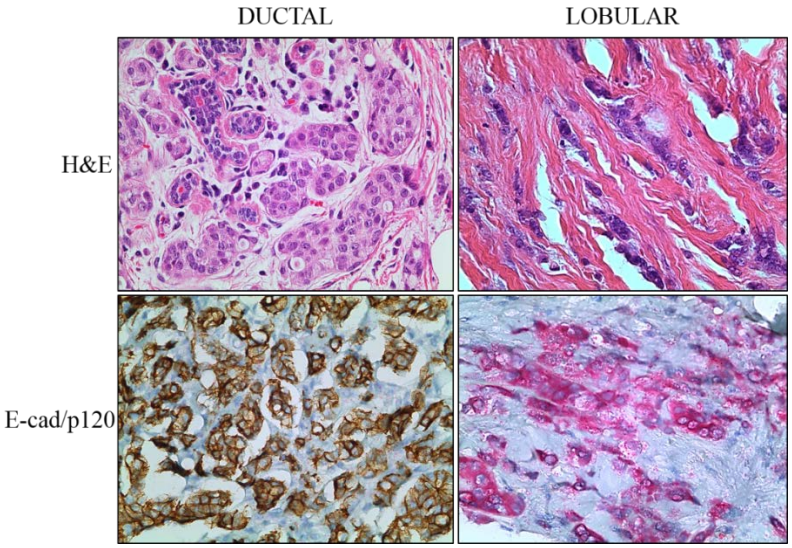

Figure 1: Ductal and lobular carcinoma: the major histological subtypes of breast cancer. H&E and E-cadherin/p120 staining depicted for both subtypes of disease.

Due to the distinct growth pattern, ILC is often diagnosed late compared to IDC because the difficulty in detection[14,17,19]. Ciriello and colleagues recently described the genomic landscape of 127 ILC tumors in The Cancer Genome Atlas (TCGA) as compared to IDC tumors[15]. Similar to previous reports, they showed that the loss of E-cadherin protein occurs in 90% of ILC, and is generally due to truncating mutations, loss of heterozygosity, or transcriptional repression[14–17]. In addition to E-cadherin alterations, they found 71% of ILC tumors harbor alterations in either *PIK3CA* (hotspot/missense mutations) or *PTEN* (truncating/missense mutation or high level copy number loss), likely leading to the high Akt activity they identified as compared to IDC[15,20,21]. ER status is also significantly different between IDC and ILC; ILC tumors are 90% ER-positive compared to 60-70% in IDC[14,15,17]. Due to this, ILC patients are treated with endocrine therapy to target ER signaling, but interestingly, data from the BIG 1-98 trials suggest that ILC tumors display resistance to traditional endocrine therapy (tamoxifen) compared to IDC[22]. In addition, results from numerous clinical studies indicate that ILC patients exhibit more frequent late recurrences associated with poorer prognosis compared to IDC, despite good prognostic markers (e.g. low Ki67 expression, high ER expression)[14,19,23,24]. This highlights the need to understand the mechanism underlying endocrine resistance and improve therapeutic options in ILC patients based on specifically activated mitogenic pathways.

1.2 INSULIN-LIKE GROWTH FACTOR AND INSULIN SIGNALING

The insulin-like growth factor (IGF) and insulin systems consist of three ligands (IGF1, IGF2, and insulin), two insulin receptor substrate proteins (IRS1/2), six IGF binding proteins (IGFBP1-6), and five receptors (insulin-like growth factor 1 receptor [IGF1R], insulin-like growth factor 2

receptor [IGF2R], insulin receptor-A and B [InsR-A and InsR-B], and IGF1/insulin hybrid receptor [HybR])[25–28]. Activation of this pathway by ligand binding plays a crucial role in normal mammary gland development and physiology and in the transition to neoplastic lesions[29]. Endocrine IGF1 ligand is produced in the liver and is released in response to growth hormone (GH) secreted by the pituitary, however autocrine and paracrine IGF1 signaling also occur[30,31].

IGF1R and InsR are both tetrameric proteins composed of two extracellular α-subunits that bind ligand, covalently linked to two intracellular β-subunits, which contain the tyrosine kinase signaling domains[32–34]. Interestingly, although IGF1R and InsR are encoded on different chromosomes with different numbers of exons, the receptors share high amino acid sequence and structural homology[35,36]. The ligand binding domains (α-subunit) share 55% amino acid similarity, and the tyrosine kinase domains (β-subunit) share 72% homology with 100% homology found in the ATP-binding domains[25,37]. The binding of ligand to IGF1R and InsR leads to conformational changes in structure and transphosphorylation of the receptor, which triggers the activation of two main intracellular signaling cascades: the phosphatidylinositol 3-kinase/Akt kinase (PI3K/Akt) pathway and the Raf kinase/mitogen activated protein kinase (Raf/ERK) pathway (Figure 2)[28]. Although IGF1R and InsR share common downstream pathways, their biological roles are not completely identical: IGF1R mainly mediates proliferation, migration, cellular transformation, and anti-apoptotic events, whereas InsR mainly controls the metabolism of glucose[38]. Nevertheless, there is extensive crosstalk between IGF1R and InsR; IGF1 can bind InsR and insulin can bind IGF1R, albeit with a lower affinity compared to their primary targeted receptors[25,39–41]. Additionally, HybRs consisting of one α/β subunit of IGF1R and one α/β subunit of InsR have been reported, and potentially exceed IGF1R content in breast tumors by greater than 75%[42–45]. Studies evaluating activity of HybR have shown that they

respond with much greater potency to IGF1 than insulin, and have different ligand binding affinity compared to non-hybrid (holo) receptors[46–49]. However, as most cells express a combination of IGF1R, InsR and HybR, and few methods exist to specifically examine activated HybR in living cells, ascribing HybR specific effects has been difficult[50,51]. We recently published a methodology to examine specific signaling and phenotypic effects due to activation of holo-IGF1R and holo-InsR compared to HybR[51]. Similar to previously published data, we demonstrated that HybR activation functions more closely to IGF1R than to InsR in promoting mitogenic signaling and proliferation, whereas InsR mainly regulated glucose uptake[25,51].

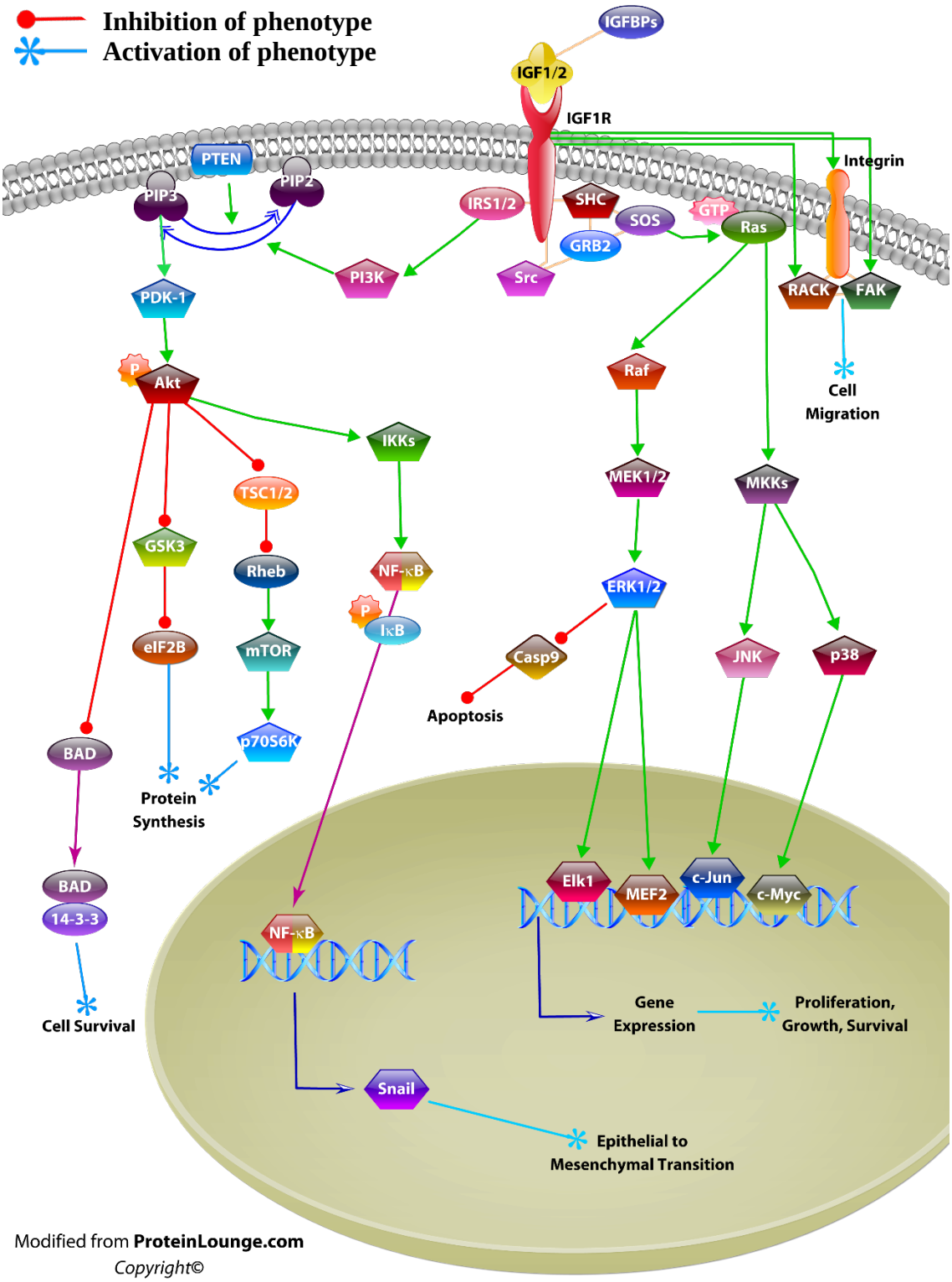

Figure 2: IGF1R signaling overview.
IGF1/2 ligand bind to IGF1R and initiates an intracellular signaling cascade mediated mainly through PI3K/Akt and Raf/MEK/ERK signaling leading to proliferation, growth, and survival. A similar signaling cascade is observed for insulin signaling via InsR. Figure was generated by modifying an existing template from ProteinLounge (access via University of Pittsburgh HSLS Library).

1.2.1 IGF1 signaling and mammary gland development

Proper GH-IGF1 signaling is required for normal mammary gland development[52]. In addition to endocrine IGF1 produced in the liver, IGF1 is secreted from the fibroblast and immune components within stroma of the mammary gland in a paracrine manner[53–55]. Paracrine IGF1 signaling is thought to be more potent than endocrine signaling (and bypasses the requirement for GH action) and initiate terminal end bud (TEB) growth and ductal branching within the mammary fat pad[54,56]. Supporting this, IGF1 null (-/-) female mice display decreased mammary gland development that can be rescued with continuous injections of IGF1[54]. Combined IGF1 and estradiol injections further increased TEB formation and ductal growth indicating that estrogen signaling synergizes with IGF1 to enhance this process[54,57,58]. Additionally, it has been demonstrated that IGF1 rescues the impaired ductal development in GH-deficient mammary glands, but that GH is unable to rescue development in IGF1-null glands, further supporting the notion that IGF1 is the critical mediator acting downstream of GH action[59].

In addition to mammary gland development, IGF1-IGF1R signaling is required for proper mammary gland morphogenesis. This was demonstrated through mammary gland transplantation assays using IGF1R-deficient embryonic mammary buds transplanted into cleared mammary fat pads of wild-type mice. These buds exhibited decreased cellular proliferation and growth potential compared to wild-type buds during mammary gland morphogenesis, highlighting the importance of epithelial IGF1R expression in the mammary gland[54,60]. The loss of IGF1-IGF1R mediated mammary gland morphogenesis is suggested to be a result of diminished cell cycle progression and elevated apoptosis in the gland[61–63]. However, although data implicates IGF1 as a potent mediator of mammary gland development, coordination with additional growth factors such as epidermal growth factor (EGF) and transforming growth factor-β (TBFβ), and other

IGF1 pathway components such as IGF1R and IGFBPs is necessary for maximal mammary gland signaling and full development to a mature gland[64,65].

1.2.2 Deregulation of IGF1R signaling in breast cancer

Similar to other growth factor signaling pathways, the GH-IGF1 axis is known to be deregulated in the progression from normal mammary gland to cancer[33,34,52]. The earliest epidemiological evidence was reported in a population of patients with primary GH insensitivity, a disease termed Laron syndrome in 1966. Laron syndrome is associated with congenital IGF1 deficiencies driven by a genetic alteration(s) in GHR affecting expression and activity. Individuals with this syndrome suffer from dwarfism and high rates of obesity, associated with high levels of GH and low levels of serum IGF1[66,67]. Strikingly, these individuals are inherently protected from cancer development compared to non-Laron wild-type relatives, suggesting the importance of this pathway in cancer development[68]. This finding was supported using an *in vivo* laboratory model of Laron syndrome – which lacks GHR/GH binding protein[69]. When crossed with transgenic models of mammary and prostate cancer, mice with this genotype displayed reduced incidence of tumor development compared to wild-type littermates[70,71]. Conversely, high levels of circulating IGF1 and IGF2 have been shown to elevate risk for cancer development, including breast, colon, and prostate cancer[72–77]. Supporting this, transgenic mice overexpressing IGF1 driven on the myoepithelial K5 promoter (*BK5.IGF1*) develop spontaneous mammary gland and skin tumors that are driven by paracrine IGF1 signaling[78–80].

Elevated IGF1-IGF1R activity in the mammary gland is thought to promote cell proliferation, survival, and epithelial to mesenchymal transition leading to breast cancer initiation and progression. Constitutively activated IGF1R (*CD8-IGF1R*) has been shown to

transform normal mammary epithelial cells (MCF10A) by promoting increased proliferation, decreased apoptosis and loss of polarity *in vitro,* and inducing tumor growth *in vivo* in immunocompromised mice. Strikingly, overexpression of other oncogenes such as ErbB2 (Her2), activated Ras, and cyclin D1 also disrupted acini formation and transformed mammary epithelial cells *in vitro,* but were not sufficient to induce tumor formation *in vivo,* emphasizing the importance of IGF1R[81,82]. Additionally, constitutively activated IGF1R has been shown to initiate epithelial to mesenchymal transition through activation of NFkB and induction of the transcription factor, Snail, leading to the downregulation of E-cadherin[81,83]. This, in combination with IGF1R crosstalk with integrins is known to mediate migratory and invasive phenotypes[81,84,85]. Data from our lab and others suggest a role for IGF1/2 signaling and efficacy of IGF1R/InsR inhibition in ER-negative (particularly triple negative [TNBC]) breast tumors and cancer stem-like cells that display EMT properties (e.g. low E-cadherin expression)[52,55,86,87].

In contrast to overexpression, inhibition of IGF1R using a tyrosine kinase inhibitor (BMS-536924) reversed transformation of CD8-IGF1R-MCF10A cells resulting in a reversion to normal acini formation, and inhibition of proliferation in multiple breast cancer cell lines[88]. In addition, IGF1R activity has been shown to promote survival to annoikis-induced apoptosis through activation of PI3K/Akt[89]. Comparable IGF1R-mediated mitogenic effects have been observed in the mammary gland *in vivo.* Transgenic female mice expressing CD8-IGF1R in the mammary gland demonstrated aberrant mammary gland development and palpable mammary gland tumor formation by 8 weeks of age[90]. Similarly, mammary glands from transgenic MMTV-IGF1R mice showed impaired ductal elongation within 55 days and palpable mammary tumor formation by 8 weeks of age. These phenotypes were associated with Akt, ERK, and STAT3 signaling activated downstream of IGF1R[91]. Conversely, inhibition of IGF1R in an

orthotopic xenograft using a C-terminal truncated (dominant negative) IGF1R lacking the receptor signaling domain was shown to inhibit migration and invasion of cancer cells and prevent the formation of lung metastasis *in vivo*[92].

1.2.3 Crosstalk between IGF1R and ER signaling

Many of the pro-tumorigenic effects of IGF1-IGF1R signaling in breast cancer may largely be due to the extensive crosstalk with the estrogen receptor (ER) signaling pathway, as demonstrated by the synergy between IGF1 and estrogen to promote proliferation[35,93]. This is likely due to the ability of IGF1 stimulation to promote phosphorylation and activation of ERα (S167). Becker and colleagues demonstrated that inhibition of the mTOR/S6K1 axis blocks IGF1-induced ERα (S167) phosphorylation and gene transcription without affecting ligand dependent ERα signaling, and additionally observed that site directed mutation of ERα (S167) reduces IGF1-mediated colony formation[94]. Similarly, estrogen induces an elevation in IGF1R and IRS1/2 expression, leading to enhanced IGF1-IGF1R signaling capacity[35,93]. In addition to estrogen-regulation of IRS1 expression, association between IRS1 and ERα in pre-pubertal mammary glands from BK5.IGF1 transgenic mice preferentially activated the PI3K/Akt pathway compared to the Ras/MAPK pathway. The authors demonstrated a switch in signaling to the Ras/MAPK pathway in post-pubertal mammary glands with decreased ERα expression, preventing the complex formation with IRS1. This highlights the crosstalk between IGF1 and ERα signaling in the mammary gland and may be especially relevant in women during times for high ERα expression in the breast, such as the pre-pubertal and post-menopausal stages of development[80]. Interestingly, tamoxifen therapy is known to decrease levels of circulating IGF1 and expression of estrogen-regulated IGF1R pathway components, providing evidence to the

notion that enhanced IGF1R activity may act as a driver or occur as a result of tamoxifen resistance[95]. In support, high IGF1R and IRS1 expression have been identified as predictors of early ER-positive breast cancer recurrence, and indicate a role for IGF1-IGF1R signaling molecules in estrogen-mediated and resistant disease progression[35,89,93].

Recently, the identification of *ESR1* mutations in breast cancer as a mechanism to endocrine therapy resistance has rejuvenated the importance of the IGF1R pathway in breast cancer. Gelsomino et al. demonstrated that mutations in the ligand binding domain of *ESR1* promote resistance to tamoxifen partially due to activation of the IGF1R signaling pathway[96]. Similarly, we have observed (Li et al.) hyperactivity of IGF1R signaling in *ESR1* mutant cells resulting in elevation of IGF1 regulated gene transcripts[97]. Additionally, we observed enhanced IGF1 signaling capacity via PI3K/Akt activation of mutant cells that was mediated by the increased IRS1 expression. Both studies demonstrated sensitivity of *ESR1* mutant cells to fulvestrant, a selective estrogen receptor downregulator, which was enhanced by the addition of IGF1R inhibitor[96,97].

1.3 STRATEGIES TO INHIBIT IGF1R ACTIVITY

Due to the large body of preclinical evidence supporting the role of IGF1R signaling as a driver of cancer and mechanism of resistance to traditional cancer therapy (e.g. chemotherapy, radiation, endocrine, Her2-targeted therapy) numerous clinical trials have been initiated to evaluate the efficacy of inhibition of this pathway[35,95,98,99]. The clinicaltrial.gov database lists over 600 clinical trials in which IGF1 was cited as either a therapeutically targeted molecule or a diagnostic marker, and over 20 clinical trials reported specifically in breast cancer since 2008[35].

Clinical studies have used three main strategies thus far to inhibit IGF1R activation, including i) small molecule tyrosine kinase inhibitors (TKI) targeting the intracellular signaling domain of IGF1R, ii) monoclonal antibodies targeting the ligand binding domain of IGF1R, and iii) monoclonal antibodies targeting the IGF1/2 ligands[33,35]. However, while many Phase I/II studies have shown promising results, many Phase III studies have been largely negative or terminated early due to limiting toxicities and/or lack of efficacy[35,100–102].

1.3.1 Classes of anti-IGF1R therapies

Most therapeutic agents developed were small molecule TKIs, such as OSI-906 or BMS-754807, that targeting the ATP-binding site of the β-subunit of IGF1R and thereby blocked intracellular signaling[103,104]. However, these drugs displayed equal efficacy against InsR and HybR due to the high sequence and structural homology of the intracellular kinase domains of both receptors (nearly 100% in ATP-binding domain)[33–35,104]. Because of this, severe limiting toxicities (e.g. grade 3 and 4 metabolic syndrome and hyperglycemia) were reported in clinical trials due to the cross inhibition of InsR and insulin signaling, and many studies were terminated prematurely often without reporting results[35,100]. An alternative approach to inhibit IGF1R more specifically was with an anti-IGF1R monoclonal antibody, such as figitumumab (CP-751, 871), which targeted the ligand-binding domain of the receptor. In 2017, Ekyalongo and Yee estimated that over 50% of clinical trials in breast cancer targeting IGF1R have used this approach, with some trials still ongoing. However, many of the preliminary results to date from the Phase III trials from this class of agents have been negative, likely due to the lack of IGF1R expression in the tumor, or compensatory mitogenic signaling of InsR—the cost of a more specific therapeutic[33,35,100].

Ligand neutralizing (blocking) antibodies have been the least used approach to targeting IGF1R. These antibodies bind and neutralize IGF1/2 in circulation to block activation of IGF1R. Two antibodies in this class, MEDI-573 (MedImmune) and BI836845 (Boehringer Ingelheim) entered Phase II clinical trials in solid tumors, including breast cancer[35]. Pharmacodynamics data reported from the Phase I trial of MEDI-573 in solid tumors indicated that the antibody suppressed circulating IGF1/2, but did not result in a dose-limiting toxicity. Based on this data, the antibody moved into Phase II development and testing, specifically in late stage metastatic ER-positive breast cancers in combination with endocrine therapy (aromatase inhibitor [NCT01446159]). Unfortunately, MedImmune has recently discontinued development of their compound, citing safety and efficacy issues on their website. In contrast to MEDI-573 though, BI836845 was shown to increase circulating non-functional IGF1 levels (found in complex with the antibody), leading to anti-proliferative effects by blocking IGF1R activation[105,106]. Promising pre-clinical and Phase I data for BI836845 has supported its transition into Phase II trials in metastatic ER-positive breast cancer in combination with everolimus (mTOR inhibitor) and exemestane (aromatase inhibitor [NCT02123823]). Additional Phase I testing is now being completed to evaluate BI836845 in combination with abemaciclib (CDK4/6 inhibitor) and various additional endocrine therapies (NCT03099174), likely to increase potential future indications for clinical approval.

1.3.2 Biomarker identification for response to anti-IGF1R therapy

It seems intuitive that IGF1R targeted therapy would be selectively effective primarily in tumors expressing the target, and indeed pre-clinical studies have indicated that lack of receptor expression is a strong negative predictor of response to anti-IGF1R therapy. Despite this, many

clinical trials proceeded irrespective of IGF1R expression, and therefore may have been enrolling and treating patients that were inherently resistant to treatment[33,107]. Supporting this, a study conducted in neuroblastoma cell lines treated with an IGF1R TKI (BMS-536924) identified high expression of IGF1R and IGF1/2 in sensitive cell lines, and high expression of IGFBP3/6 in resistant cell lines[108]. Additionally, anti-IGF1R antibody therapy lacked efficacy in breast cancer cells lacking expression of IRS1/2, further suggesting that activation of IGF1R in combination with expression of downstream signaling molecules is important in mediating response[109]. However, more comprehensive assessment is required to identify patients that would receive beneficial response from IGF1R targeted therapy.

Studies evaluating changes in gene expression have sought to identify expression signatures indicative of IGF1 response in cancer cells and tumors with the overarching goal of selecting patients who may benefit to IGF1R targeted therapy[87,110–112]. As expected, gene expression changes induced by IGF1 in an immortalized breast epithelial cell line (184tert) were determined to regulate transcription, cell cycle, metabolism, and angiogenesis, and further these genes typically contained transcription factor binding sites for CRE/AP1/AP2 in conjunction with SP1 and ETS sites in the proximal promoter[110]. Similarly, a study from our lab showed that a set of greater than 800 genes were responsive to IGF1 stimulation in MCF-7 breast cancer cells, including genes regulating cell proliferation, survival, metabolism, and DNA repair pathways. This gene set was termed the IGF1-signature (IGF1-sig), and was then compared with gene expression profiles of multiple breast tumor cohorts. The IGF1-sig was found to correlate with the expression profiles of ER-negative breast tumors and a subset of ER-positive tumors that had low expression of ER. Additionally, the IGF1-sig correlated with pathologic features (e.g. high grade, larger tumors, nodal involvement) and poor overall patient survival[112]. In a

subsequent study, we observed that cell lines and xenograft models with high IGF1-sig were sensitive to anti-IGF1R therapy (BMS-754807) and that the IGF1-sig was reversed following treatment[87]. However, the IGF1-sig is likely similar to other growth factor pathway signatures and may not be sufficient to solely identify the patient populations that would benefit from IGF1R targeted therapy. Therefore, the goal of this project was to a complementary proteomics approach to gene expression profiling to determine novel mediators of IGF1R and InsR signaling with the goal of determining potential biomarkers for response to anti-IGF1R therapy.

2.0 PROTEOMIC SCREENING AND LASSO REGRESSION REVEAL NOVEL REGULATORS OF THE IGF1 AND INSULIN SIGNALING PATHWAYS

2.1 INTRODUCTION

Activation of IGF1R and InsR have been shown to promote mammary tumorigenesis, metastasis, and resistance to anti-cancer therapy, and are associated with an increased risk for breast cancer[73,74,81,90,92,98,113,114]. However, although IGF1R inhibition has been effective in pre-clinical *in vitro* and *in vivo* studies, the receptor has proven difficult to specifically target in humans—likely due to crosstalk with InsR and a lack of biomarkers for patient selection (see Chapter 1)[33,34,84,92,95,99,115]. Understanding the relationship between the IGF1R and InsR signaling networks and their combined role in breast cancer is crucial to developing improved therapeutic strategies and a personalized medicine approach to oncology treatment.

To gain insight and improved understanding of cellular signaling networks, such as the IGF1R and InsR pathways, an experimental methodology with the ability to track time-dependent evolution of signaling is necessary. Technological advancements have led to the development of numerous proteomic approaches such as mass spectrometry[116] and live cell imaging[117] that allow for the quantification of multiple proteins across a large number of samples. Similarly, reverse phase protein array (RPPA) serves as a high-throughput technique that provides quantification of the expression of both phosphorylated and total proteins using validated antibodies[118]. This approach has previously been used for biomarker prediction[119], classification of signaling response due to activation of upstream mediators[120], and drug response[121]. Here, we used an RPPA data set obtained from a panel of 21 breast cancer cell lines

stimulated with IGF1 or insulin for a 48-hour time course to construct models of time-dependent signaling with the goal of characterizing differential signaling dynamics and interactions downstream of the two functionally similar growth factor signaling pathways. Finally, we validated two *in silico* predictions for novel mediators of the IGF1 and insulin growth factor signaling pathways: E-cadherin and acetyl-CoA carboxylase (ACC1/2).

2.2 MATERIALS AND METHODS

2.2.1 Cell culture and Reverse Phase Protein Array (RPPA)

The data set (deposited in NCBI's Gene Expression Omnibus (GEO) database with series accession number GSE80233) was generated at the RPPA Core Facility (MD Anderson Cancer Center, Houston, TX). Twenty-one breast cancer cell lines from the ATCC SPORE collection (AU565, BT20, BT474, Cama-1, HCC70, HCC1954, HS578T, MCF7, MCF10A, MDA-MB-134-VI, MDA-MB-231, MDA-MB-361, MDA-MB-415, MDA-MB-435 (re-classified as melanoma cell line), MDA-MB-453, MDA-MB-468, SKBR3, T47D, UACC812, and ZR75.1) were cultured in complete growth medium consisting of DMEM, DMEM/F-12, RPMI, L15 or McCoy's 5A with 10% FBS or horse serum according to the conditions provided by Neve et al. (*Cancer Cell*, 2006)[122]. Cells were plated in triplicate 6 cm dishes per treatment time point and then switched to serum-free medium (SFM). Cells were serum starved for 24 hrs, then treated with 10nM IGF1 (GroPep BioReagents #CU100) or insulin (Sigma #12643) for 5 min, 10 min, 30 min, 6 hr, 24 hr, or 48 hrs. Cells treated with vehicle (Vhc) were collected at 5min, 24 hr, and 48 hr.

Cell lysates were washed in ice-cold PBS twice, and lysed immediately in RPPA lysis buffer with protease inhibitor (1% Triton X-100, 50mM Hepes, 150mM NaCl, 1.5mM MgCl2, 1mM EGTA, 100mM NaF, 10mM NaPPi, 10% Glycerol, 1mM Na3VO4, 1mM PMSF, 10ug/ml Aprotinin). Lysates were sonicated and centrifuged at 14,000 rpm at 4°C for 10 min. Protein concentrations were determined by BCA and lysates diluted to 1ug/ml final concentration with 4X SDS/β-mercaptoethanol sample buffer. Each lysate was printed in duplicate with five 2-fold dilutions on a single nitrocellulose-coated FAST slide (945 lysates, printed 10 times; GE Healthcare). Then, each slide was probed with a primary antibody and a biotin-conjugated secondary antibody. Levels of 134 proteins or phospho-proteins were measured using corresponding antibodies. The signal, amplified by the Dako Cytomation-catalyzed system (Dako), was visualized by DAB colorimetric reaction. The slides were then scanned and quantified using Microvigene (VigeneTech) software. Super-curve fitting was used for loading correction of each sample[123]. Yu-fen Wang (graduate student), Dr. Beate Litzenburger (postdoctoral fellow) and Dr. Angelo Casa (postdoctoral fellow) completed the culturing, stimulation and lysis of cells in 2009 while our lab (PI: Dr. Adrian Lee) was located at Baylor College of Medicine (Houston, TX).

2.2.2 Quality control of RPPA antibodies

Internal quality control on the specificity and validity of the 134 antibodies used in the RPPA experiment was performed. Validation required obtaining a single or dominant band for the antibody in question on immunoblots run for the dynamic range of the RPPA data conditions. Pearson correlation coefficients of 0.8 between RPPA and immunoblot results were used as a cutoff to determine if the antibody was specific for the intended target. The RPPA Core Facility

routinely updates their list of available reliable antibodies based on experiences in hundreds of conditions and cell lines. With the combination of information from our experience and others, 26 of the antibodies were labeled as “non-specific” under the specific experimental conditions, and were excluded from all subsequent analyses.

2.2.3 Data processing and construction of linear statistical models

Briefly, the data acquired from the RPPA experiment was pre-processed to reduce noise, and modeled using lasso regression to create predictions of IGF1 and insulin signaling interactions. Validation of models was completed using a synthetic data set and performance tested using a leave-one-out cross validation methodology. Statistical analysis on the validation experimental results were performed using Student’s t-test with significance level of $p<0.05$. All simulations and analyses were completed in Matlab, versions 2014a and 2015a (MathWorks). Cemal Erdem (graduate student; laboratory of Drs. Timothy Lezon and D. Lansing Taylor in the Department of Computational and Systems Biology at the University of Pittsburgh) completed all computational biology methodology related to this study. Modeling predictions were then validated using wet-bench experimentation. Complete methods can be found in our *Molecular and Cellular Proteomics* publication (Erdem and Nagle et al. 2016, PMID: 27364358)[124].

2.2.4 Stable shRNA infection

T47D cell line was acquired from ATCC and cultured in RPMI+10% FBS. Stable CDH1 knockdown T47D cells were generated using a retro-viral infection of Renilla targeting control (shSCR [5’ TGCTGTTGACAGTGAGCGCAGGAATTATAATGCTTATCTAT

AGTGAAGCCACAGATGTATAGATAAGCATTATAATTCCTATGCCTACTGCCTCGGA]) and CDH1 (shCDH1 [5’ TGCTGTTGACAGTGAGCGCAAGTGTGTTCATTA ATGTTTATAGTGAAGCC ACAGATGTATAAACATTAATGAACACACTTATGC CTACTGCCTCGGA]) short-hairpin RNAs (shRNA). Following infection, cells were selected using growth media supplemented with 1ug/ml Puromycin (Life Technologies #A11138-03) and were routinely cultured in the selection media. Dr. Tiffany Katz (post-doctoral fellow in the laboratory of Dr. Steffi Oesterreich) generated these cells.

2.2.5 Transient siRNA knockdown

MCF-7 cell line was acquired from ATCC and cultured in DMEM+10%FBS. MCF-7 cells were reverse transfected with either 50nM of ON-TARGETplus Non-targeting pool (Dharmacon #D-001810-10) or 25nM each of SMARTpool ON-TARGETplus *ACACA* and *ACACB* (acetyl co-A carboxylase) siRNA (Dharmacon # L-004551-00 and L-004759-00) following the Lipofectamine RNAiMAX manufacturer’s protocol (Life Technologies #13778-150) for 48 hours.

2.2.6 IGF1/insulin stimulation

Cells were plated to approx. 70% confluency, serum starved overnight then stimulated with 10nM HCl (Vhc), IGF1, or insulin for 5 min or 10 min time points as indicated.

2.2.7 Immunoblotting

Samples for immunoblot analysis were collected using RIPA buffer (50mM Tris pH 7.4, 150mM NaCl, 1mM EDTA, 0.5% Nonidet P-40, 0.5% NaDeoxycholate, 0.1% SDS) supplemented with 1x HALT protease and phosphatase cocktail (Thermo Fisher #78442), water bath sonicated for 15 minutes (1 min on, 30 sec off), and centrifuged at 14,000rpm at 4˚C for 12 minutes. Protein concentration was assessed using BCA assay (Thermo Fisher #23225) and 50ug of protein per sample was run on 12% SDS-PAGE gel (except when blotting for ACC – then 7% SDS-PAGE gel was used) then transferred to PVDF membrane. Membranes were blocked for 1 hour using Odyssey PBS Blocking Buffer (LiCor #927-40000) then probed using the following primary antibodies and concentrations: pERK Thr202/Tyr204 (Cell Signaling #4377; 1:1000), total ERK (Cell Signaling #9102; 1:1000), pAkt S473 (Cell Signaling #4060; 1:1000), total Akt (Cell Signaling #9272; 1:1000), E-cadherin (BD Biosciences #610182; 1:1000), ACC1/2 (Cell Signaling #3676; 1:500) and β-actin (Sigma #A5441; 1:5000). Membranes were then washed in TBST, incubated in LiCor secondary antibody (1:10,000) for 1 hour (anti-rabbit 800CW [LiCor #926-32211]; anti-mouse 680LT [LiCor #925-68020]), then imaged using the Odyssey Infrared Imager.

2.3 RESULTS

2.3.1 Large-scale proteomic screening of IGF1/insulin signaling in breast cancer cell lines

To further our understanding of the IGF1 and insulin signaling networks using a systems biology approach, we performed a proteomic screen using reverse phase protein array (RPPA) on samples from 21 breast cancer cell lines of various histological subtypes. Cells were stimulated with vehicle (Vhc), 10nM IGF1, or 10nM insulin for six time-point analyses (5, 10, 30m, 6h, 24h, 48h). RPPA analysis included 134 different antibodies against phosho- and total proteins. However, twenty-six antibodies were excluded from this study (see Methods), leaving a remaining set of 108 proteins for analysis. An overview of the data produced from the phospho-antibodies revealed that IGF1 and insulin (data not shown) stimulation induced phosphorylation of IGF1R (pIGF1R) at Tyr1135/1136 in all cell lines (Figure 3). Additionally, maximal activation generally occurred at 5 – 10 minutes following stimulation and declined thereafter as expected. However, activation of downstream targets, such as Akt (pAkt) and phosphorylation of ribosomal protein S6 (pS6), following IGF1 stimulation was only observed in approximately half of the cell lines. The cell lines MCF-7, MCF10A, T47D, MDA-MB-134, MDA-MB-231, and ZR75.1 (among others) were found to be highly IGF1 responsive and exhibited maximal activation of downstream IGF1R signaling.

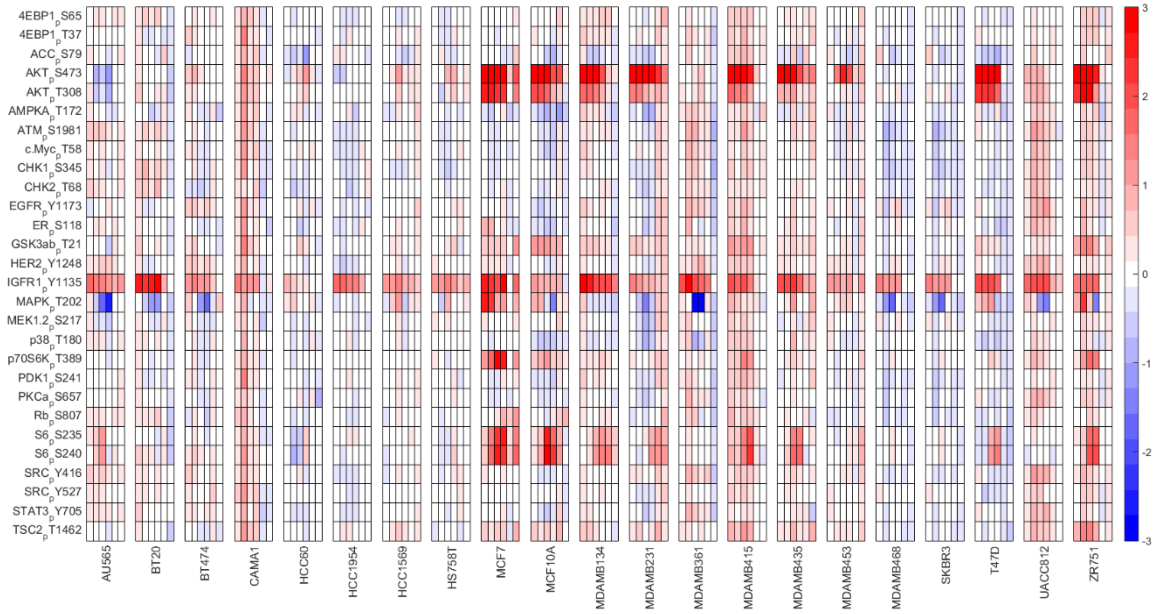

Figure 3: IGF1-induced phospho-protein expression profiles in 21 breast cancer cell lines.
The heat map shown depicts the change in the expression of 28 phospho-proteins following a 48 hr time course of IGF1 stimulation as determined by RPPA analysis. Six columns are shown for each cell line, with each column representing a single time point (5, 10, 30 min, 6, 24, 48 h). The values shown represent the difference in log2 expression level relative to the serum-starved condition. Red color corresponds to up-regulation and blue color represents down-regulation of signal compared relative to serum-starved cells. Row headings indicate the arrayed proteins with phosphorylation sites indicated after the subscript 'p'.

2.3.2 Time dependent modeling predicts novel mediators of IGF1 and insulin signaling

We collaborated with Drs. Timothy Lezon and D. Lansing Taylor (and graduate student – Cemal Erdem), in the Department of Computational and Systems Biology at the University of Pittsburgh to develop a computational model to better understand the IGF1 and insulin signaling networks, and potentially determine differential mediators of these pathways. Work from their lab resulted in the development of a novel time dependent model based on lasso regression that when combined with perturbation analysis predicted mediators of IGF1 and insulin signaling. The result of the model consisted of the *'perturbed'* protein that if altered under conditions of IGF1 and/or insulin stimulation affected the expression level of the *'output'* protein. The *output*

was arbitrarily set as phosphorylated Akt (S473 or Thr308) and ERK (Th202/204) due to their roles as major downstream signaling hubs of pIGF1R/InsR. A depiction of the top exclusive interactions for IGF1 and insulin stimulation, as well as the top differential interactions revealed the complexity of the system (Figure 4).

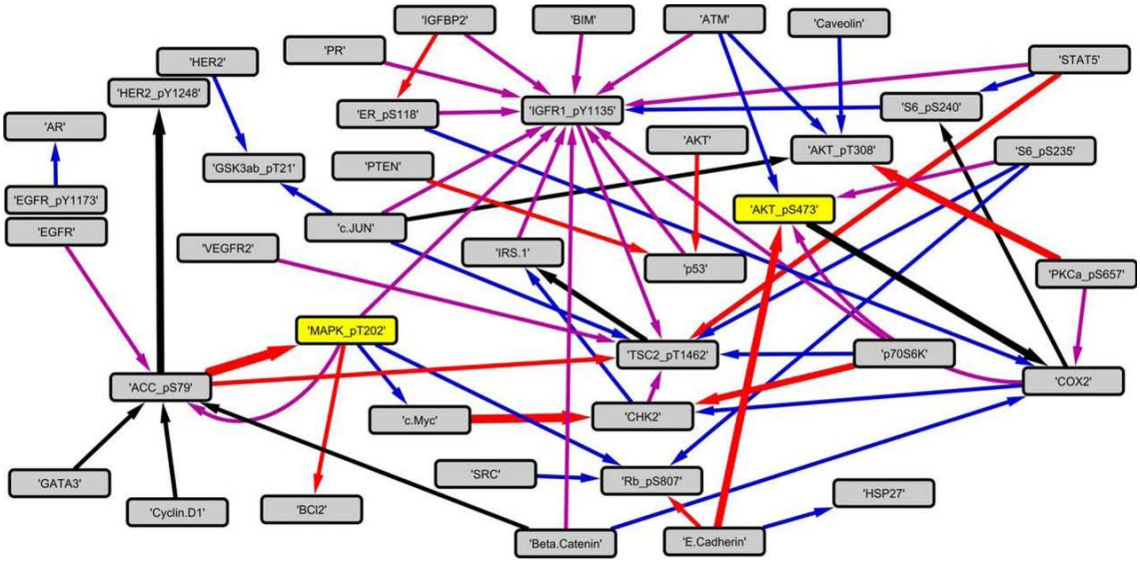

Figure 4: Computationally inferred network of signaling interactions in the IGF1/insulin pathways. The schematic depicts the signaling interactions inferred by the lasso regression computational model moving from the vehicle to the 10 min time-point of growth factor stimulation. The major downstream signaling hubs (pAkt (S473) and ERK (Th202/204)) are labeled in yellow ('output'). The purple lines represent the top 20 exclusive interactions present in IGF1 model only and the blue lines represent the interactions inferred only in the insulin model. The red lines represent the interactions present in both models, but with magnitudes stronger in the IGF1 model and the black lines also represent the interactions present in both models, but with higher magnitudes in the insulin model.

Additionally, the computational model predicted the time point that the interaction was most evident and the ligand (IGF1 or insulin) predicted to have the greatest effect (Table 1) on signaling magnitude. The two signaling interactions predicted by the model that we focused on for this study, due to their novelty and potential impact, included i) E-cadherin regulation of

IGF1/insulin-induced Akt phosphorylation and ii) acetyl-CoA carboxylase (ACC1/2) regulation of IGF1/insulin-induced ERK phosphorylation.

Table 1: *In silico* predictions for novel IGF1/insulin signaling mediators.
The table depicts the top candidate predictions for novel IGF1 and/or insulin signaling interactions as predicted by the lasso regression computational model. Outlined are the 'perturbed' proteins that if altered may affect IGF1 and insulin signaling through Akt and ERK at the given time points.

Perturbation	*Output*	*Ligand*	*Time (min)*
E-cadherin	Akt (S473)	IGF1	10, 30
ACC1/2	ERK (Thr202)	IGF1	5, 10
ATM	Akt (S473)	Insulin	5, 10, 30
ATM	Akt (Thr308)	Insulin	5, 10
Cyclin B1	ERK (Thr202)	IGF1	30
COX2	Akt (S473)	IGF1	10, 30

2.3.3 Validation of IGF1/insulin signaling mediators predicted *in silico*

To validate these predictions, we used shRNA/siRNA knockdown of E-cadherin (*CDH1)* and acetyl-CoA carboxylase (*ACACA/ACACB*) in breast cancer cell lines, followed by stimulation with IGF1 and insulin to assess changes in downstream Akt or ERK signaling. Cell lines chosen for the experimental validation express both high levels of the protein target for knockdown and are IGF1/insulin responsive based on our proteomic data. First, the effect of E-cadherin loss on IGF1/insulin-induced Akt (S473) signaling was assessed. Following shRNA knockdown of CDH1 (shCDH1) in T47D cells, enhanced IGF1/insulin-induced phosphorylation of Akt following 5 and 10 min of stimulation was observed (Figure 5). The fold change induction of

pAkt (S473) over vehicle in shCDH1 cells was greater compared to control cells (shSCR) with stimulation of both growth factors at the 5 min time point (shCDH1 IGF1=9-fold [$p<0.01$]; shCDH1 insulin=4-fold [$p<0.005$]). Similarly, both IGF1 and insulin induced greater fold change induction in pAkt in shCDH1 cells compared to shSCR at the 10 min time point. The magnitude of change was greatest with IGF1 stimulation compared to insulin; therefore, we focused on the regulation of the IGF1 signaling pathway by E-cadherin for the remainder of the study (Chapters 3 and 4), with the assumption that similar results would be observed following insulin stimulation.

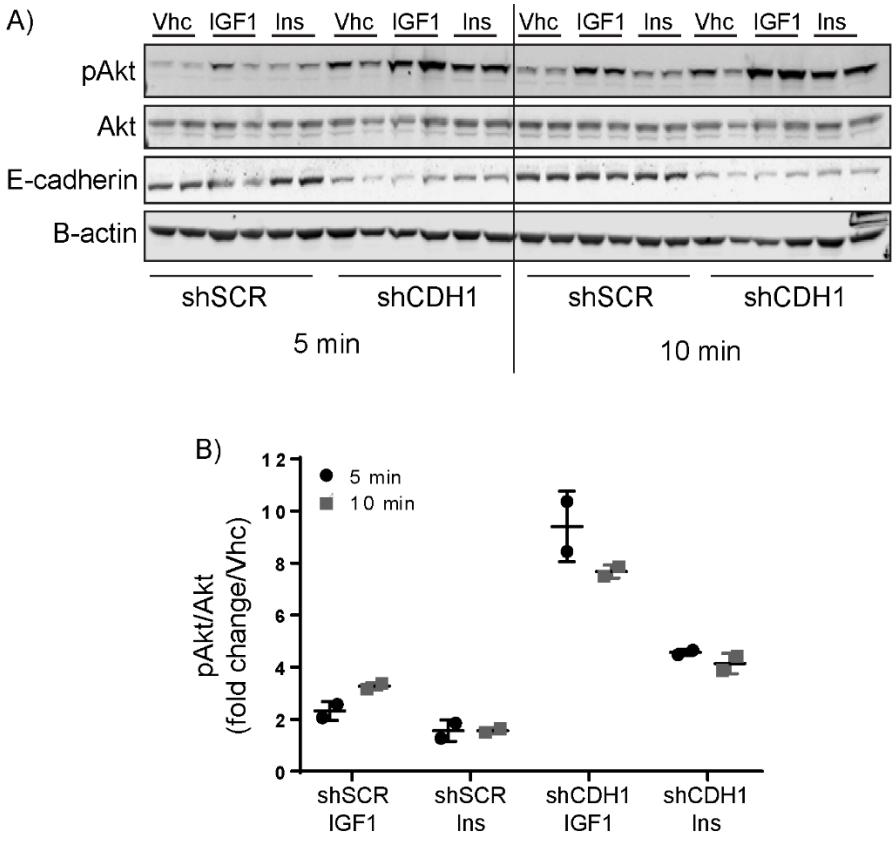

Figure 5: Knockdown of E-cadherin (*CDH1*) enhances IGF1- and insulin-induced Akt signaling. (A) T47D breast cancer cells stably expressing Renilla (shSCR) or CDH1 (shCDH1) shRNA were stimulated with IGF1 (10nM) for 5 or 10 min. Akt signaling (pAkt (S473) and total Akt) and levels of E-cadherin were assessed by immunoblot. (B) Quantification of immunoblot was done using LiCor software and is displayed as relative pAkt/Akt levels as a fold change over vehicle for each time point. Data shown is from one independent experiment with n=2 biological replicates.

Next, the effect of ACC1/2 knockdown in MCF-7 cells on IGF1/insulin-induced ERK signaling was assessed. The fold change induction of ERK signaling (pERK Th202/204) by IGF1 in cells with knockdown of ACC (siACC) was increased compared to siSCR cells at the 5 min time point (siACC IGF1=3-fold increase ($p<0.05$) [Figure 6]). Conversely, the fold change induction of ERK signaling by insulin at the same time point in siACC cells was decreased compared to siSCR cells (siACC insulin=0.8-fold decrease ($p<0.05$)). Additionally, there was a trend toward down-regulation of pERK signaling in siACC compared to siSCR cells at the 10 min time point with both IGF1 and insulin stimulation.

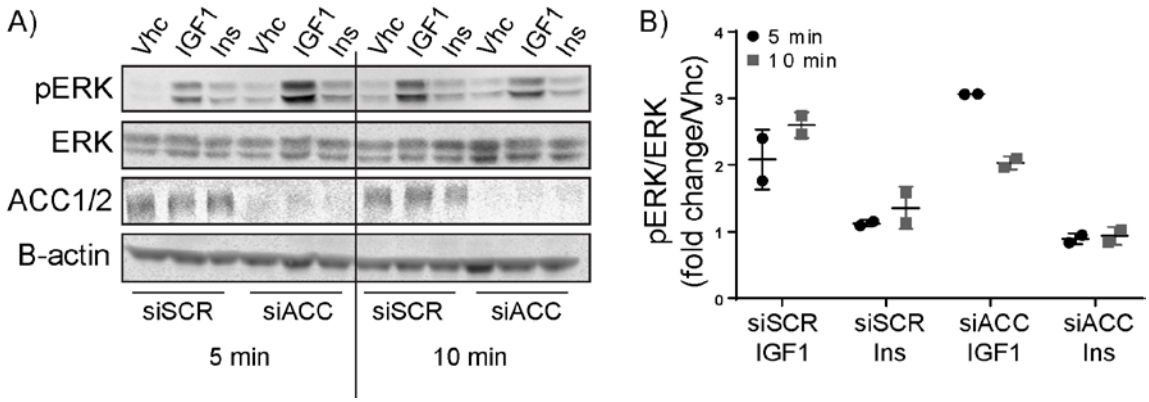

Figure 6: Knockdown of acetyl coA-carboxylase (*ACC1/2*) divergently alters IGF1- and insulin-induced ERK signaling.
(A) MCF-7 breast cancer cells transfected with scramble (siSCR) or ACC (siACC) siRNA were stimulated with IGF1 (10nM) for 5 or 10 min. ERK signaling (pERK (Th202/204) and total ERK) and levels of ACC1/2 were assessed by immunoblot. (B) Quantification of immunoblot was done using LiCor software and is displayed as relative pERK/ERK levels as a fold change over vehicle for each time point. Data shown is from one independent experiment with n=2 biological replicates.

2.4 DISCUSSION

In the study presented in this chapter, we assessed the temporal dynamics of the IGF1 and insulin signaling pathways to identify differences in downstream signaling and uncover novel interacting mediators. We assessed the expression of 108 phospho- and total proteins in a large panel of breast cancer cell lines following IGF1 and insulin stimulation over a 48-hour time course using a high-throughput proteomic approach. A novel, unbiased computational model was then developed to understand how signaling interactions in the IGF1 and insulin growth factor pathways change over time, and to determine differential signaling components in these highly similar pathways. The model was internally validated in two ways using the inherent existence of post-translational modifications within the data: i) levels of non-phosphorylated protein predicted the ability of the same protein to become phosphorylated (e.g. PKCα and Rb1 [data not shown]) and ii) the presence of known interactions between kinase and substrate were observed (e.g. p70S6K levels predicted phosphorylation of S6 ribosomal protein [data not shown])[124]. Additionally, the model predicted *in silico* that alterations in E-cadherin and ACC1/2 affect Akt and ERK signaling, respectively, in IGF1 and insulin-stimulated cells, and these predictions were validated experimentally *in vitro*. The *in vitro* validations provide further confidence that future predictions of signaling mediators may be defined and validated successfully using this approach.

Based on the *in silico* predictions, we show that the loss of E-cadherin in breast cancer cells enhances IGF1 and insulin-induced Akt signaling. The interaction of E-cadherin with IGF1/insulin signaling has high translational relevance for two reasons. First, E-cadherin is a critical regulator of epithelial to mesenchymal transition (EMT) and metastasis in breast cancer. One of the significant features of EMT is reduction in E-cadherin expression, combined with

increases in expression of the mesenchymal markers N-cadherin and vimentin[83,125,126]. While it has been established that IGF1-IGF1R signaling induces an EMT phenotype and drives E-cadherin repression, the reverse regulation of signaling has not been well characterized[81,83,84]. Consistent with our findings, it has been shown that endogenous E-cadherin negatively regulates Akt signaling activation by sequestering β-catenin leading to increased PTEN transcriptional activation and decreased Akt phosphorylation[127,128]. Additionally, it has been demonstrated that overexpression of E-cadherin reduces growth factor-signaling activation by reducing both receptor mobility and ligand binding affinity[129,130]. Further detail regarding the regulation of growth factor pathways by E-cadherin is discussed in Chapter 3.

Second, invasive lobular carcinoma (ILC), a subtype of breast cancer accounting for 10-15% of total breast cancer cases, is defined by loss of functional E-cadherin protein. This occurs in 90% of ILC and is frequently due to truncation mutations in *CDH1*, hemizygous deletion of the *CDH1* locus, or transcriptional repression[15]. Our proteomic data indicates that an ILC cell line, MDA- MB-134, is one of the most IGF1 responsive cell lines used in the study (Figure 3). We focus on and highlight the importance of the IGF1-IGF1R pathway in ILC in Chapter 4.

Additionally, we validate that the loss of ACC in MCF-7 cells divergently effects IGF1 and insulin-induced ERK signaling. ACC is activated by phosphorylation of AMP-activated protein kinase (AMPK) and functions to catalyze the irreversible carboxylation of acetyl-CoA to produce malonyl-CoA to regulate a rate limiting step in fatty acid synthesis. Cancer cells often overexpress genes that regulate lipogenic signaling such as fatty acid synthase (FASN), stearoyl-CoA desaturase (SCD1), and ACC1/2 to drive oncogenic signaling in low nutrient and highly oxidative tumor microenviornments[131]. Evidence suggests that the activation of AMPK, as a result of decreased hepatic glucose following treatment with the diabetes drug, metformin,

induces ACC levels leading to enhanced insulin signaling and reduced insulin resistance[132]. Despite this mechanism linking ACC to insulin signaling, we found no previously reported link between ACC and ERK signaling. Therefore, of note, there is no clear hypothesis for how this novel interaction influences IGF1 induction of ERK signaling.

In summary, although preclinical and epidemiological evidence suggest IGF1R to be a beneficial therapeutic target in breast cancer, the compensatory and activating feedback mechanisms in tumor cells have likely prevented the efficacy of anti-IGF1R/InsR therapy in clinical trials to date[33,35,36]. Only after understanding the dual IGF1R/InsR network dynamics, could we identify the tumor subclasses suitable for inhibition of this pathway. The computational model of the IGF/insulin signaling networks introduced in this study provide us with a framework to uncover novel experimental targets of pharmacological importance in these pathways.

3.0 LOSS OF FUNCTIONAL E-CADHERIN ENHANCES IGF1R SIGNALING IN BREAST CANCER

3.1 INTRODUCTION

IGF1 is a circulating endocrine peptide hormone that is a major regulator of organismal growth and development[34]. IGF1, in combination with estrogen, is essential for normal mammary gland development, and this pathway is deregulated in the initiation and progression of breast cancer[133–136]. Many studies, including from our laboratory, have shown the ability of IGF1 receptor (IGF1R) to promote mammary tumorigenesis and metastasis both *in vitro*[81,88] and *in vivo*[81,90,92]. Additionally, we showed that when constitutively activated, IGF1R transformed mammary epithelial cells, increased migration and invasion, and induced epithelial to mesenchymal transition (EMT) via the NFkB pathway and upregulation of Snail[81,84].

Based on these observations, both small molecule tyrosine kinase inhibitors and monoclonal antibodies against IGF1R were tested in clinical trials in breast cancer. Unfortunately, although as many as 50% of breast tumors express IGF1R[52], these trials only identified a small subset of patients showing a therapeutic response to IGF1R targeted therapy, suggesting that predictive biomarkers are required to identify which patients' tumors will be responsive[33,35,36,137].

We previously developed an IGF1-signature (IGF-sig) based on microarray analyses, and more recently reported on a novel computational method to identify putative biomarkers of IGF1 signaling using a systems biology approach[112,124]. The latter was based on a proteomic screen using reverse phase protein array (RPPA) on 21 breast cancer cell lines of various histological

subtypes stimulated with IGF1 over a time course (discussed in Chapter 2)[124]. This computational model identified E-cadherin as a putative regulator of IGF1 signaling, and data in this chapter indicate that loss of E-cadherin expression directly increases IGF1R pathway activation and associated phenotypes in breast cancer. Insight into how E-cadherin regulates IGF1R is necessary to aid in our understanding of the oncogenic signaling network, specifically because the loss of E-cadherin i) is implicated in the ability of tumor cells to escape the primary tumor to potentially seed metastatic lesions and ii) is transcriptionally repressed and/or genetically lost in subsets of breast tumors[126,138–141]. The latter will be discussed in depth in Chapter 4.

3.2 MATERIALS AND METHODS

3.2.1 Cell Culture

All cell lines were authenticated (most recent date listed in [ ] below following each cell line) by the University of Arizona Genetics Core and mycoplasma tested (Lonza #LT07-418). Lab stocks were made following authentication and were used for this study. MCF-7 (ATCC; DMEM+10% FBS [06/29/16]), T47D (ATCC; RPMI+10% FBS [02/08/17]), ZR75.1 (ATCC; RPMI+10% FBS [10/13/16]), and MDA-MB-231 (ATCC; DMEM+10% FBS [10/13/16]) cells were cultured with indicated media conditions. Julie Scott (Oesterreich Lab) and Beth Knapick (Lee Lab) assisted with cell line propagation and authentication.

3.2.2 Transient siRNA knockdown

Cells were reverse transfected with 25nM final concentration of siGENOME human SMARTpool control siRNA (Dharmacon #D-001206) or siGENOME human SMARTpool CDH1 siRNA (Dharmacon #M-003877-02) using standard Lipofectamine RNAiMAX (Invitrogen #13778) protocol. Downstream assays were typically performed 48-72 hours following transfection. For experiments involving IGF1 (GroPep BioReagents #CU100) stimulation, cells were serum starved overnight and then pulsed with IGF1 (1nM, 10nM, or 100nM) for 10 minutes.

3.2.3 Stable shRNA infection

Stable CDH1 knockdown T47D cells were generated using a retro-viral infection of Renilla targeting control (shSCR [5’ TGCTGTTGACAGTGAGCGCAGGAATTAT AATGCTTATCTATAGTGAAGCCACAGATGTATAGATAAGCATTATAATTCCTATGCC TACTGCCTCGGA]) and two CDH1 (sh-1 [5’ TGCTGTTGACAGTGAGCGCA AGTGTGTTCATTAATGTTTATAGTGAAGCCACAGATGTATAAACATTAATGA ACACACTTATGCCTACTGCCTCGGA] and sh-2 [5’ TGCTGTTGACAGTGAGCGA CCGGGACAACGTTTATTACTATAGTGAAGCCACAGATGTATAGTAATAAACGTTGTC CCGGGTGCCTACTGCCTCGGA]) short-hairpin RNAs (shRNAs). Following infection, cells were selected using growth media supplemented with 1ug/ml Puromycin (Life Technologies #A11138-03) and were routinely cultured in the selection media. These cells were generated by Dr. Tiffany Katz (postdoctoral fellow, Oesterreich Lab).

3.2.4 Plasmid DNA overexpression

MDA-MB-231 cells were stably transfected using FUGENE6 with empty or hE-cadherin-pcDNA3 vector (Addgene #45769) using 15ug DNA per 10cm plate of cells. Cells were selected using growth media supplemented with 800ug/ml G418 (Invitrogen #10131-035) and were routinely cultured in the selection media until a stable population of cells grew out.

3.2.5 Immunoblotting

Samples for immunoblot analysis were collected using RIPA buffer (50mM Tris pH 7.4, 150mM NaCl, 1mM EDTA, 0.5% Nonidet P-40, 0.5% NaDeoxycholate, 0.1% SDS) supplemented with 1x HALT protease and phosphatase cocktail (Thermo Fisher #78442), probe sonicated for 15 seconds (20% amplitude), and centrifuged at 14,000rpm at 4˚C for 12 minutes. Protein concentration was assessed using BCA assay (Thermo Fisher #23225) and 50ug of protein per sample was run on 12% SDS-PAGE gel then transferred to PVDF membrane. Membranes were blocked for 1 hour using Odyssey PBS Blocking Buffer (LiCor #927-40000) then probed using the following primary antibodies and concentrations: pIGF1R Y1135 (Cell Signaling #3918; 1:500), total IGF1R β-subunit (Cell Signaling #3027; 1:1000), pAkt S473 (Cell Signaling #4060; 1:1000), total Akt (Cell Signaling #9272; 1:1000), E-cadherin (BD Biosciences #610182; 1:1000), and β-actin (Sigma #A5441; 1:5000). Membranes were then washed in TBST, incubated in LiCor secondary antibody (1:10,000) for 1 hour (anti-rabbit 800CW [LiCor #926-32211]; anti-mouse 680LT [LiCor #925-68020]), then imaged using the Odyssey Infrared Imager.

3.2.6 IGF1-induced cell cycle and viability analysis

For cell cycle: MCF-7 and ZR75.1 cells were reverse transfected as described above for 48 hours. Cells were then serum starved for 30 hours, and pulsed with 10nM IGF1 for 17 hours. Cells were then trypsinized, washed 2x with PBS, and fixed in 70% EtOH for 30 minutes at 4˚C. Cells were washed 2x with PBS then incubated in 50ng/ul RNase A (Qiagen #1007885) for 15 minutes at 37˚C. Cell DNA content was then stained using 50ng/ul propidium iodide (Sigma #P4170) for 30 minutes at 4˚C. Cell cycle profiles were analyzed using the BD LSRII flow cytometer. Statistical difference in percent of cells in S- or G2/M phase in IGF1 treated cells over vehicle control in experimental groups was evaluated using a two-tailed student's t-test ($p<0.05$).

For viability: T47D short hairpin control (shSCR) and E-cadherin knockdown (shCDH1) cells were plated in serum-free media in 96 well plates (9,000 cells per well) and then stimulated with IGF1 (10nM) for 6 days. The FluoReporter Blue Fluorometric DNA content Quantitation Kit was used to measure dsDNA as a measure of cell viability. Statistical difference in Hoechst fluorescence in IGF1 treated cells over vehicle control in each cell line was evaluated using a two-tailed student's t-test ($p<0.05$).

3.2.7 Immunofluorescence microscopy and proximity ligation assay

Cells were plated on coverslips for the assay and then fixed in 4% paraformaldehyde for 30 minutes at 37˚C. Coverslips were washed 2x with PBS and then permeabilized for 1 hour using 0.3% Triton X-100 diluted in PBS. For immunofluorescence, coverslips were blocked in 5% goat serum diluted in PBS and then incubated in primary antibody overnight (total IGF1R β-subunit

[Cell Signaling #3027; 1:300] and E-cadherin [BD Biosciences #610182; 1:100]), followed by Alexa Fluor secondary antibody incubation for 1 hour (anti-rabbit Alexa Fluor 488 [Life Technologies #A11070] and anti-mouse Alexa Fluor 546 [Life Technologies #A11018]; 1:200). Coverslips were imaged by confocal microscopy.

For *in situ* proximity ligation assay, coverslips were processed using the Duolink red mouse/rabbit kit using the protocol provided (Sigma #DUO92101) with the same antibody dilutions as described above. Confocal microscopy was used for imaging. The ratio of puncta/nuclei for each experimental condition was calculated by counting all puncta and nuclei in five 60x images. One-way ANOVA was used to compare the ratios between the experimental conditions (VHC, 30m, 6hr, 24hr).

3.2.8 Dose response growth assays

MCF-7, ZR75.1 and T47D cells were reverse transfected with control or CDH1 siRNA as described above into 96-well plates (9,000 cells per well) in 100ul of media per well. The following day, cells were treated with 3x vehicle (DMSO), OSI-906 (Selleckchem #S1091) or BMS-754807 diluted in 50ul of media for a final volume in each well of 150ul (n=6 per concentration). Adherent and suspension plates (2D and ultra-low attachment [ULA; Corning #3474]) were collected on day 6 and viability was measured using CellTiter Glo Viability assay (Promega #G7572) according the manufacturer protocol. EC_{50} values for viability were calculated by non-linear regression and statistical differences evaluated using sum-of-squares Global f-test ($p<0.05$).

3.3 RESULTS

3.3.1 Loss or inhibition of E-cadherin results in enhanced IGF1R activity

To validate our previously published data (Chapter 2)[124] and to further understand the regulation of the IGF1 signaling pathway by E-cadherin, we silenced E-cadherin (*CDH1*) by siRNA knockdown in a panel of three estrogen receptor (ER)-positive IDC cell lines and then stimulated with a dose series of IGF1 (0, 1, 10, 100nM). MCF-7, ZR75.1, and T47D E-cadherin knockdown (siCDH1) cells showed enhanced sensitivity to IGF1 compared to the scramble control (siSCR) cells, most notable at the 1nM dose of IGF1, resulting in increased levels of IGF1R and Akt phosphorylation (Figure 7A-C). As a complementary approach, we inhibited E-cadherin function in MCF-7 cells using the HECD-1 monoclonal antibody that binds the extracellular domain of E-cadherin and prevents adherens junction formation. Similar to the knockdown of E-cadherin, HECD-1 treated cells showed increased IGF1R and Akt phosphorylation compared to control (Figure 7D). Additionally, we evaluated confluency-dependent IGF1R signaling to understand the effect of increased cell-cell contacts. A confluent monolayer of MCF-7 cells lost the ability to initiate IGF1R signaling upon ligand stimulation compared to a sub-confluent monolayer (approx. 50%), however, the knockdown of E-cadherin rescued this signaling in both confluency conditions (Figure 7E). We evaluated the functional effect of enhanced IGF1 signaling by examining the effect of IGF1 on the cell cycle profile in MCF-7 and ZR75.1 cells with reduced E-cadherin. CDH1 knockdown cells showed a significant increase ($p=0.03$ and $p=0.0005$, respectively) in the percentage of cells progressing into the S- and G2/M-phases of the cell cycle following IGF1 treatment compared to the siSCR cells (Figure 7F). Similarly, slight increases in

IGF1-induced cell viability in E-cadherin knockdown cells compared to SCR in T47D cells were observed (Figure 25).

We overexpressed E-cadherin in MDA-MB-231 cells, an ER-negative IDC cell line with undetectable E-cadherin protein by immunoblot to determine if overexpression represses signaling. Although adherens junction formation was not observed (data not shown), E-cadherin overexpressing cells demonstrated decreased phosphorylation of IGF1R and Akt compared to empty vector control cells, and significantly less cell cycle progression in response to IGF1 stimulation ($p=0.011$; Figure 26A-B).

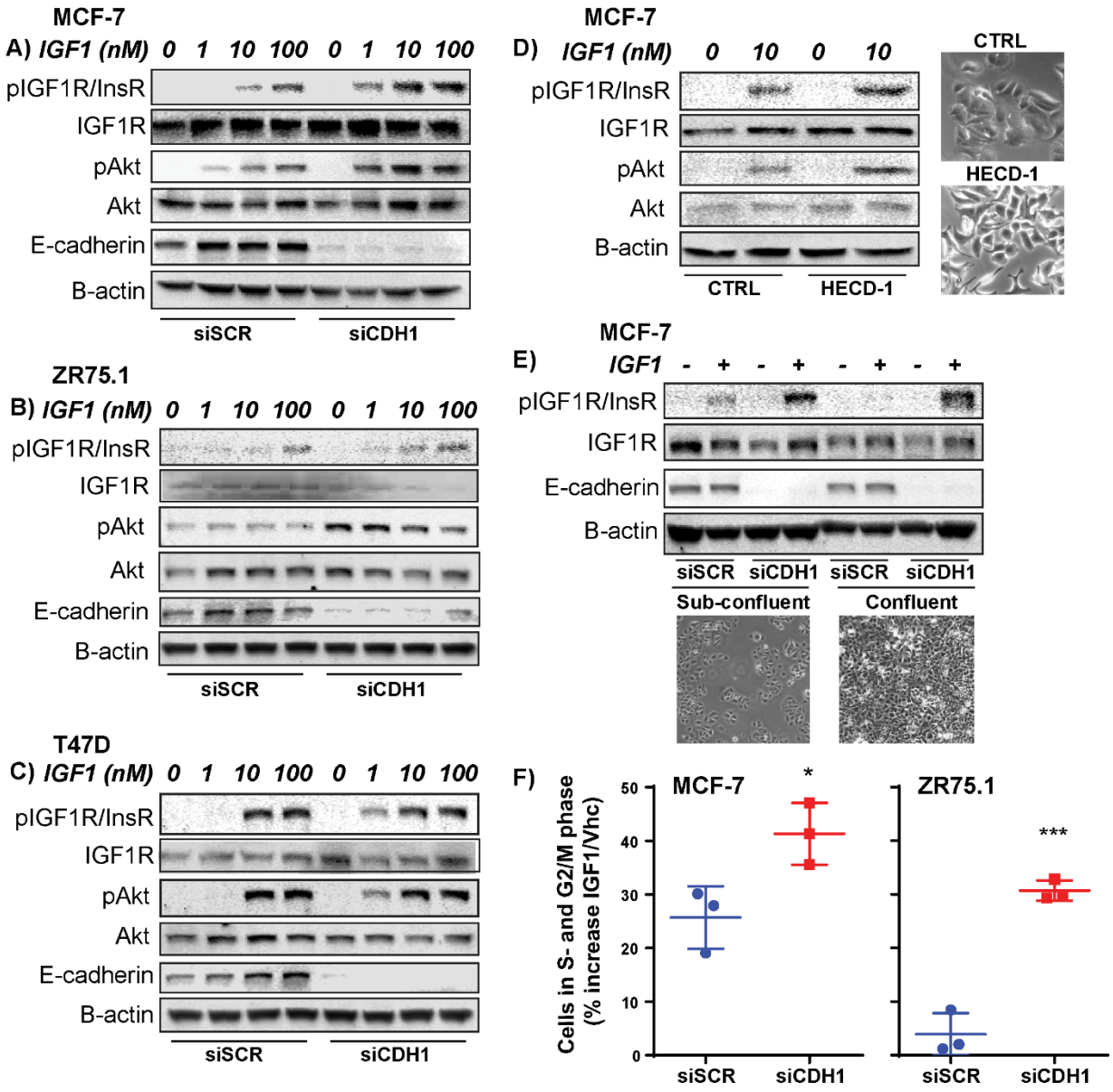

Figure 7: Loss or inhibition of E-cadherin enhances IGF1R signaling.
(A) MCF-7, (B) ZR75.1, and (C) T47D breast cancer cells transfected with SCR (siSCR) or CDH1 (siCDH1) siRNA were stimulated with increasing doses of IGF1 (0-100nM) for 10 min. IGF1R and Akt signaling was assessed by immunoblot. Of note, IGF1R expression could routinely not be detected in ZR75.1. (D) MCF-7 cells were treated with 25ug/ml HECD-1 antibody for 24 hours and imaged by phase-contrast microscopy for dissociation of adherens junctions. Cells were stimulated with Vhc or 10nM IGF1 for 10 min and IGF1R and Akt signaling assessed by immunoblot. (E) MCF-7 cells were plated at sub-confluency (200k cells in 6-well) or high confluency (800k cells) and then stimulated with either Vhc or 10nM IGF1 for 10 min. IGF1R signaling was assessed by immunoblot. Representative phase-contrast microscopy images of the cell plating densities are shown. (F) MCF-7 and ZR75.1 siSCR and siCDH1 cells were serum-starved and stimulated with 10nM IGF1 for 17 hours and DNA stained with propidium iodide to measure cell cycle profile. The percent of cells in the IGF1/Vhc conditions in the S- and G2/M phases of the cell cycle for siSCR and siCDH1 are shown (representative experiment shown; n=2 or 3 each with 3 biological replicates).

3.3.2 Loss of E-cadherin enhances sensitivity to IGF1R inhibition

Due to the enhanced sensitivity of E-cadherin knockdown cells to IGF1 stimulation, we determined if loss of E-cadherin in ER+ IDC also increased sensitivity to the IGF1R ATP-competitive small molecule inhibitors, OSI-906 (OSI) and BMS-754807 (BMS). Specifically, we tested the effect of loss of E-cadherin on sensitivity to OSI and BMS in MCF-7, ZR75.1, and T47D cells. In addition to 2D adherent culture, ultra-low attachment suspension growth (ULA) conditions was examined, since we observed increased cell viability in E-cadherin knockdown cells under these conditions (Tasdemir et al, manuscript in preparation), possibly due to the reported annoikis resistance of cells lacking E-cadherin expression[142]. MCF-7 siCDH1 cells displayed significantly decreased viability in response to OSI treatment, compared to siSCR cells in both 2D ($p<0.0001$; Figure 8A) and ULA ($p=0.0003$; Figure 8B) growth conditions resulting in a shift in the EC_{50}. Additionally, ZR75.1 siCDH1 cells showed significantly decreased viability and a shift in the EC_{50} when grown in ULA ($p<0.0001$; Figure 27A-B) in response to OSI treatment, but not in the 2D growth condition. However, there was no change in viability between T47D siSCR and siCDH1 cells in response to OSI in either growth condition (Figure 28A-B).

Similarly, MCF-7 and T47D siCDH1 cells showed decreased viability in response to BMS compared to siSCR cells grown in the ULA growth condition ($p<0.0001$ and $p<0.05$, respectively), but no significant difference in 2D (Figure 8C-D, Figure 28C-D). However, ZR75.1 siCDH1 cells did not display enhanced sensitivity to BMS compared to siSCR cells in either growth condition (Figure 27C-D). Overall, these data suggest that the loss of E-cadherin enhances breast cancer cell sensitivity to IGF1R inhibition. We also tested the growth response of MCF-7 siSCR and siCDH1 cells treated with ICI 182,780 (ICI), a selective estrogen receptor

downregulator (SERD), and observed no statistical difference in EC_{50} suggesting that the loss of E-cadherin does not generally sensitize cells to all small molecule drug treatments (Figure 29).

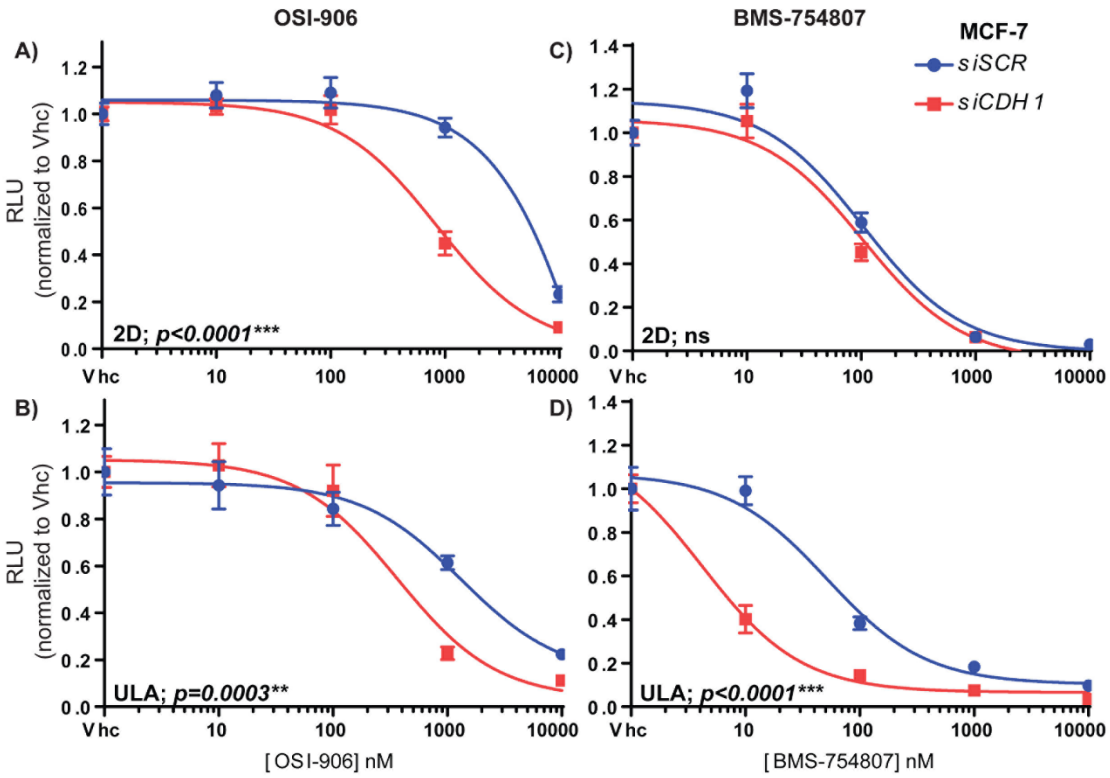

Figure 8: Knockdown of E-cadherin increases sensitivity to IGF1R inhibition.
MCF-7 cells were reverse transfected with SCR or CDH1 siRNA and seeded into 96-well 2D or ULA plates and treated with IGF1R inhibitor (OSI-906 or BMS-754807) for 6 days. Conditions in the panels as follows: (A) OSI-906; 2D, (B) OSI-906; ULA, (C) BMS-754807; 2D, (D) BMS-754807; ULA. The CellTiter Glo assay was used to assess cell viability (relative luminescence). EC50 values for viability were calculated by non-linear regression and statistical differences evaluated using sum-of-squares Global f-test ($p<0.05$; representative experiment shown; n=3 each with 6 biological replicates).

3.3.3 IGF1R and E-cadherin directly interact in ER+ breast cancer cells resulting in recruitment of IGF1R to adherens junctions

To understand how E-cadherin regulates IGF1R, we assessed whether IGF1R and E-cadherin directly interact in breast cancer cells using *in situ* proximity ligation assay (PLA). The

sensitivity and specificity of PLA allows for detection of endogenous interacting proteins within proximity of no further than 40nm. Because the protocol requires probes to be within nanometer proximity for effective ligation and signal detection, it is suggested that both primary antibodies bind in the same orientation to the proteins of interest, either extracellular or cytoplasmic. Therefore, using a rabbit IGF1Rβ cytoplasmic subunit antibody and a mouse E-cadherin cytoplasmic antibody, PLA showed that IGF1R and E-cadherin directly interact in both MCF-7 and T47D cells, as shown by the red fluorescent puncta (Figure 9A-B). To demonstrate the specificity of the detection, we used MCF-7 knockdown cells lacking E-cadherin (siCDH1) or IGF1R (siIGFR) as negative controls, stained for E-cadherin and IGF1R, and observed the red fluorescent puncta signal greatly diminished (Figure 9C-D, Figure 30A-C).

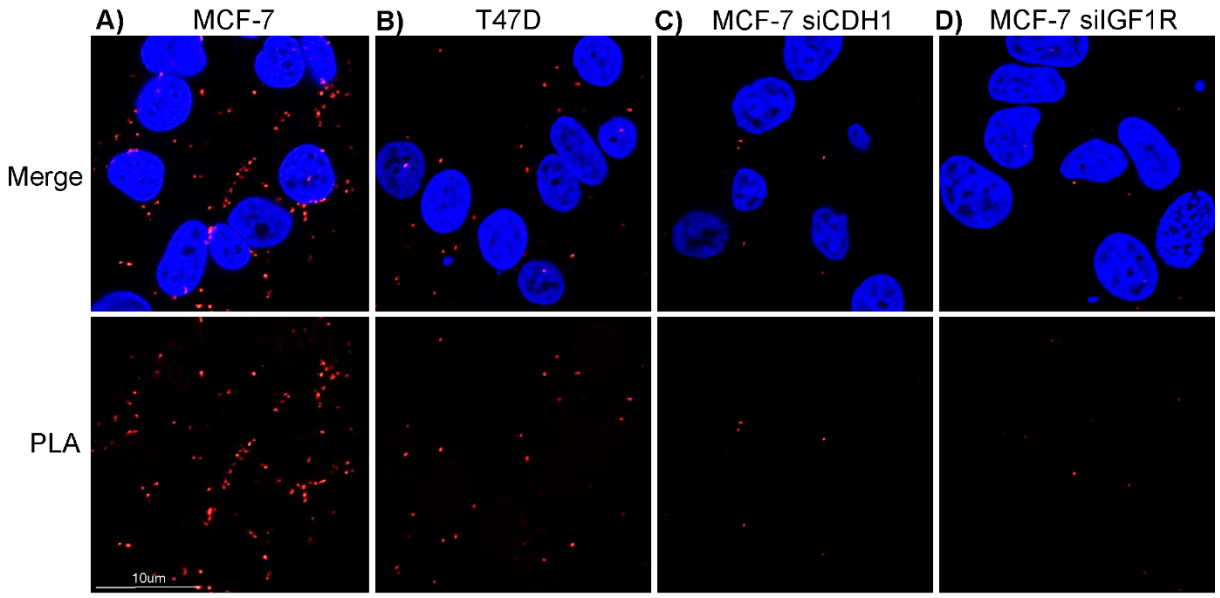

Figure 9: Proximity ligation assay reveals a direct interaction between IGF1R and E-cadherin. (A) MCF-7 and (B) T47D cells were plated on coverslips, fixed, and stained with IGF1R and E-cadherin antibody overnight. The Duolink (Sigma) *in situ* PLA protocol was followed and coverslips were imaged using confocal microscopy to reveal red puncta. (C) MCF-7 siCDH1 and (D) siIGF1R cells were used as negative controls for the assay to assess primary antibody specificity.

Additionally, the specificity of the secondary antibodies was confirmed by using each primary antibody alone and a no primary antibody control and did not detect significant levels of PLA puncta over background (Figure 30D-F). The interaction between IGF1R and E-cadherin following IGF1 stimulation was examined using PLA. In MCF-7 cells, IGF1 treatment (30 min, 6 hr, 24 hr) caused a significant decrease in number of fluorescent puncta ($p=0.003$), suggesting that the interaction between the two proteins needs to be disrupted for proper IGF1R function (Figure 10A-E). This possibly explains why siCDH1 cells have an increased IGF1R signaling capacity compared to control cells. We stained MCF-7 cells for endogenous IGF1R and E-cadherin and determined that IGF1R and E-cadherin co-localize to adherens junctions.

Interestingly, co-localization was prominent at the points of cell-cell contact, and noticeably absent or reduced on portions of the membrane where there was no cell-cell contact (Figure 11A). This suggests that E-cadherin recruits IGF1R to adherens junctions, perhaps to sequester the receptor as a mechanism of signaling repression. Upon knockdown of E-cadherin the expression pattern of IGF1R appears to redistribute equally to the entire cell membrane (Figure 11B) supporting the idea that E-cadherin influences and regulates IGF1R localization.

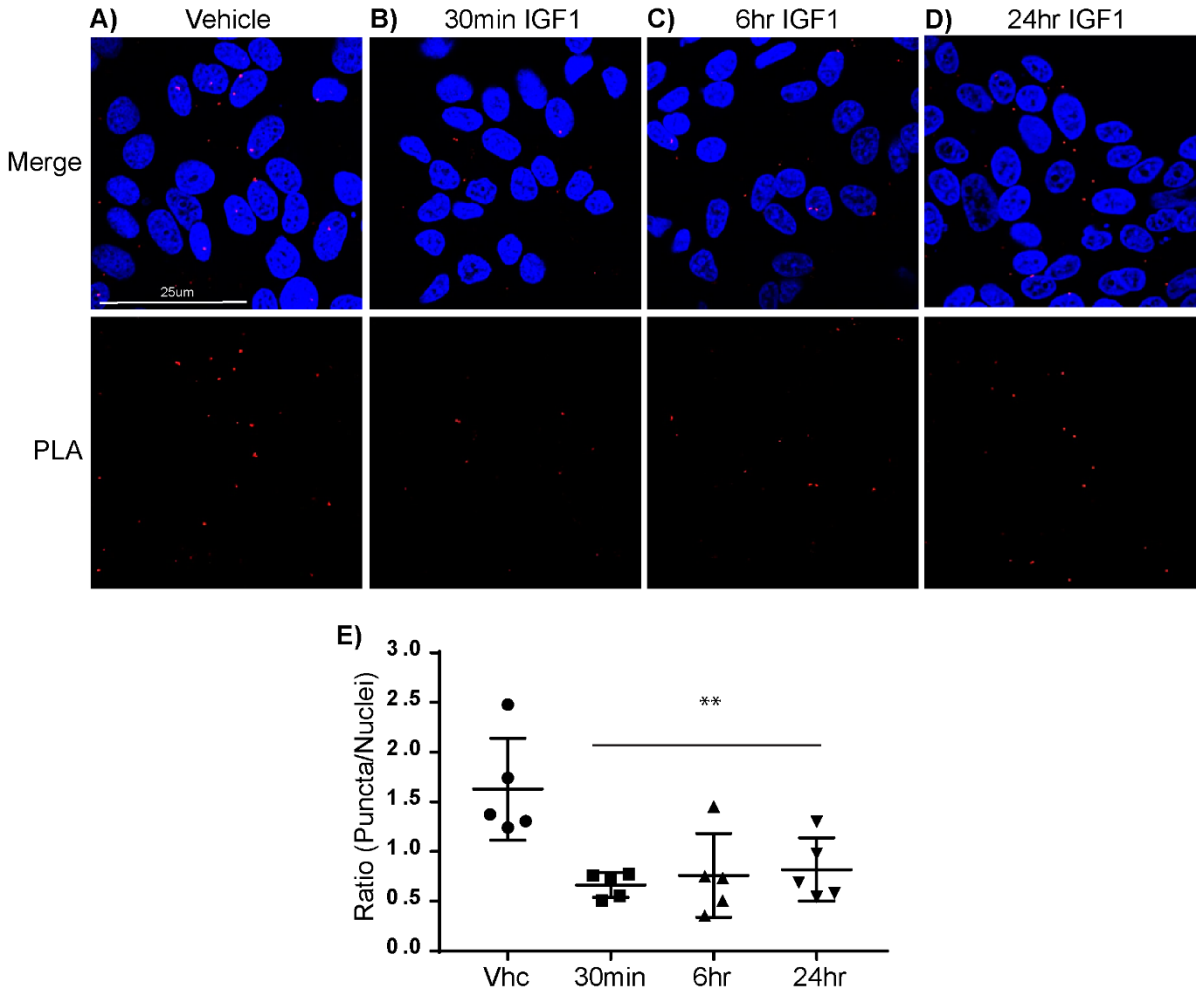

Figure 10: IGF1 stimulation induces the disruption of the IGF1R-E-cadherin complex.
MCF-7 cells were plated on coverslips and treated with either (A) Vhc or 10nM IGF1 for (B) 30 min, (C) 6 hr, or (D) 24 hr using PLA protocol. (E) Red puncta and nuclei (DAPI) were quantified and displayed as a ratio of puncta/nuclei. All puncta and nuclei in 60x images were counted (n=5). Statistical difference determined by one-way ANOVA ($p<0.05$; representative experiment shown). Data shown is from 1 independent experiment with n=5 fields counted (experiment repeated twice).

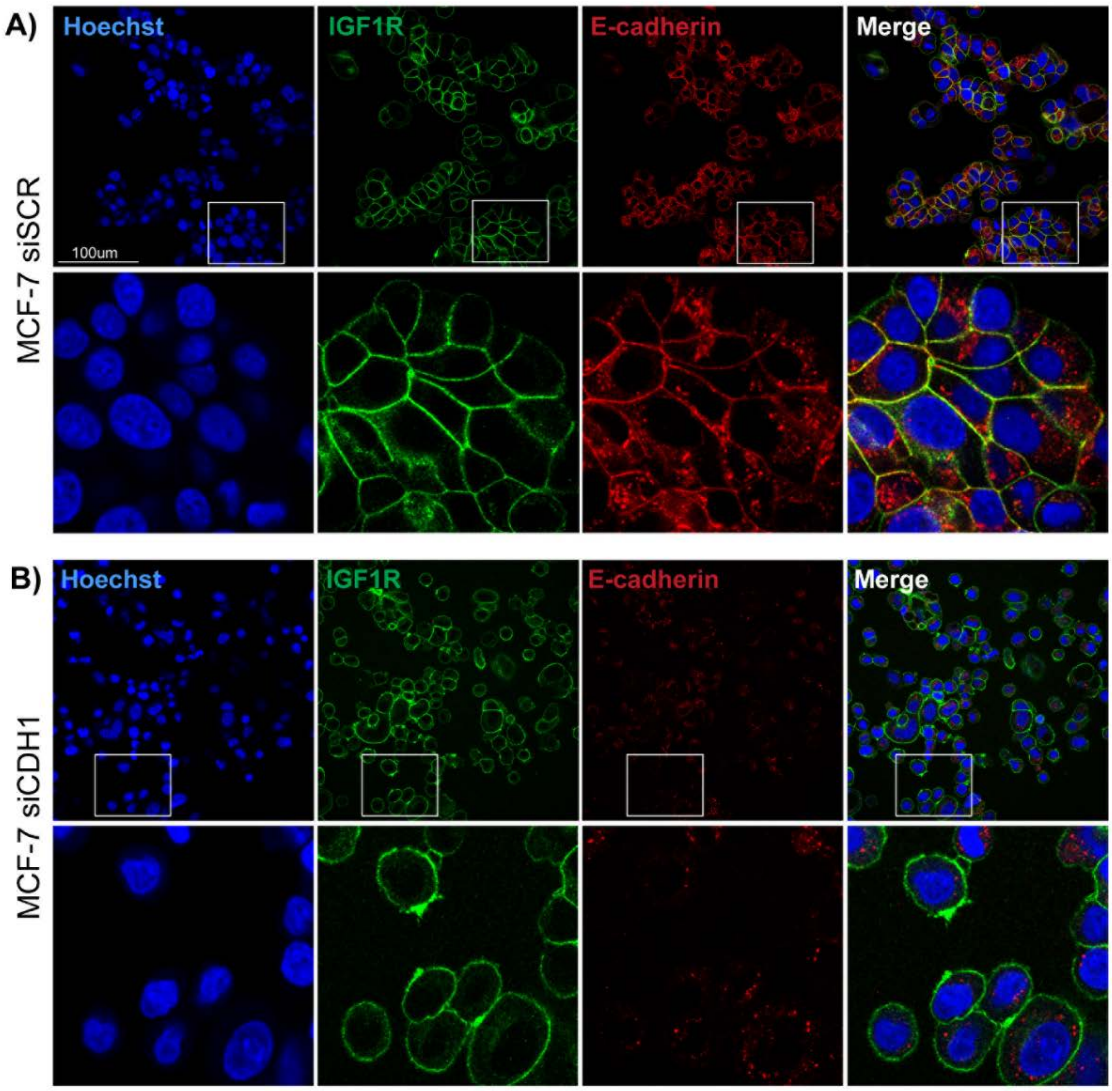

Figure 11: IGF1R and E-cadherin co-localize at points of cell-cell contact.
MCF-7 (A) siSCR and (B) siCDH1 cells were plated on coverslips, fixed, and stained with IGF1R and E-cadherin antibody overnight. The co-localization of IGF1R (green) and E-cadherin (red) was analyzed by immunofluorescence confocal microscopy.

3.4 DISCUSSION

Despite a large body of preclinical evidence supporting the use of IGF1R inhibitors for the treatment of breast cancer, the outcomes of clinical trials testing the efficacy of these drugs in patients thus far have been disappointing. However, these trials proceeded with a lack of appropriate biomarkers for predicting positive therapeutic efficacy and little to no understanding of which tumor types would benefit[33,35,36,143]. In response, in recent years the field has emphasized the need to understand and identify gene expression or proteomic biomarkers that predict a positive response to targeted therapy. Along this thought process, we previously published a gene expression signature used to identify tumors that are IGF1 responsive[112] and here we focus on one proteomic biomarker, E-cadherin, identified through an integrative computational approach recently published by our group[124]. It is known that constitutive IGF1R activation drives E-cadherin transcriptional repression through EMT via NFκB induction of Snail[81,84], however, the reverse regulation of IGF1R by E-cadherin has not been previously characterized. Our data suggest that loss of E-cadherin in breast tumors highlights a subset of tumors that may be responsive to IGF1R inhibition, and we begin to describe the mechanism by which this regulation occurs.

We demonstrate that in breast cancer cells, IGF1R in breast cancer cells is endogenously localized to cell-cell contacts, similarly to data published by in MCF-7 cells overexpressing IGF1R[144] and in corneal epithelial cells[145]. We show a direct, endogenous interaction between IGF1R and E-cadherin using *in situ* proximity ligation assay. To our knowledge interaction between IGF1R and E-cadherin in breast cancer cells has only been demonstrated by immunoprecipitation (IP)[144]. Our data provide confirmation of this interaction using a technique

known to be higher in specificity and sensitivity with less cell manipulation (e.g. cell lysis or scraping), compared to IP which often results in pull-down of entire protein complexes. This data suggests that IGF1R is recruited to adherens junctions by E-cadherin, possibly resulting in receptor sequestration and signaling repression.

This process is similar to the sequestration of EGFR into the adherens junction and the subsequent loss of receptor mobility, a well characterized mechanism of EGFR signaling repression[129,130,146]. However, that action is suggested to be mediated through the tumor suppressor, Merlin, responsible for coordinating stabilization of the adherens junction and thereby regulating contact-inhibition growth[146]. Although IGF1R signaling is controlled in a contact-dependent manner (Figure 7E), Curto et al. additionally showed that IGF1 activity is not regulated by Merlin, indicating that IGF1R regulation by E-cadherin likely occurs independently of this factor[146]. Although there may be a yet undefined intermediate regulator similar to Merlin, our data indicate that E-cadherin plays a role in coordinating the recruitment and sequestration of IGF1R within the adherens junction and functions to inhibit IGF1R signaling. When E-cadherin is lost and junction formation is disrupted (such as in ILC cells discussed in Chapter 4), IGF1R is released and re-localizes to the entirety of the cell membrane where signaling is more easily initiated upon IGF1 ligand binding.

Supporting this concept, our data indicate that the knockdown of E-cadherin in three ER+ breast cancer cell lines not only enhanced IGF1-induced signaling via IGF1R but also increased sensitivity of the cells to ligand. This is similar to the relationship reported between EGF-EGFR and IGF1-IGF1R upon adherens junction disruption via calcium-depletion[130]. Because of the increased IGF1R pathway activation and proliferative phenotype associated with the loss of E-cadherin, the knockdown cells in turn became more sensitive to IGF1R inhibition. In our

previous work we described sensitivity of ER-negative breast tumors to IGF1R inhibition (BMS-754807)[87], specifically mesenchymal-like triple negative tumors lacking expression of E-cadherin[147]. However, we did not find a direct correlation between EC_{50} of BMS-754807 and E-cadherin expression level in cell lines upon recent re-analysis of the data (data not shown). This suggests that multiple biomarkers may need to be used in combination, such as in combination with activation of the IGF1 gene signature, or perhaps there is a threshold by which E-cadherin expression in IDC tumor cells needs to be below to predict response to IGF1R inhibitor; a subset of ER-negative cells may be below that threshold.

In summary, we present a diverse set of data indicating that the loss of E-cadherin enhances IGF1R pathway activity and sensitivity to anti-IGF1R therapy. We show that IGF1R and E-cadherin directly interact, and this leads to the sequestration and potential repression of IGF1R within the adherens junction. Overall, this study begins to shed light on a previously unrecognized mechanism of IGF1R regulation by E-cadherin and highlights a potential therapeutic strategy of exploiting the IGF1R pathway in breast cancer subtypes with low E-cadherin expression.

4.0 HYPERACTIVE IGF1-IGF1R PATHWAY IN INVASIVE LOBULAR BREAST CARCINOMA PRESENTS A NOVEL THERAPEUTIC STRATEGY

4.1 INTRODUCTION

The data presented in Chapter 3 suggests that a loss of functional E-cadherin enhances IGF1R pathway activation leading to a hyperproliferative phenotype and increased sensitivity to IGF1R inhibition. Therefore, we hypothesize that subsets of breast cancer with diminished E-cadherin expression may be susceptible to IGF1R pathway inhibition.

One such subtype of breast cancer with lack of E-cadherin expression is invasive lobular breast carcinoma (ILC), accounting for 10-15% (~30,000 cases/year in the United States) of total breast cancer cases. ILC is defined by the loss of functional E-cadherin *(CDH1*), which occurs in 95% of ILC due to truncating mutations, loss of heterozygosity, and transcriptional repression[14,15]. Due to the loss of E-cadherin protein, ILC cells grow in linear patterns throughout the breast tissue, lacking the ability to form adherens junctions, in contrast to the solid mass growth of the most frequent subtype of breast cancer, invasive ductal breast carcinoma (IDC)[16]. Interestingly, one of the most IGF1 responsive cell lines in our proteomic data set (Chapter 2) was an ILC cell line, MDA-MB-134, that lacks E-cadherin protein expression and cell-cell junctions[124]. In this chapter, we characterize the IGF1-IGF1R pathway activity in ILC, and provide evidence that inhibition of IGF1R in E-cadherin deficient breast cancers, such as ILC, could potentially serve as an effective therapeutic strategy.

4.2 MATERIALS AND METHODS

4.2.1 Cell Culture

All cell lines were authenticated (most recent date listed in [ ] following the cell lines below) by the University of Arizona Genetics Core and mycoplasma tested (Lonza #LT07-418). Lab stocks were made following authentication and were used for this study. MDA-MB-134-VI (ATCC; 50/50 DMEM/L15+10% FBS [02/08/17]), SUM44PE (Asterand; DMEM/F12+2% CSS with 5ug/ml insulin, 1ug/ml hydrocortisone, 5mM ethanolamine, 5ug/ml transferrin, 10nM triodothyronime, and 50nM sodium selenite [02/08/17 – no reference profile exists in database]), and BCK4[148] (MEM+5% FBS with 1nM insulin and 1x NEAA [10/13/16 – no reference profile exists in database) cells were cultured with indicated media conditions. BCK4 cells were kindly provided by Dr. Britta Jacobsen (UC Denver). Julie Scott (Oesterreich Lab) and Beth Knapick (Lee Lab) assisted with cell line propagation and authentication.

4.2.2 Immunoblotting

Samples for immunoblot analysis were collected using RIPA buffer (50mM Tris pH 7.4, 150mM NaCl, 1mM EDTA, 0.5% Nonidet P-40, 0.5% NaDeoxycholate, 0.1% SDS) supplemented with 1x HALT protease and phosphatase cocktail (Thermo Fisher #78442), probe sonicated for 15 seconds (20% amplitude), and centrifuged at 14,000rpm at 4˚C for 12 minutes. Protein concentration was assessed using BCA assay (Thermo Fisher #23225) and 50ug of protein per sample was run on 12% SDS-PAGE gel then transferred to PVDF membrane. Membranes were blocked for 1 hour using Odyssey PBS Blocking Buffer (LiCor #927-40000) then probed using

the following primary antibodies and concentrations: pIGF1R Y1135 (Cell Signaling #3918; 1:500), total IGF1R β-subunit (Cell Signaling #3027; 1:1000), E-cadherin (BD Biosciences #610182; 1:1000), and β-actin (Sigma #A5441; 1:5000). Membranes were then washed in TBST, incubated in LiCor secondary antibody (1:10,000) for 1 hour (anti-rabbit 800CW (LiCor #926-32211); anti-mouse 680LT (LiCor #925-68020)), then imaged using the Odyssey Infrared Imager.

4.2.3 Immunofluorescence microscopy

Cells were plated on coverslips for assay then fixed in 4% paraformaldehyde for 30 minutes at 37˚C. Coverslips were washed 2x with PBS and then permeabilized for 1 hour using 0.3% Triton X-100 diluted in PBS. Coverslips were blocked in 5% goat serum diluted in PBS and then incubated in primary antibody overnight (total IGF1R β-subunit [Cell Signaling #3027; 1:300] and E-cadherin [BD Biosciences #610182; 1:100]) followed by Alexa Fluor secondary antibody incubation for 1 hour (anti-rabbit Alexa Fluor 488 [Life Technologies #A11070] and anti-mouse Alexa Fluor 546 [Life Technologies #A11018]; 1:200). Confocal microscopy was used for imaging.

4.2.4 Dose response growth assays and synergy experiments

SUM44PE and MDA-MB-134-VI cells were plated in 96-well ULA plates (Corning #3474; 18,000 cells per well) in 100ul of media per well. The following day, cells were treated with 6x vehicle (DMSO), OSI-906, BMS-754807, or BEZ235 (Selleckchem #S1009) diluted in 25ul of media such that the combination of two drugs resulted in 150ul of total volume in each well (n=2

per experiment). Plates were collected on day 6 and viability was measured using CellTiter Glo Viability assay (Promega #G7572) according to the manufacturer's protocol. Synergy was calculated using the Median-Effect Principle and Combination Index-Isobologram Theorem (Chou-Talalay)[149] using the computer program Calcusyn (Biosoft, Cambridge, UK). Values less than one indicate synergistic drug interactions. Combination index values for ED50, ED75, ED90 are shown as a mean ± SEM from n=3 independent experiments.

4.2.5 *In vivo* ILC xenograft growth and explant culturing

MDA-MB-134, BCK4, and WHIM9[150] cells ($5x10^6$ cells) were injected into the right inguinal mammary fat pads of NOD.Cg-Prkdcscid Il2rgtm1Wjl/SzJ (NSG; The Jackson Laboratories [MM134 and WHIM9]) or CB17.Cg-PrkdcscidLystbg-J/Crl (SCID-beige; Charles River [BCK4]) mice, respectively (implanted with slow release estradiol (0.36mg) pellet [Innovative Research of America #SE-121]) and collected at a tumor volume of approximately $350mm^3$. Tumors were then collected, processed, and minced into 1-$2mm^3$ chunks of tumor tissue. Julie Scott (Oesterreich Lab) assisted with tissue implantation, harvesting, and processing. Tissue chunks were then plated on Vetspon Absorbable Hemostatic Gelatin sponges (Patterson Veterinary #07-849-4032) in 12-well tissue culture plates containing 1.5mls of explant media (DMEM/F12+10% FBS with 10mM HEPES, 1mg/ml BSA, 10ug/ml insulin, 10ug/ml hydrocortisone, 1x antibiotic-antimycotic solution (Thermo Fisher #15240-062)). Explant media conditions were provided by Dr. Damir Vareslija (PI: Dr. Leone Young). Media was treated with vehicle or 1uM BMS-754807 or 100nM BEZ235 for 72 hours. Tissue chunks were collected by formalin fixation followed by paraffin embedding. Sections were stained for ki67 (Dako #M7240; 1:100) as a marker of proliferation using standard immunohistochemistry technique. Nuclei were quantified by counting all clearly

defined nuclei within each explant tissue section (n=3-8). A two-tailed student's t-test was used to determine statistical difference between vehicle and BMS treatment or a one-way ANOVA to determine the difference between vehicle, BMS, and BEZ treatment ($p<0.05$). Justin Kehm and Kara Burlbaugh (undergraduates; Lee and Oesterreich Labs) assisted with quantification of Ki67 staining.

4.2.6 TCGA data analysis

TCGA RNA-Sequencing (RNA-seq) expression data were downloaded as transcripts per million (TPM) from the Gene Expression Omnibus database (GEO: GSE62944) and log2(TPM+1) for gene-level results were used. TCGA Reverse Phase Protein Array (RPPA) data were downloaded as median-normalized, batch-corrected expression values from TCPA (Level 4, version 4.0). ER+ IDC (n=417) and ILC (n=137) samples with both RNA-Seq and RPPA data were used for all analyses. Mann-Whitney U tests were used to compare expression, Spearman's rho to compare correlations, and a chi-square test to compare proportions between ILC and IDC tumors. All were calculated using R (version 3.4.1). The median expression values for IGF1 and pIGF1R across ER+ IDC and ILC tumors (n=554) for correlation were used as cutoffs. Kevin Levine (graduate student; Oesterreich Lab) completed all bioinformatic analysis.

4.3 RESULTS

4.3.1 Invasive lobular breast cancer (ILC) displays enhanced IGF1-IGF1R pathway activation

Because knockdown or inhibition of E-cadherin induces hyperactivity of the IGF1R pathway in cell line models, we investigated whether IGF1R pathway activity is also hyperactivated in ILC, a subtype of breast cancer that accounts for 10-15% of all breast cancer cases and is molecularly classified by its genetic loss of E-cadherin[15]. Because 90-95% of ILC tumors are ER+ we focused on this cohort[15]. IGF1R expression and localization was examined in the ER+ ILC cell lines: SUM44PE (Figure 12A), MDA-MB-134 (Figure 12B), and BCK4 (Figure 12C). As expected, ILC cells showed a lack of membranous E-cadherin staining. Additionally, IGF1 signaling response in a panel of ILC cell lines (MM134, SUM44PE, BCK4, and MM330) was compared to MCF-7 cells, which is thought of as the most highly IGF1 responsive breast cancer cell line. Of note, MM330 cells express E-cadherin protein, but harbor alterations in α-catenin rendering their adherens junctions non-functional and therefore, are classified as an ILC cell line. The ILC cells displayed a greater or equal level of phosphorylation of IGF1R in response to IGF1 compared to MCF-7 cells indicating a high level of IGF1R activity (Figure 31).

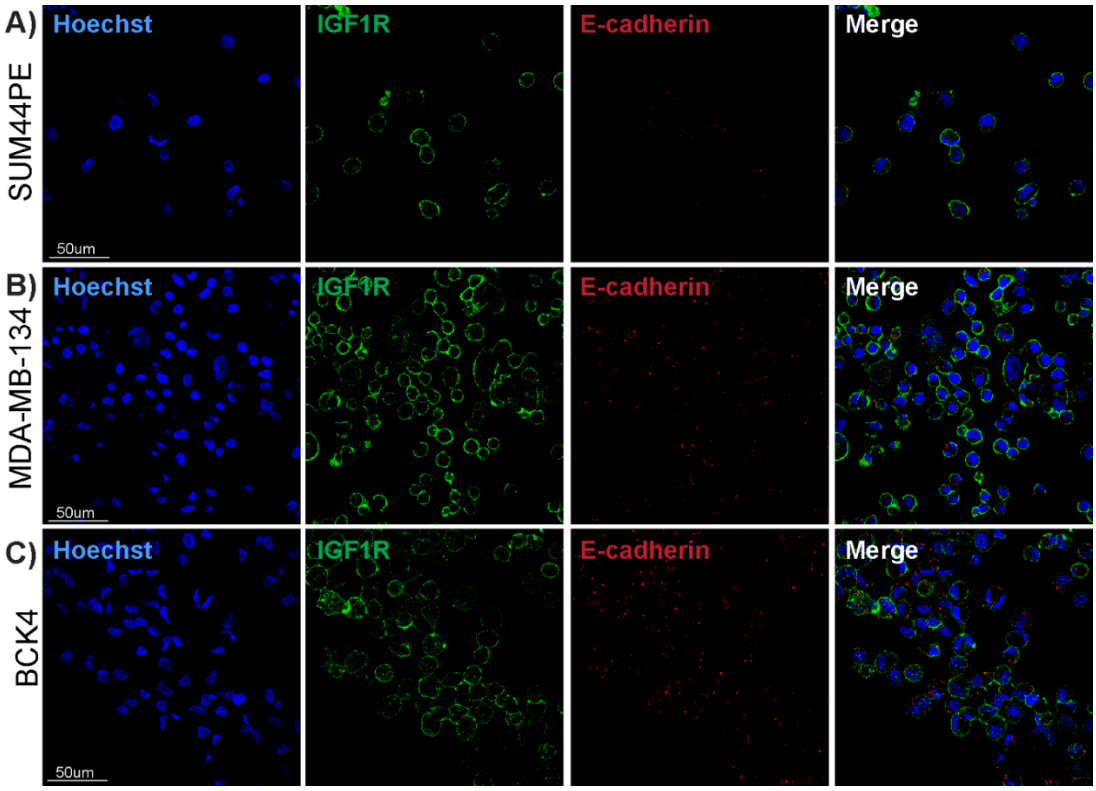

Figure 12: ILC cell lines express membranous IGF1R
(A) SUM44PE, (B) MDA-MB-134, and (C) BCK4 ILC cells were immunostained for IGF1R (green) and E-cadherin (red) and imaged by confocal microscopy. Nuclei were stained with Hoechst. Of note, BCK4 cells were imaged at an increased exposure compared to MM134 and SUM44PE cells.

To compare IGF1R activity in ER+ ILC (n=137) and IDC (n=417) tumors, CDH1 and IGF1 ligand mRNA expression, and IGF1R phosphorylation (pIGF1R; Y1135/Y1136) were examined using RNA-sequencing and Reverse Phase Protein Array data from The Cancer Genome Atlas (TCGA). Concurrent with a decrease in CDH1 mRNA expression (p=9.06e-52; Figure 13A), IGF1 ligand mRNA expression (p=1.3e-15; Figure 13B) and pIGF1R levels (p=2.15e-08; Figure 13C) were significantly increased in the ILC tumors compared to IDC tumors. Interestingly, ILC tumors exhibited a significant positive correlation (Spearman rho=0.21; p=0.012), despite having significantly reduced total IGF1R expression compared to IDC (data not shown; Figure 13D). In contrast, IDC tumors did not show a correlation

(Spearman rho=0.06; p=0.22) suggesting that presence of IGF1 ligand did not necessarily activate IGF1R in IDC. Strikingly, the percentage of tumors with higher than median expression (across all breast tumors) of both IGF1 and pIGF1R is significantly higher in ILC (56.2%) compared to IDC (21.3%), suggesting that IGF1 ligand activates IGF1R signaling in these tumors more efficiently with the loss of E-cadherin (chi-square test, p= 2.5e-14; Figure 13D). Interestingly, when assessing activation of the IGF-sig[112] (gene signature indicative of active IGF1 signaling) in ER+ ILC versus IDC in the TCGA cohort we did not observe a statistically significant difference in expression score (data not shown).

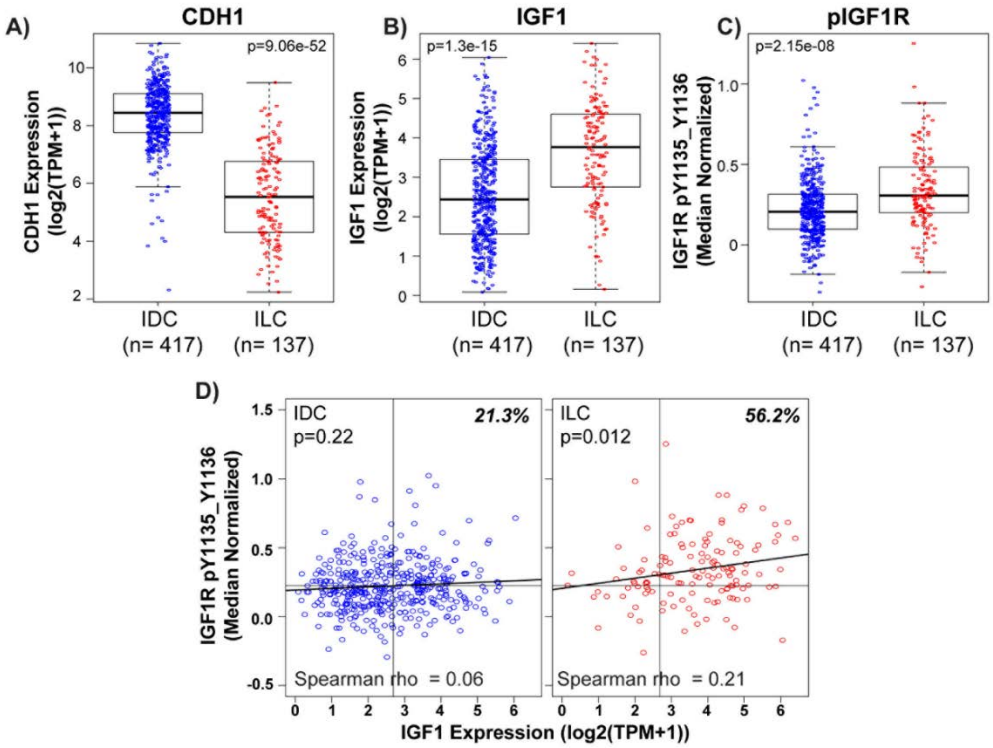

Figure 13: IGF1-IGF1R pathway is active in ILC with genetic loss of E-cadherin
(A) CDH1 mRNA, (B) IGF1 mRNA, (C) and pIGF1R Y1135 & Y1136 levels in ER+ IDC compared to ER+ ILC in TCGA were plotted using RNAseq (log2 TPM+1) and RPPA (median normalized) data. The TCGA cohort includes n=417 IDC cases and n=137 ILC cases that have matched data for RNAseq and RPPA. Man-Whitney test was used to determine significant differences in expression level between the two subtypes ($p<0.05$). (D) Correlation between pIGF1R and IGF1 ligand expression is plotted for IDC (left) and ILC (right). Spearman's rank correlation was used to demonstrate the correlation between the two variables with significance as defined by $p<0.05$. Bioinformatic analysis was completed by Kevin Levine (Oesterreich Lab).

4.3.2 IGF1R inhibitors and endocrine therapy synergize to decrease viability in ILC cells

Clinically, patients with ER+ ILC are treated with endocrine therapy targeting ER, however, data from the BIG 1-98 trial suggest that ILC tumors demonstrate resistance to tamoxifen therapy compared to IDC[22]. Additionally, results from multiple clinical studies indicate that ILC patients have a poorer prognosis with more frequent late recurrences compared to IDC [19,23,24]. This highlights the need to improve therapeutic options in ILC patients based on uniquely activated pathways and therefore, we evaluated efficacy of IGF1R pathway inhibitors in ER+ ILC cell lines in combination with endocrine therapy. Recent data published from our lab suggest that tamoxifen, a selective estrogen receptor modulator (SERM), can act as a partial ER agonist activating ER activity in some ILC cell lines, rather than a pure antagonist as in IDC cells[151], in line with the data from the BIG1-98 study. Therefore, we tested efficacy of the SERD, ICI 182,780 (ICI) in combination with two IGF1R inhibitors used in Chapter 3 (OSI and BMS) and a PI3K/mTOR inhibitor (BEZ235 (BEZ)) in our studies. SUM44PE and MM134 cells were treated with increasing doses of OSI (Figure 14A-B; Figure 32A-B), BMS (Figure 14C-D; Figure 32C-D), and BEZ (Figure 14E-F; Figure 32E-F) in combination with increasing doses of ICI. With all three IGF1R pathway inhibitors decreased cell viability was observed with the addition of increasing doses of ICI. Formal testing the synergy of the drug combinations using the Median-Effect Principle and Combination-Index Isobologram Theorem, commonly referred to as the Chou-Talalay method[149] revealed combination index (CI) values less than 1 for drug interactions at the ED50, ED75, and ED90 indicating a high level of synergy for the three sets of inhibitor combinations (Figure 14, Figure 32, Table 3). The lowest CI values were observed for the BMS+ICI drug combination in SUM44PE cells (ED50=0.127, ED75=0.081, ED90=0.099). Additionally, a minimum dose reduction index (DRI) for ICI of 8-fold for all drug combinations

in SUM44PE cells and 2-fold in MM134 cells at the EC50 was seen. This data suggests that adding an IGF1R pathway inhibitor in combination with ICI reduces the concentration of ICI necessary to achieve that same inhibitory effect as ICI alone.

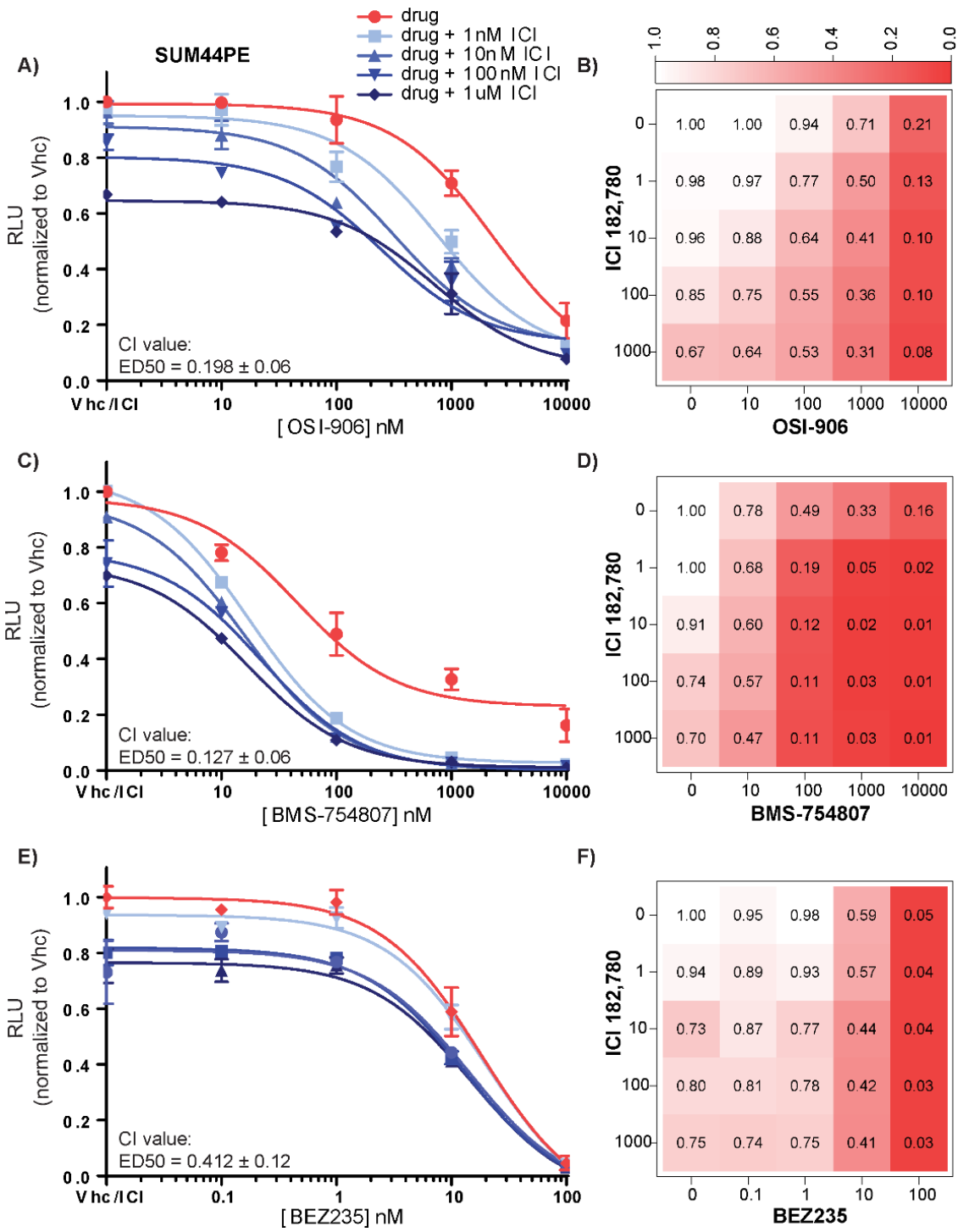

Figure 14: IGF1R pathway inhibitors and endocrine therapy synergize to inhibit cell viability in ILC
SUM44PE ILC cells were plated into 96-well ULA plates and treated for 6 days with increasing doses of (A, B) OSI-906, (C, D) BMS-754807, or (E, F) BEZ235 in combination with increasing doses of ICI 182,780. The dose response curves and heat maps shown indicate inhibition of cell viability (relative luminescence measured using CellTiter Glo). Representative experiment shown; n=3 independent experiments each with 2 biological replicates per combination of doses.

4.3.3 Ex vivo IGF1R pathway inhibition inhibits proliferation in ILC xenografts

Finally, we evaluated the efficacy of an IGF1R inhibitor in ILC in vivo. However, there are a limited number of ILC patient-derived xenograft (PDX) and cell line xenograft models, and their slow growth rates makes large scale *in vivo* studies challenging. We therefore treated two ILC cell line xenografts and one ILC PDX *ex vivo* as explant cultures, as previously described from our lab and others[152–155]. The advantages of this technique include less tissue requirement for the assay compared to an *in vivo* study and rapid understanding of the therapeutic efficacy of the inhibitor. Additionally, data published by Majumder et al.[155] suggest a high concordance between *ex vivo* and *in vivo* tumor response to drug treatment. MM134 and BCK4 cells (a weakly ER responsive ILC cell line, not used for synergy experiments due to slow growth *in vitro*) were grown as xenografts, harvested and plated as explant culture, and then treated the media with vehicle or BMS (1μM) for 72 hours. The tissue was collected and stained for Ki67 as a marker of proliferation. We observed a significant decrease in Ki67 positive nuclei in both tumor models treated with BMS (Figure 15). In the MM134 tumor we observed a significant decrease ($p=0.002$) in Ki67 positive nuclei from 47% in the vehicle to 22% in the BMS treated tumor tissue (n=3 or 4; Figure 15A-C). Similarly, in the BCK4 tumor we observed a significant decrease ($p=0.005$) in Ki67 positive nuclei from 25% in vehicle to 11% in BMS treated tumor tissue (n=6; Figure 15D-F).

In addition to the cell line xenografts, the ER+ ILC PDX, WHIM9, was treated with BMS and BEZ as an explant. Because this tumor harbors a *PIK3CA* hotspot mutation (H1047R), inhibition of the PI3K pathway using BEZ was included[150]. We observed a trend toward a decrease in Ki67 positive nuclei from 27% in the vehicle to 23% in the BMS treated tumor

tissue, and observed a significant decrease ($p<0.01$) in to 8% in BEZ treated tumor tissue ($n=7$ or 8; Figure 33). This data suggests that targeting the IGF1R pathway in ILC tumors may be a useful strategy to inhibit tumor cell proliferation.

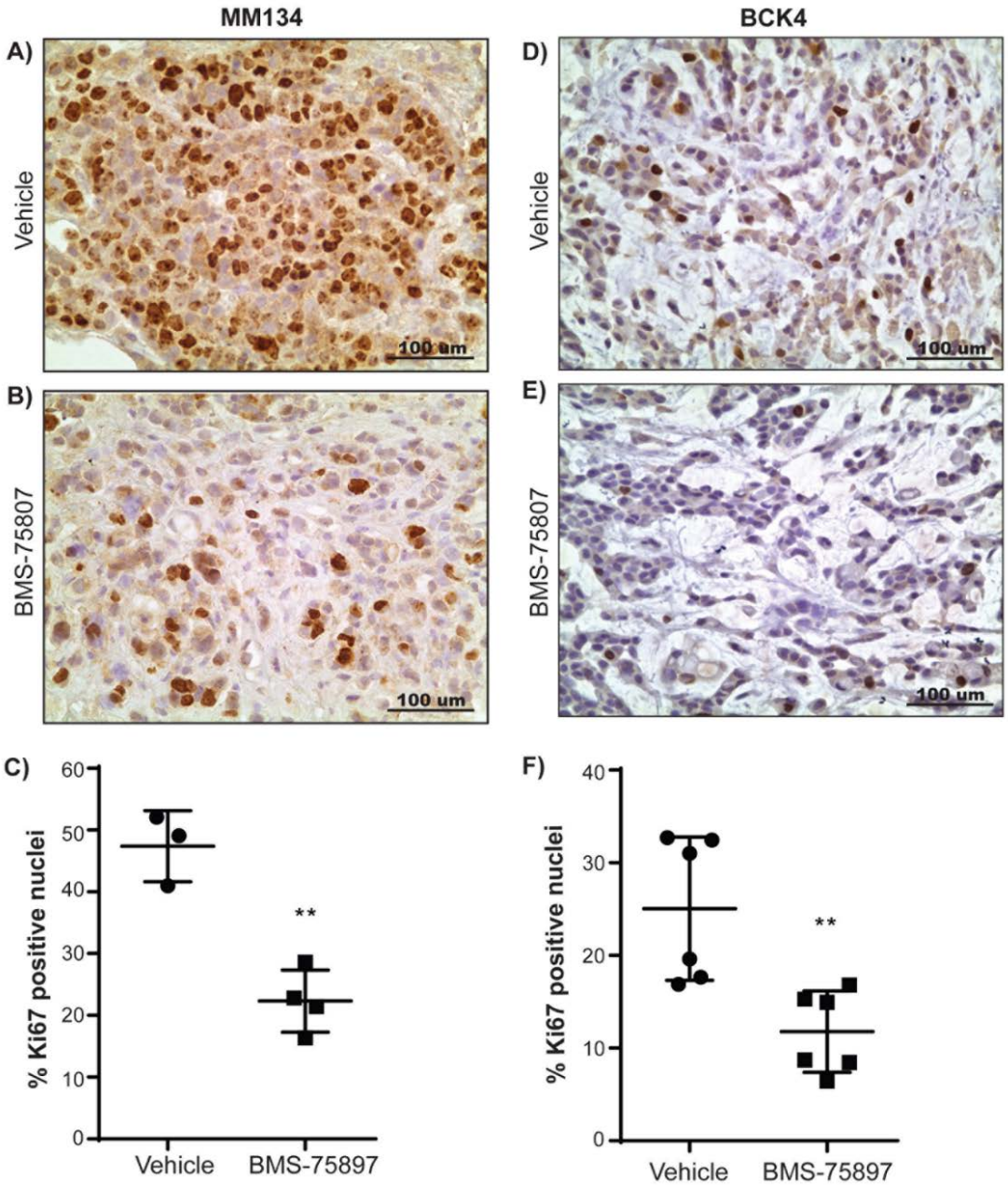

Figure 15: IGF1R inhibition reduces proliferation in ILC tumor *ex vivo* cultures.
MM134 and BCK4 xenograft tumors were harvested from immunocompromised mice, minced into 1-2mm^3 tumor chunks and then plated on gelatin sponges in 12-well plate containing 1.5ml media. Media was treated with DMSO Vhc or 1uM BMS-75807 for 72 hours. Tumor pieces were harvested by FFPE and stained for Ki67 as a marker of proliferation (A-B, MM134; D-E, BCK4). Staining was quantified by counting all clearly defined nuclei in 20x images (C and F). Statistical difference was assessed using a Student's t-test ($p<0.05$; n=3-6). Ki67 staining quantification was completed by Justin Kehm and Kara Burlbaugh (undergraduates; Oesterreich and Lee Labs).

4.4 DISCUSSION

We believe that the IGF1-IGF1R signaling may be particularly important in ILC, an understudied subtype of breast cancer, due to the complete loss of E-cadherin protein and/or adherens junction formation. In this subtype, the loss of E-cadherin may serve as a biomarker of IGF1 activity. Indeed, we demonstrate that ILC have increased IGF1 pathway activation (IGF1 ligand expression and pIGF1R levels) compared with IDC. This is similar to the results of two studies analyzing differences between ILC and IDC that found increased IGF1 ligand and IGF1R expression levels in ILC[20,156]. Consistent with this, we found that ILC cell lines are susceptible to IGF1R inhibition and importantly, that IGF1R pathway inhibitors (OSI, BMS, BEZ) synergize with a standard of care endocrine therapy (ICI) resulting in further reduced cell growth. Future studies will focus on validating these therapies in additional ILC tumors and understanding the synergistic interaction between IGF1R inhibitors and ICI. This data may be especially meaningful due to the fact that there is an increased prevalence of late recurrences in ER+ ILC compared to ER+ IDC tumors treated with endocrine therapy, indicating the need for improved therapy options for patients with ILC[22,23].

One limitation for the use of IGF1R inhibitors in ILC is the relatively high prevalence of mutations in the PI3K/Akt signaling pathway. Recently, Ciriello et al. comprehensively characterized ILC tumors compared to IDC tumors and described the mutational landscape of 127 ILC tumors[15]. They found 48% of ILC tumors harbor hotspot/missense mutations in *PIK3CA* and 13% to carry either a truncating/missense mutation or high level copy number loss in *PTEN*, similar to what had been previously described[20,21]. These genetic alterations likely lead to the high Akt activity in these tumors as defined by an Akt signature they reported. Our data

suggest that the remaining tumors may also have high Akt signaling activity due to aberrant IGF1R activity. But, because the alterations in *PIK3CA/PTEN* occur downstream of IGF1R, the effectiveness of IGF1R inhibition in this setting is unclear, as demonstrated in Figure 33. Resistance to other upstream kinase inhibitors in tumors harboring activating alterations in *PIK3CA/PTEN* has been previously observed[157] and therefore, it would be important to screen patients for these alterations before considering use of receptor tyrosine kinase inhibitor therapy, including against IGF1R.

Interestingly, the use of an Akt pathway inhibitor, such as BEZ235, may be mutually beneficial in targeting the *PIK3CA/PTEN* alterations and the enhanced IGF1R pathway activation observed in these tumors. Cantley and colleagues recently reported that high levels of insulin promote resistance to PI3K inhibitors in tumors with *PIK3CA* mutations[158], and therefore there may be a role for combinatorial IGF1R and PI3K inhibition as well. Future studies will investigate these relationships using additional *ex vivo* or *in vivo* screening of ILC tumors. Overall, this study begins to shed light on a previously unrecognized mechanism of IGF1R regulation by E-cadherin and highlights a potential therapeutic strategy of exploiting IGF1R pathway activity in ILC tumors.

5.0 DEVELOPMENT OF AN IGF1-DRIVEN TRANSGENIC MODEL OF ILC

5.1 INTRODUCTION

A major roadblock to ILC research is the lack of appropriate *in vivo* models that accurately recapitulate disease observed in humans. These models are required for improved mechanistic understanding of disease initiation and progression, and the development of novel therapeutic strategies to target ILC. The currently available models, similar to other types of cancer, include cell line xenografts, patient derived xenografts (PDX), and transgenic models. However, there are major drawbacks to many models currently available in the ILC field, as described below. Importantly, a common problem with *in vivo* models of ILC, similar to all breast cancer models, in that it is challenging to develop and sustain ER-positive (ER+) disease[159,160]. Due to the fact that approximately 90% of all ILC tumors are ER+, the presence and functionality of ER is a crucial aspect of the *in vivo* models used in research studies[15].

The use of cell line and patient derived xenograft models of ILC relies exclusively upon the ability of the cells or tissue to grow within an immunocompromised mouse, and this process is often lengthy in time or inefficient (e.g. low-take rates of tumors or large number of cells required) for ILC. Currently, we have only three ER+ cell lines available for use in cell line xenograft studies that are also markedly estrogen responsive (SUM44PE, MDA-MB-134, BCK4). Data from our lab (Tasdemir et al. unpublished) suggests that these cell lines may take up to five months to form palpable tumors of 350-500mm^3 in size. Additionally, these mice need to be treated with estrogen pellet supplementation to support tumor growth, causing bladder and kidney toxicity resulting in loss of mice from the study prior to tumor formation. In addition to cell line xenografts, there are

a select number of ER+ ILC PDX models available for use, but similar to cell lines many have slow growth rates and low take-rates. Among the available ER+ ILC PDXs, there are differences in tumor growth rate, mutational status (ER, PIK3CA, p53), and estrogen dependence among these models. The select PDXs (e.g. WHIM20, WHIM23) with increased growth and/or take rate are highly proliferative, and therefore do not mimic the typical low proliferative rate of classic ILC found in patients[15]. The availability of an ER+ ILC PDX model is study dependent based on the tumor characteristics required.

The overall use of xenograft models allows for the understanding of mechanisms for disease progression and response to therapeutics, but these models are not best suited for studies focused understanding tumor initiation and formation. In contrast, transgenic mouse models of ILC allow this, along with understanding of disease progression and response to therapeutics. Multiple models of mouse ILC have been developed, mainly by Drs. Jos Jonkers and Patrick Derksen, some with tumor latencies shorter than or equal to that required for xenograft studies[142,161–163].

Initial studies in the field of transgenic ILC mouse modeling, began with an unrelated study by Boussadia and Kemler, et al (2002)[164], in which they assessed the effect of loss of E-cadherin on mammary gland development and remodeling following pregnancy, lactation, and involution. Using an MMTV-Cre driven recombination of floxed E-cadherin alleles (*MMTV-Cre;CDH1flox*), E-cadherin was inactivated in the differentiated alveolar cells of the mammary gland. While the mammary glands of female mice with homozygous somatic inactivation of E-cadherin developed normally up to 18 days of pregnancy, following parturition the mammary gland underwent massive apoptosis resulting in a lack of milk protein production and inability of dams to nurse pups. This resembled the status of the normal gland during involution when total remodeling via apoptosis is

in process. Further, this study suggests that the loss of E-cadherin function in the mammary gland is not sufficient to induce mammary tumorigenesis in mice.

Despite the lack of tumor formation in the *MMTV-Cre;CDH1flox* model, Derksen and Jonkers et al. (2006) developed the first transgenic mouse ILC model using a similar Cre-recombination based strategy[142]. However, they combined somatic inactivation of the tumor suppressor, p53 with the inactivation of E-cadherin, hypothesizing that the p53 inactivation would protect the cells with homozygous loss of E-cadherin from apoptosis-induced cell death leading to the formation of mouse ILC (mILC). The model they developed used a K14-driven Cre-recombinase (*K14Cre;CDH1flox;TRP53flox*). Using this model, the authors confirmed the results of the study described above from Boussadia and Kemler et al. (2002), such that *K14Cre;CDH1*$^{fl/fl}$ mice did not exhibit the formation of mammary gland tumors. As expected, the loss of p53 alone (*K14Cre;TRP53*$^{fl/fl}$*)* induced development of both non-metastatic skin and mammary tumors with a tumor latency of 330 days. Excitingly, the introduction of homozygous *CDH1* floxed alleles (*K14Cre;CDH1*$^{fl/fl}$*;TRP53*$^{fl/fl}$*)* to create the triple transgenic model resulted in significantly decreased tumor latency (214 days), increased metastatic capacity, and led to changes in tumor phenotype. Mammary tumors from this genotype were described as mILC due to their histological similarity with human ILC. The authors described the cells as large, discohesive spindle shaped cells with pleomorphic nuclei expressing epithelial markers, but unfortunately, the tumors did not express ER. Additionally, it is estimated that only 8% of ILC tumors harbor alterations in *TP53*, rendering this model potentially applicable for studying only a small subset of the disease.

In a second study, Derksen and Jonkers et al. (2011) developed a nearly genetically identical model of mILC, except they used the Wap promoter, rather than the K14 promoter. The authors indicate that the main benefit to switching the promoter was to circumvent the high number

of skin tumors produced by driving tumorigenesis on the K14 non-specific epithelial promoter[161]. The Wap (whey acidic protein) promoter is expressed in the luminal compartment of the mammary gland and while the promoter is most highly active during lactation, low basal activation occurs. Consistent with the previously published data, *WapCre;CDH1*$^{fl/fl}$ female mice did not develop mammary tumors, despite multiple rounds of pregnancy, and *WapCre;CDH1*$^{fl/fl}$*;TRP53*$^{fl/fl}$ mice developed ER-negative mILC tumors with pleomorphic features with a median latency of 194 days. Interestingly, inducing lactation did not affect tumor onset, latency, or metastatic formation in *WapCre;CDH1*$^{fl/fl}$*;TRP53*$^{fl/fl}$ mice, indicating that the basal activity of the Wap promoter was sufficient to induce mILC tumor formation.

In 2016, Boelens and Jonkers et al. published a novel strategy to develop a mILC transgenic model, following the comprehensive profiling of ILC in The Cancer Genome Atlas (TCGA)[15]. TCGA data suggest that at least 13% of ILC tumors harbor alterations in *PTEN* resulting in enhanced PI3K/Akt signaling activation. However, an additional 48% of tumors harbor activating alterations in *PIK3CA* also resulting in hyperactivation of the PI3K/Akt pathway. Therefore, the development of a novel mILC model to mimic PI3K/Akt activation as a tumor driver would potentially represent as many as 61% of total ILC cases. To do this, the authors followed a similar strategy as used by Derksen and Jonkers et al. (2011), except they replaced somatic inactivation of *TRP53* with inactivation of *PTEN*[163]. This resulted in a *WapCre;CDH1*$^{fl/fl}$*;PTEN*$^{fl/fl}$ mouse that developed mILC with a tumor latency of 109 days. Consistent with previous findings, the authors note that *WapCre;CDH1*$^{fl/fl}$ mammary gland display enhanced apoptotic activity, reinforcing the idea that somatic inactivation of E-cadherin alone is not sufficient to induce tumor formation. However, they do disclose that these mice develop hyperplastic and dysplastic ducts filled with discohesive cells by 6 weeks of age, a phenotype not previously reported, prior to the gland

undergoing apoptosis. Importantly, the mILC tumors that develop in the *WapCre;CDH1*$^{fl/fl}$*;PTEN*$^{fl/fl}$ mice express ER in 26% of tumor cells, a marked improvement from the ER-negative p53 model previously developed. However, to our knowledge the functionality of ER in this model has yet to be assessed. A summary of the mILC transgenic models of note are found in Figure 16.

Due to the lack of comprehensive mILC transgenic models, including models of ER+ disease, we sought to develop a novel model of ER+ mILC using the data we generated indicating hyperactivation of the IGF1-IGF1R pathway in ILC. The IGF1 transgenic mice (*BK5.IGF1*) constitutively overexpress IGF1 driven by the myoepithelial K5 promoter leading to numerous phenotypes including the development of skin and mammary tumors via paracrine IGF1-IGF1R signaling[78,79]. While mammary tumor formation is enhanced with DMBA treatment, BK5.IGF1 female mice develop ER+ mammary tumors with an incidence of 31% by 55 weeks of age without treatment[78]. Aside from tumor formation, the BK5.IGF1 transgenic pups are often small, weak and developmentally delayed compared to wild-type pups. Their phenotype includes, scruffy skin, and acromegalic features, such as: enlarged paws, snout, and ears. Therefore, we are currently developing a model that mimics the breeding schemes of the previously above-described transgenic models, but using overexpression of IGF1 in combination with WapCre-driven somatic inactivation of E-cadherin to induce tumor formation.

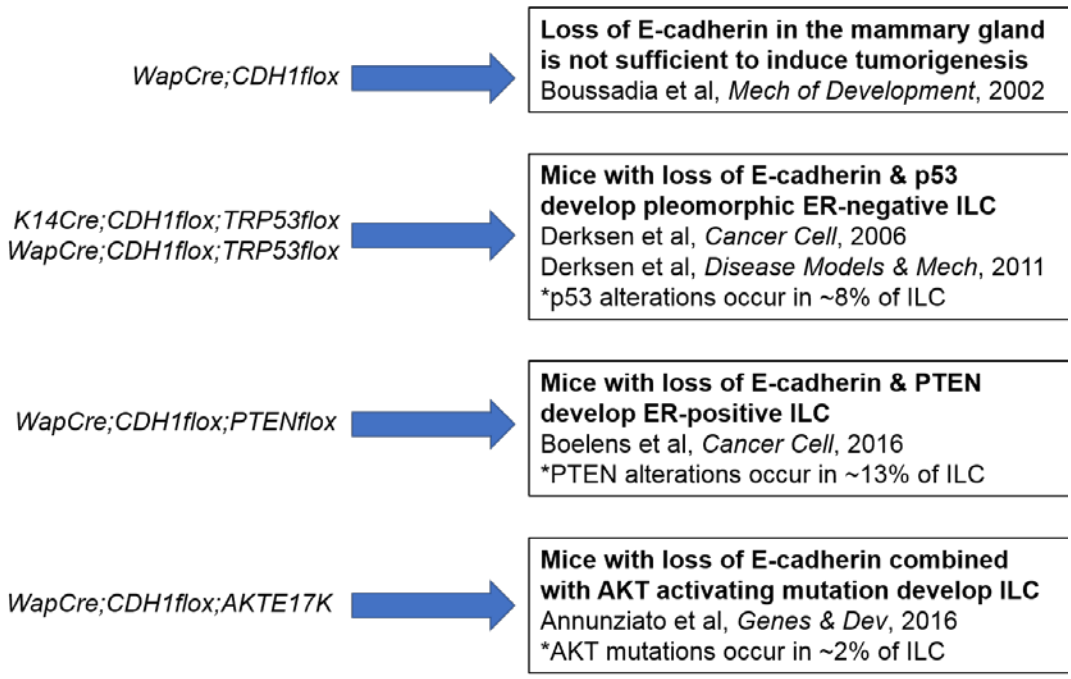

Figure 16: Summary of currently available mILC transgenic models.
Descriptions include genetic background of transgenic mice, type of mILC formed, reference to primary publication, and frequency of alteration as found in human ILC.

5.2 MATERIALS AND METHODS

5.2.1 Development of *WapCre;CDH1flox* transgenic mouse line

We ordered the *WapCre* mouse[165] from the NCI Mouse Repository (strain #01XA8). There is no cost associated with obtaining mice from the NCI Mouse Repository, however this process was quite lengthy because the stain was cryoarchived and required recovery prior to shipment. We received 1 female and 2 male B6.Cg-Tg(WAP-Cre)11738M mice and 1 male and 2 female C57BL/6NCr (wild-type) mice on 8/25/2015. The breeders that were sent to our animal facility were contaminated with MNV (mouse norovirus) and therefore pups generated between a wild-type/transgenic breeding pair needed to be cross-fostered. Following cross-fostering and quarantine, the colony was expanded and maintained as a hemizygous colony. All *WapCre*

transgenic colonies are maintained with hemizygous *WapCre* expression because it is not possible to determine hemi- from homozygous positive mice based on genotyping. The mice were tail snipped and ear tagged at the time of weaning for genotyping. The following primer set was used to verify *WapCre* expression: forward 5' TAG AGC TGT GCC AGC CTC TTC and reverse 5' CAT CAC TCG TTG CAT CGA CC. This primer set is labeled as "WAP". Detailed information on the protocol used for genotyping, including PCR settings, can be found at the NCI Mouse Repository webpage. The *WapCre* PCR product appears as a 210bp band on a DNA gel following PCR.

We ordered the *CDH1flox* transgenic mouse (B6.129-Cdh1^{tm2Kem}/J) from Jackson Laboratories (Stock #005319). These mice were additionally cryoarchived and required recovery prior to shipment. We received heterozygous *CDH1flox* mice from Jackson Labs. The colony was expanded and mice were tail snipped and ear tagged at weaning for genotyping. The following primer set was used to determine *CDH1flox* allele status: forward 5' GGG TCT CAC CGT AGT CCT CA and reverse 5' GAT CTT TGG GAG AGC AGT CG. This primer set is labeled as "IMR". Detailed information on the genotyping protocol used, including PCR settings, can be found at the Jackson Labs webpage. The *CDH1wt* allele PCR product appears as a 243bp band and the *CDH1fl* allele product appears as a 310bp band on a DNA gel following PCR.

To create the *WapCre;CDH1*$^{wt/fl}$ mouse needed for our studies, we crossed (cross #1) the *WapCre* mouse with the *CDH1*$^{wt/fl}$ mouse (Figure 17). This mouse was on the C57BL/6 background. Following the creation of the double transgenic mouse (*WapCre;CDH1*$^{wt/fl}$), we backcrossed the C57BL/6 transgenic mouse three generations into a FVB/N background using mice purchased from Taconic. This was necessary due to the low penetrance of mammary tumors in C57BL/6 mice; FVB/N are known to have higher mammary tumor penetration in transgenic

models induced by multiple oncogenes[166,167]. Three backcrosses into FVB/N resulted in the "3rd backcross (bc) FVB" *WapCre;CDH1*$^{wt/fl}$ transgenic line that was 87.5% FVB/N and 12.5% C57BL/6. These mice were genotyped using the primers described above. This work was initiated by Dr. Tiffany Katz, a postdoctoral fellow in Dr. Steffi Oesterreich's laboratory in 2015.

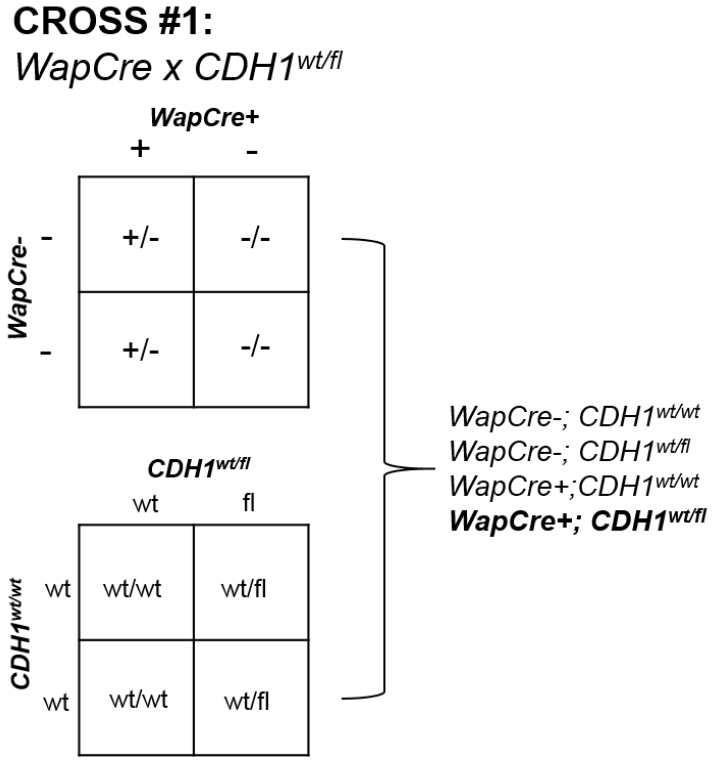

Figure 17: Genetic cross (cross #1) required to produce *WapCre;CDH1flox* double transgenic strain. Depiction of the Mendelian genetics (Punnett squares) associated with the cross between *WapCre x CDH1*$^{wt/fl}$ mouse lines to produce the *WapCre;CDH1*$^{wt/fl}$ strain. The genotype of interest is highlighted in bold; additional genotypes not highlighted were euthanized.

5.2.2 *BK5.IGF1* transgenic mice

We imported the BK5.IGF1 transgenic mouse line as a collaboration with Dr. Robin Fuchs-Young, an investigator at Texas A&M (originally developed by DiGiovanni and Kiguchi et al. (2000)[79]).

These mice do not to be genotyped due to the evident phenotype as described above. Additionally, they have the capacity to lose heat due to expression of the IGF1 transgene constitutively in their skin, and the MWRI veterinarian, Dr. Sara Andux, also suggested that these mice may be hypersensitive the light. This line is typically maintained by breeding through the male. Although, female BK5.IGF1 mice can breed successfully, due to the phenotype, cycling in the female is irregular results in inefficient and unpredictable breeding. The only downfall to this strategy is that only approximately 50% of male BK5.IGF1 mice are able/willing to mate. Additionally, the breeding life of these mice is considerably shortened compared to a wild-type animal – approximately 6-8 months of reliable breeding. The colony is maintained as a hemizygous colony by breeding male *BK5.IGF1* mice with female outbred CD-1 mice ordered from Envigo.

5.2.3 Breeding scheme for development of IGF1-driven mILC model

WapCre;CDH1$^{wt/fl}$ (3rd backcross FVB/N) female mice were crossed with male *BK5.IGF1* mice (cross #2; Fig 18). This mating resulted in 8 genotypes of mice with a combination of one of each of the three transgenes: 1) *WapCre- or WapCre+,* 2) *CDH1*$^{wt/wt}$, or *CDH1*$^{wt/fl}$*, and 3) IGF1- or IGF1+*.

We then bred female *WapCre;CDH1*$^{wt/fl}$*;IGF1-* and male *WapCre;CDH1*$^{wt/fl}$*;IGF1+* mice obtained from cross #2 to produce the "IGF1-ILC" tumorigenesis study cohort (cross #3; Figure 19). All other unused pups from cross #2 were euthanized. This mating resulted in 12 genotypes of mice with a combination of one of each of the three transgenes: 1) *WapCre- or WapCre+,* 2) *CDH1*$^{wt/wt}$, *CDH1*$^{wt/fl}$*, or CDH1*$^{fl/fl}$*, and 3) IGF1- or IGF1+*. All male and *WapCre-* pups were euthanized from cross #3. Once the females in this cohort reach(ed) breeding age, they are mated for one cycle of pregnancy to induce maximal Wap promoter expression. Nursing of pups occurs for 5-8 days, and

then pups are euthanized to initiate mammary gland involution. Females in the cohort that do not become pregnant are indicated, such that potential differences in tumor formation or latency can be monitored. Julie Scott and Beth Knapick assisted with colony maintenance, cage weaning, and weekly palpation. Scientific management of the IGF1-ILC mILC project will be transitioned to Dr. Jennifer (Atkinson) Xavier (Lee Lab).

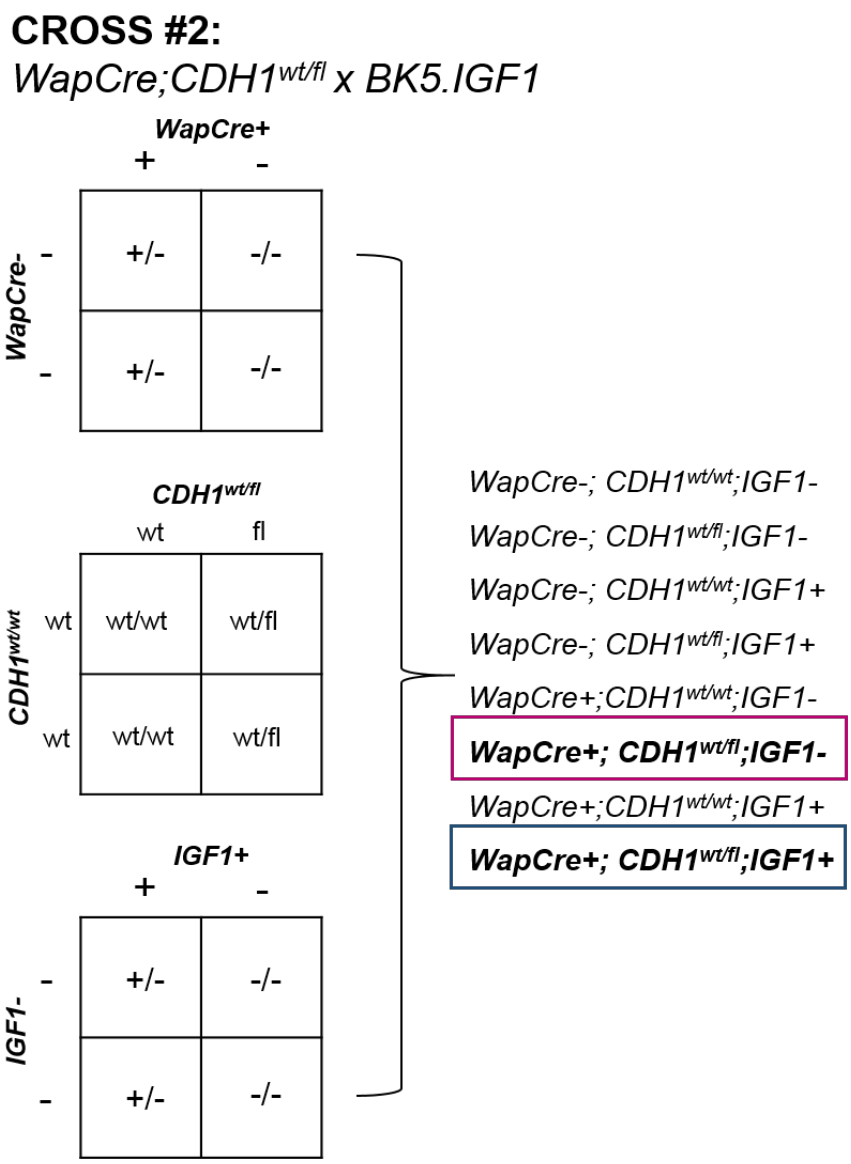

Figure 18: Genetic cross (cross #2) required to produce WapCre;CHD1flox;IGF1 triple transgenic mouse strain.
Depiction of the Mendelian genetics (Punnett squares) associated with the cross between *WapCre;CDH1$^{wt/fl}$* (female) x BK5.IGF1 (male) mouse lines to produce the triple transgenic *WapCre;CDH1$^{wt/fl}$;IGF1*. The genotypes of interest are highlighted in bold (pink=female, blue=male); additional genotypes not highlighted were euthanized.

CROSS #3:

WapCre;CDH1$^{wt/fl}$;BK5.IGF1- x *WapCre;CDH1$^{wt/fl}$;BK5.IGF1+*

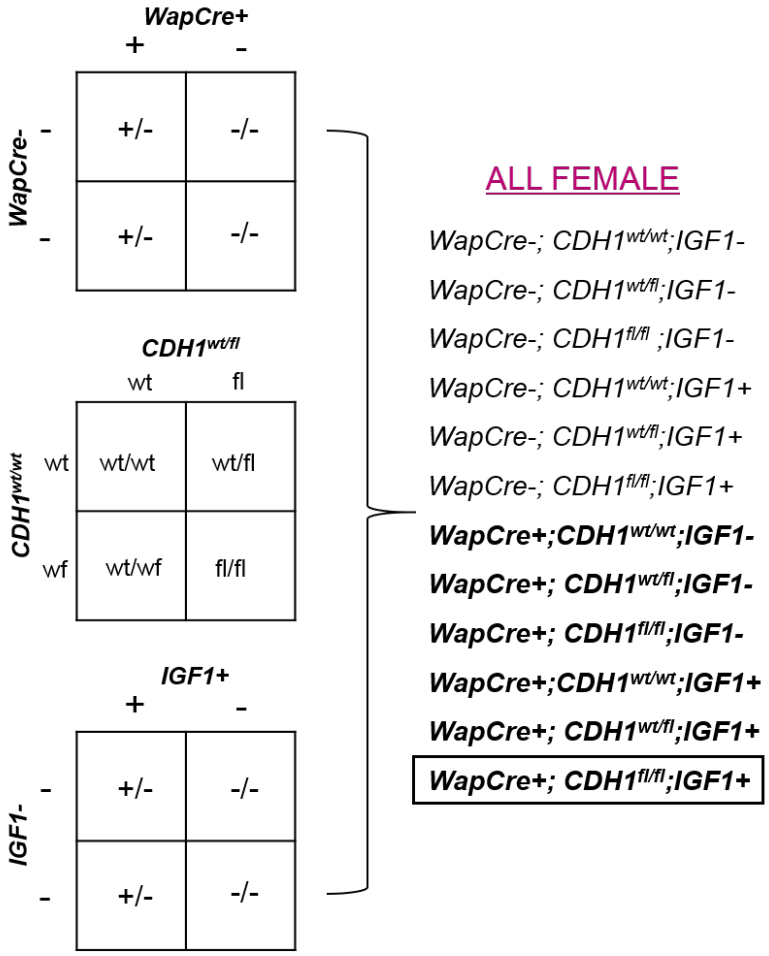

Figure 19: Genetic cross (cross #3) required to produce the cohort of female mice for the IGF1-ILC tumorigenesis study.

Depiction of the Mendelian genetics (Punnett squares) associated with the cross between *WapCre;CDH1$^{wt/fl}$;IGF1-* (female; pink) x *WapCre;CDH1$^{wt/fl}$;IGF1+* (male; blue) mouse lines to produce the triple transgenic female pups for the mILC tumorigenesis study . The genotypes of interest are highlighted in bold; all male pups and additional genotypes not highlighted were euthanized.

5.3 RESULTS

We anticipate that female mice of the *WapCre;CDH1$^{fl/fl}$;IGF1+* genotype may potentially develop mILC due to the somatic inactivation of E-cadherin combined with activation of the oncogenic IGF1-IGF1R pathway. We anticipate the tumors to be ER+ because the mammary gland tumors formed in the BK5.IGF1 transgenic females are ER+[78]. To date, we have not observed tumor formation, likely because the cohort has not reached optimal age (oldest female in cohort born 9/29/2017). Table 2 describes the total number of female mice in the IGF1-ILC tumor cohort to date (current as of 03/01/2018) per each of the six genotypes. We are continuing to breed (cross #3 repeated) to expand this cohort. Mice are currently monitored for tumor formation by palpation once per week.

Table 2: Summary table outlining current number of female mice of each genotype in the IGF1-ILC tumorigenesis cohort.
In bold (*WapCre;CDH1$^{fl/fl}$;IGF1+)* is the genotype we anticipate may develop mILC. Number of animals is updated as of 03/01/2018. To date no tumor development has occurred.

	IGF1-	*IGF1+*
CDH1$^{wt/wt}$	10	8
CDH1$^{wt/wt}$	21	12
CDH1$^{wt/wt}$	7	**13**

5.4 DISCUSSION

Due to the lack of ER+ mILC transgenic models, the development of novel mILC model would benefit the ILC research community in total. Importantly, this would be the first mILC transgenic model to use growth factor activation of oncogenic signaling in combination with somatic inactivation of E-cadherin to drive tumor formation. The ability of IGF1 to induce ILC tumor initiation and progression would indicate the importance of the IGF1-IGF1R signaling pathway in this disease. This would shed light on a possible mechanism of ILC development, providing insight on novel targets and therapeutic strategies. Additionally, because the increased IGF1 mRNA in the model mimics the increased mRNA levels observed in ILC from TCGA (discussed in Chapter 4), this would validate our research findings that the loss of E-cadherin enhances IGF1R activity and that the IGF1-IGF1R signaling axis is hyperactivated in human ILC.

This model could be used to understand the potential for use of IGF1R inhibitors in the treatment of ILC. New strategies of inhibiting the IGF1-IGF1R axis are currently in progress. One such strategy in development is the use of an IGF1/2 ligand neutralizing antibody (BI 836845, Boehringer Ingelheim) to prevent IGF1/2 ligand binding to activate the IGF1R and downstream signaling[105,106]. BI 836845 is a fully humanized antibody that has high affinity IGF1/2. In preclinical studies, this drug has been shown to reduce phosphorylation of IGF1R and inhibit cancer cell proliferation. *In vivo*, BI 836845 treatment induces high levels of serum inactive IGF1 and elevated growth hormone (GH) levels. Elevated GH levels indicate an endocrine site of action for the compound, and therefore, our model (if successful) would be useful to assess the capacity of the antibody to inhibit signaling induced by paracrine IGF1 in mammary tumors. We have a signed MTA with Boehringer Ingelheim, and anticipate being able to complete a study to address

this question. To our knowledge, this has not yet been tested and the site(s) of mechanism of action of the neutralizing antibody, BI 836845, are not comprehensively understood.

6.0 CONCLUSIONS

IGF1R signaling acts as a major mediator for normal mammary gland development and the progression to breast cancer. Pre-clinical evidence suggests that IGF1R activity drives malignant transformation in mammary epithelial cells and induces tumor growth and metastasis in murine models[34,52,64,81]. However, despite the vast amount of *in vitro* and *in vivo* evidence suggesting that targeting IGF1R in breast cancer would be a clinically beneficial therapeutic option, the results of clinical trials thus far using anti-IGF1R therapeutics have been largely unsuccessful[33,35]. This is thought to be mainly due to the lack of predictive biomarkers or criteria for beneficial response to therapy, and therefore, patients were not selected in a meaningful manner—often without confirmation that the tumor even expressed IGF1R. Additionally, due to IGF1R pathway crosstalk with insulin signaling, many therapeutics (e.g. receptor tyrosine kinase inhibitors) non-specifically inhibited InsR inducing metabolic syndrome in patients leading to dose limiting toxicities[35]. Recently, however, an innovative class of anti-IGF1R therapy, IGF1/2 ligand binding antibody, have been initiated in pre-clinical studies and clinical trials in breast cancer. This therapeutic strategy inhibits IGF1/2 ligand binding to IGF1R to inhibit oncogenic signaling and importantly, seems to exhibit reduced side effects compared to previously used IGF1R/InsR tyrosine kinase inhibitors and anti-IGF1R monoclonal antibodies[35,105,106]. The advancement of the IGF1/2 ligand antibody, BI836845 (xentuzumab, Boehringer Ingelheim) into Phase 2 clinical trials presents a unique opportunity to develop biomarkers for response to anti-IGF1R therapy to optimize and refine the subsets of patients that would most highly benefit from treatment.

Along this thought process, our goal was to define novel proteomic biomarkers of IGF1 and insulin signaling. Using a large proteomic screen in a panel of twenty-one breast cancer cell lines stimulated with IGF1 and insulin we developed an innovative computational model to predict signaling mediators. Through this process we identified a list of candidate proteins, including E-cadherin (*CDH1*) and acetyl coA-carboxylase (*ACC1/2*), thought to regulate IGF1- and insulin-induced Akt and ERK signaling, respectively[124]. In Chapter 2 we provide *in vitro* validation of the computational predictions, and focus on the negative regulation of IGF1 signaling by E-cadherin. The predicted association between E-cadherin and IGF1 signaling was of interest due to the role of E-cadherin in epithelial to mesenchymal transition (EMT), thought to be a major regulator of cancer cell metastasis. Our lab and others have previously published studies describing the repression of E-cadherin by IGF1 signaling via activation of EMT programming. The reverse negative regulation of IGF1R by E-cadherin has been largely uncharacterized. This finding reveals a novel concept whereby the interaction between IGF1R and E-cadherin may be controlled by a feed forward loop—with the loss of E-cadherin activating IGF1R signaling via EMT programming, which further downregulates E-cadherin expression leading to cancer phenotypes (Figure 20).

Our studies, described in Chapter 3, indicate that the loss or functional inhibition of E-cadherin enhances IGF1R pathway activation and results in increased IGF1-induced cell cycle progression and proliferation. Due to this, E-cadherin knockdown cells showed increased sensitivity to anti-IGF1R treatments compared to control cells. We additionally found that E-cadherin directly regulates IGF1R, as the two proteins were found in complex endogenously by proximity ligation assay in breast cancer cells and co-localize at the adherens junction. This suggests that IGF1R is recruited to points of cell-cell contacts by E-cadherin as a method of

growth factor signaling repression, similar to a mechanism of repression described for EGFR[129,130,146]. In summary, this data suggests that IGF1R has an increased signaling capacity when E-cadherin expression is diminished. Future studies will focus on fully understanding the mechanism of IGF1R signaling repression by E-cadherin, including i) determining whether a repressive signaling hub, containing negative regulators of IGF1R, is formed upon IGF1R association with E-cadherin, ii) determining whether there is a shift in the binding kinetics of IGF1 ligand to IGF1R in the presence or absence of E-cadherin, and iii) determining the specific domains of E-cadherin that are responsible for mediating IGF1R signaling (e.g. extracellular domain or p120 binding domain).

Importantly, a histological subtype of breast cancer termed invasive lobular carcinoma (ILC) displays loss of function E-cadherin protein in approximately 95% of total cases[14,15]. We hypothesized that this subtype may display hyperactive IGF1R signaling and investigated this association in Chapter 4. Because 90% of ILC tumors are ER+, we focused on this molecular subtype during our analyses[15]. Using gene expression and proteomic data from The Cancer Genome Atlas (TCGA) we determined that both IGF1 ligand mRNA expression and pIGF1R levels were enhanced in estrogen receptor-positive (ER+) ILC tumors compared to invasive ductal carcinoma (IDC) tumors, parallel with a significant decrease in CDH1 mRNA expression. This is similar to work published by Nakagawa et al. and Bertucci at al. that demonstrated increased IGF1 ligand expression in ILC compared to IDC tumors[20,156]. Further, we determined that ILC cell lines displayed increased IGF1-induced IGF1R phosphorylation compared to the IDC cell line, MCF-7, classically referred to as the most highly IGF1 responsive breast cancer cell line. IGF1 is typically produced in the stroma by fibroblasts and immune cells, and a recent study by Ireland and colleagues demonstrated high expression of IGF1/2 secreted from tumor-

associated macrophages[30,31,53–55]—a significant point because ILC cells are surrounded by increased levels of stroma compared to IDC, rendering increased IGF1 ligand availability in this tumor type[14,156]. The availability of ligand in the stromal compartment may specifically contribute to the hyperactivation of IGF1R in ILC in contrast to activation of other receptor tyrosine kinases, such as EGFR, where the EGF ligand is not overexpressed (data not shown [TCGA]).

Further, we showed that ER+ ILC cell lines and xenografts are sensitive to IGF1R inhibition, and in combination with endocrine therapy show synergistic inhibition of cell viability. Therefore, our data suggest that targeting IGF1R may be appropriate in this setting due to the hyperactivity of the IGF1-IGF1R pathway and ability to couple to existing endocrine therapy. This is a striking and clinically relevant finding because although ILC tumors are treated with endocrine therapy, patients with this disease suffer increased incidence of endocrine therapy resistance and more late recurrences compared to IDC, as demonstrated by multiple clinical studies[19,22–24]. Therefore, there exists a unique challenge and opportunity to uncover novel therapeutic targets for ILC based on pathways that are specifically activated. However, one caveat that requires further study is understanding the efficacy of IGF1R inhibition in ILC tumors harboring mutations in *PIK3CA* or *PTEN* downstream of IGF1R that result in hyperactive Akt activity—these alterations are quite frequent in this subtype of breast cancer (61%)[15]. Therefore, we investigated the combination of a small molecule PI3K/mTOR inhibitor with endocrine therapy in ER+ ILC cells, and also observed a synergistic inhibition of cell viability. This approach may potentially serve as an alternative to targeted IGF1R therapy in tumors harboring *PIK3CA/PTEN* alterations to inhibit this mutation-induced pathway activation more directly. There may also be a benefit in combining PI3K targeted therapy in combination with

anti-IGF1R therapy in tumors harboring *PIK3CA* mutations. Recent data from Cantley and colleagues suggest that elevated levels of insulin may provide a mechanism of resistance to tumors harboring *PIK3CA* that are treated with PI3K targeted therapy[158]. Because the insulin and IGF1 signaling pathways are highly homologous, it is possible that IGF1 plays a similar role as a resistance mechanism. Future studies will serve to elucidate these interactions using *in vivo* and *ex vivo* drug screening to assess the combinations of IGF1R, PI3K, mTOR, and ER targeted therapy in ILC tumors of various genetic backgrounds (e.g. *PIK3CA* mutant, *PTEN* null, wild-type).

Overall, our data suggest that the loss of E-cadherin may be used a biomarker for IGF1R activity and therefore, a predictor for response to anti-IGF1R therapy. The loss of E-cadherin in ILC is genetic, however, other tumor types, such triple negative breast cancers that have undergone EMT, have an epigenetic and/or transcriptional downregulation of E-cadherin—and similar to data published by our lab, the basal and mesenchymal subtypes of TNBC are thought to be in part driven by IGF1-IGF1R signaling[87,112,168]. We hypothesize these tumors may also be susceptible to anti-IGF1R therapy. We will test this in future studies with similar methodology as described for ILC tumors, however, combining IGF1R pathway inhibitors with standard of care chemotherapy in TNBC with low E-cadherin expression. In addition, a number of studies have previously investigated and provided evidence for predictive biomarkers for IGF1R targeted therapy—including increased levels of circulating IGF1, and expression of IGF1R, IRS1/2, and IGFBP3[107,109,169,170]. The results from these studies highlight the importance of determining whether the IGF1-IGF1R pathway is active when treating with anti-IGF1R therapy and therefore, these factors would also need to be assessed in tumors with loss of E-cadherin to ensure the treatment would be useful. In conclusion, the data presented in this dissertation

indicate that the loss of E-cadherin induces IGF1R pathway hyperactivation, and therefore, E-cadherin deficient breast tumors such as ILC may be susceptible to anti-IGF1R therapy.

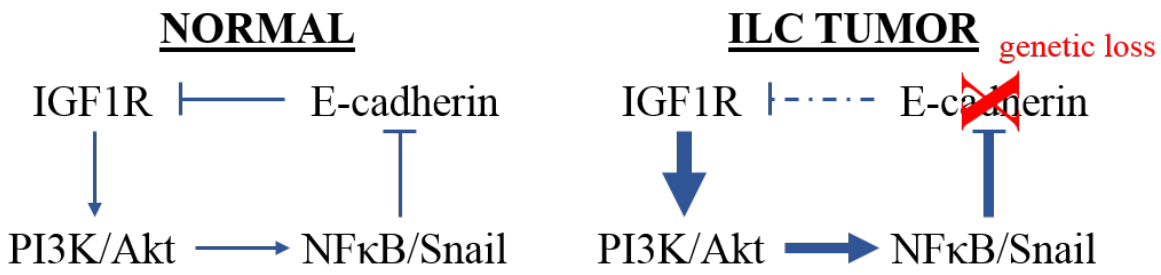

Figure 20: Schematic for IGF1R/E-cadherin bi-directional signaling repression in normal mammary gland and dysregulation in ILC tumors.
A simplified schematic depicting the bi-directional repression of E-cadherin and IGF1R in the normal mammary gland and the loss of repression in ILC tumors. A similar repression likely occurs in TNBC with low E-cadherin levels via epigenetic or transcriptional repression, rather than genetic loss as in ILC.

APPENDIX A

EVALUATING THE ACTIVITY OF THE GH-GHR AXIS IN BREAST CANCER

A.1 INTRODUCTION

Growth hormone (GH)-mediated signaling begins at an endocrine level with growth hormone releasing hormone secretion from the hypothalamus, which subsequently induces the release of GH from the anterior pituitary gland. GH stimulates production of insulin-like growth factor-1 (IGF1) by the liver to regulate normal growth[171]. GH binds the homodimerized growth hormone receptor (GHR), a membrane spanning receptor belonging to the cytokine Type I receptor family, to induce a conformational change that allows for the phosphorylation of the tyrosine kinases JAK2 and c-SRC. This leads to activation of downstream signaling through the JAK/STAT and PI3K/Akt pathways[172,173].

The GH/IGF1 axis is a major regulator of body growth and longevity, likely in part due to its regulation of multiple stem cell lineages[29,171,174,175]. Deregulation of the GH/IGF1 axis has been implicated in breast cancer, in part by contributing to the proliferation and expansion of cancer stem cells[174,176]. Strikingly, spontaneous dwarf rats that lack GH are completely refractory to carcinogen-induced mammary cancer, and supplementation with GH restores tumor development[177,178]. Similarly, by blocking GHR function with the antagonist, pegvisomant (FDA approved for the treatment of acromegaly), we demonstrated effective growth inhibition of

MCF-7 xenograft tumors[179]. Conversely, overexpression of GH transforms mammary epithelial cells and increases proliferation of breast cancer cells[180–182].

While GH acts in an endocrine manner, it is also secreted locally by breast cancer cells in an autocrine and paracrine fashion, promoting proliferation, migration and invasion, epithelial to mesenchymal transition, expansion of the progenitor population, and resistance to radiation therapy[176,181–185]. Lombardi and colleagues showed that GH regulates mammary stem cell number and function, and that GH is increased in early breast premalignant lesions[176]. It is possible that GH is a critical regulator of cancer stem cells or tumor initiating cells driving tumor formation or recurrence following treatment[176,184]. We hypothesize that breast tumors may have a population of cells with hyperactivity of the GH-GHR signaling pathway and therefore, may be effectively targeted by inhibiting GHR action.

A.2 MATERIALS AND METHODS

A.2.1 Cell culture

All cell lines were acquired from ATCC and cultured in the indicated media conditions: T47D (RPMI+10% FBS), MDA-MB-453 (MM453; DMEM+10% FBS), MDA-MB-415 (MM415; DMEM+10% FBS), HCC1806 (RPMI+10% FBS), HCC1954 (RPMI+10% FBS), BT549 (RPMI+10% FBS), and MCF10A (DMEM/F12+5% horse serum supplemented with 10ug/ml insulin, 20ng/ml EGF, 0.1ug/ml cholera toxin, and 2.5ug/ml hydrocortisone).

A.2.2 Growth factor (hGH/IGF1) stimulation and treatment with GHR blocking antibody

T47D cells were plated and then serum-starved overnight. As indicated, cells were stimulated with vehicle (10mM HCl), 100ng/ml or 1ug/ml human growth hormone (hGH; Sigma #H5916) and 50ng/ml IGF1 (GroPep BioReagents #CU100) to assess signaling (45 min) or viability (6 or 8 days). For signaling experiments assessing the effect of GHR blocking antibody, serum-starved T47D cells were treated with 100ng/ml hGH in combination with 1ug/ml GHR blocking antibody (R&D Systems #AF1210) for 1 or 4 hours.

A.2.3 Immunoblotting

Samples for immunoblot analysis were collected using RIPA buffer (50mM Tris pH 7.4, 150mM NaCl, 1mM EDTA, 0.5% Nonidet P-40, 0.5% NaDeoxycholate, 0.1% SDS) supplemented with 1x HALT protease and phosphatase cocktail (Thermo Fisher #78442), probe sonicated for 15 seconds (20% amplitude), and centrifuged at 14,000rpm at 4˚C for 12 minutes. Protein concentration was assessed using BCA assay (Thermo Fisher #23225) and 50ug of protein per sample was run on 12% SDS-PAGE gel then transferred to PVDF membrane. Membranes were blocked for 1 hour using Odyssey PBS Blocking Buffer (LiCor #927-40000) then probed using the following primary antibodies and concentrations: GHR (EMD Millipore #ABC444; 1:500), pSTAT5 (Y694, Cell Signaling #9350; 1:500), pSTAT3 (Y705, Cell Signaling #9145; 1:500), STAT5A/B (Cell Signaling #9363; 1:500), STAT3 (Cell Signaling #4904; 1:500), and β-actin (Sigma #A5441; 1:5000). Membranes were then washed in TBST, incubated in LiCor secondary antibody (1:10,000) for 1 hour (anti-rabbit 800CW [LiCor #926-32211]; anti-mouse 680LT [LiCor #925-68020]), then imaged using the Odyssey Infrared Imager.

A.2.4 Transient siRNA knockdown

Cells were reverse transfected into 96-well (2D adherent) plates with 50nM final concentration of ON-TARGETplus non-targeting control pool siRNA (Dharmacon #D-001810) or ON-TARGETplus human GHR siRNA (Dharmacon #L-010402) using standard Lipofectamine RNAiMAX (Invitrogen #13778) protocol.

A.2.5 Viability assays

Following reverse transfection of SCR or GHR siRNA in 2D 96-well plates, cell viability was assessed on day 6 using the FluoReporter Blue Fluorometric DNA Quantitation Kit (Thermo Fisher #F2962) following the manufacturer's protocol. Statistical difference in Hoechst fluorescence in siSCR compared to siGHR cells in each cell line was evaluated using a two-tailed student's t-test ($p<0.05$). Following growth factor stimulation (hGH/IGF1) in ultra-low attachment suspension (ULA) 96-well plates, viability was assessed on days 6 and 8 using CellTiter Glo Viability assay (Promega #G7572) according to the manufacturer's protocol. Statistical difference in relative luminescence in experimental growth conditions on days 6 and 8 was evaluated using two-way ANOVA and Tukey's multiple comparison test ($p<0.05$).

A.3 RESULTS

A.3.1 Expression level of GHR varies in breast cancer cell lines and predicts response to GHR knockdown

To assess the levels of GHR expression in breast cancer, we probed a panel of cell lines (T47D, MM453, MM415, MCF10A, HCC1806, HCC1954, BT549) for GHR protein expression by immunoblot. The highest GHR expression was observed in MCF10A (normal mammary epithelial cell line) and HCC1954 cells, and the lowest expression in HCC1806 and BT549 cells. T47D, MM453, and MM415 cells expressed an intermediate level of GHR compared to the high and low expressing cell lines (Figure 21).

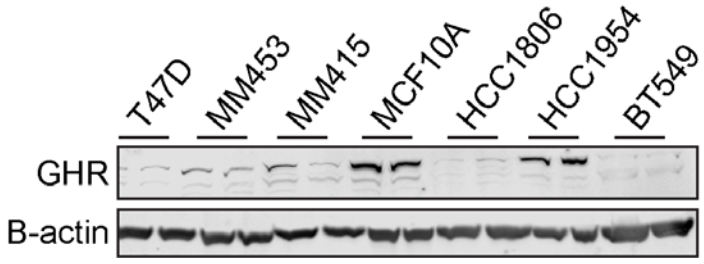

Figure 21: Growth hormone receptor (GHR) expression is variable among breast cancer cell lines. A panel of breast cancer cell lines ((T47D, MM453, MM415, MCF10A, HCC1806, HCC1954, BT549) was assessed by immunoblot for GHR expression.

Then, we silenced GHR in these cell lines using siRNA and assessed the effect on cell viability to determine if the level of GHR expression is predictive of response to GHR knockdown. There was significantly decreased viability in MCF10A ($p<0.0001$), T47D ($p<0.0001$), HCC1954

(p=0.0007), and MM415 (p=0.0404) cells (high to intermediate basal expression of GHR) following GHR knockdown (siGHR) as compared to control (siSCR) cells (Figure 22A-D).

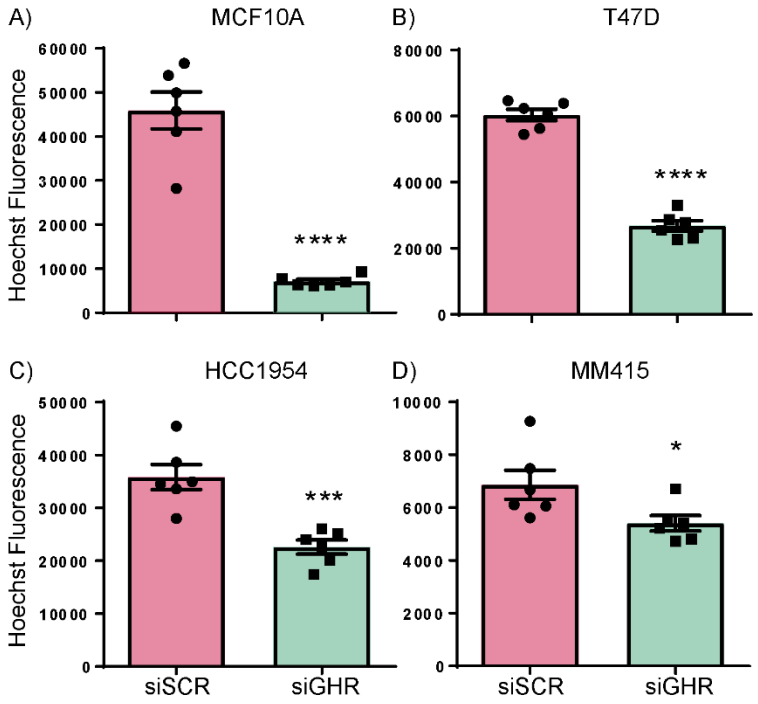

Figure 22: A subset of breast cancer cell lines are growth inhibited by GHR knockdown.
(A) MCF10A, (B) T47D, (C) HCC1954, and (D) MM415 cell lines were reverse transfected with control (siSCR) and GHR (siGHR) siRNA for 6 days. Viability was assed using FluoReporter Blue Fluorometric DNA Quantitation Kit following the manufacturer's protocol to measure DNA content. Statistical difference in Hoechst fluorescence in siSCR compared to siGHR cells in each cell line was evaluated using a two-tailed student's t-test ($p<0.05$*, $p<0.005$***, $p<0.001$****).

Conversely, there was no difference in viability between siGHR and siSCR cells in the MM453, HCC1806, and BT549 cell lines (low to intermediate basal expression of GHR [Figure 23A-C]). Knockdown was verified by qRT-PCR (data not shown). These results indicate that the protein expression level of GHR in breast cancer cells may be useful in predicting sensitivity to GHR knockdown or inhibition.

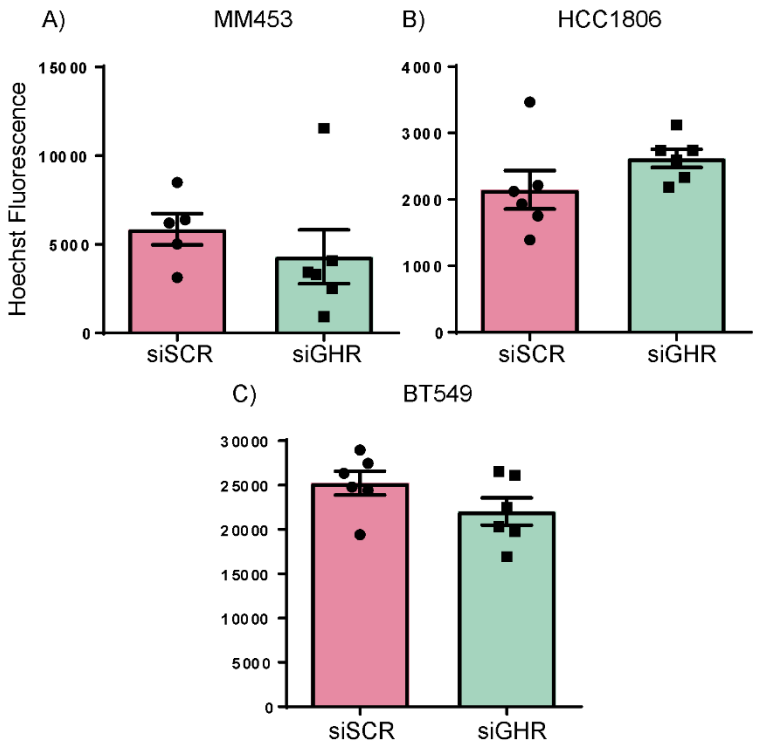

Figure 23: A subset of breast cancer cell lines are resistant to GHR knockdown.
(A) MM453, (B) HCC1806, and (C) BT549 cell lines were reverse transfected with control (siSCR) and GHR (siGHR) siRNA for 6 days. Viability was assed using FluoReporter Blue Fluorometric DNA Quantitation Kit following the manufacturer's protocol to measure DNA content. Statistical difference in Hoechst fluorescence in siSCR compared to siGHR cells in each cell line was evaluated using a two-tailed student's t-test ($p<0.05$). No significant difference was detected between siSCR and siGHR in these cell lines.

A.3.2 Growth hormone stimulation induces STAT3/5 activation that cannot be blocked by treatment with GHR blocking antibody

To understand signaling downstream of GHR and its effects on cell proliferation, we stimulated T47D cells with human growth hormone (hGH). T47D cells are known to be highly hGH responsive, supported by our data that knockdown of GHR reduces cell viability (Figure 22)[186,187]. Following serum-starvation, T47D cells were stimulated with 100ng/ml or 1ug/ml doses of hGH and phosphorylation of STAT5 and STAT3 was observed (Figure 24A). Interestingly, similar to previously published data, treatment with a GHR blocking antibody was

unable to inhibit hGH-induced STAT5 activation (Figure 24B)[186]. We then evaluated the effect of hGH stimulation on growth of T47D cells. Additionally, we combined hGH and IGF1 stimulation to determine if there was an additive effect on growth, since these growth factors are in the same signaling family. Following serum-starvation and growth factor simulation, we observed statistically significant increases in viability in cells stimulated with both hGH and hGH+IGF1 compared to VHC cells on days 6 and 8 ($p<0.0001$; Figure 24C).

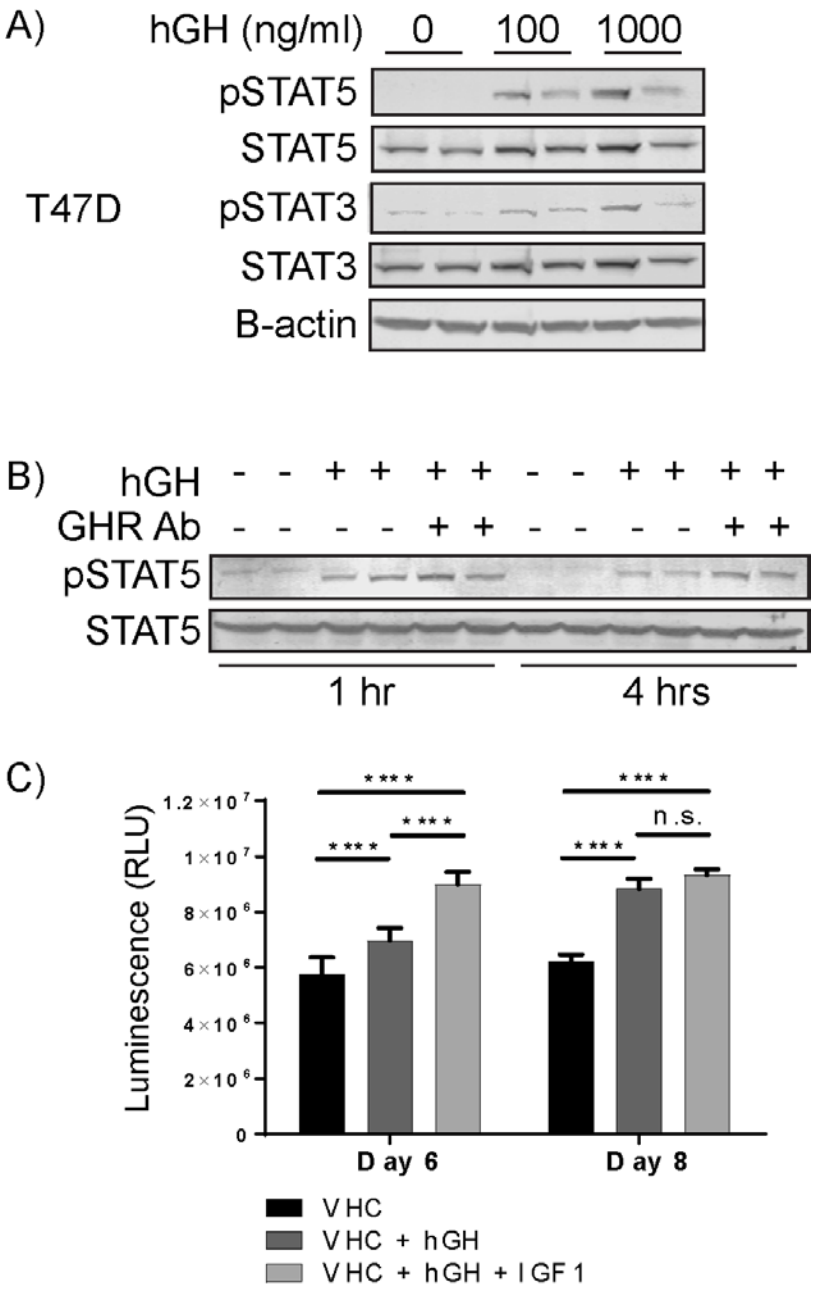

Figure 24: Growth hormone (hGH) stimulation induces JAK-STAT signaling and enhances viability of T47D cells.

(A) T47D cells were serum-starved overnight and stimulated with 100 or 1000ng/ml hGH for 45 minutes or (B) stimulated with 100ng/ml hGH -/+ 1ug/ml GHR neutralizing antibody for 1 or 4 hours. JAK-STAT signaling (pSTAT5 (Y694)/pSTAT3 (Y705)) was assessed by immunoblot. (C) T47D cells were serum-starved and plated into 96-well ULA plates and stimulated with either vehicle, 100ng/ml hGH, or hGH + 50ng/ml IGF1. Viability was assessed on days 6 and 8 using CellTiter Glo Viability assay. Statistical difference in RLU in growth conditions on days 6 and 8 was evaluated using two-way ANOVA and Tukey's multiple comparison test ($p<0.05$, $p<0.0001$****)

A.4 DISCUSSION

In addition to the role of endocrine GH in regulating normal body growth and longevity, autocrine GH via GHR has been implicated as a potential driver for breast cancer. We sought to understand the effect of GHR knockdown on breast cancer cell viability and determine whether GHR protein expression serves as a biomarker for response to knockdown. Our data indicate that the breast cancer cell lines with higher expression of GHR (e.g. HCC1954, MM415) showed greater inhibition in cell viability following GHR silencing as compared to the lower expressing cell lines (e.g. HCC1806, BT549). However, T47D cells were significantly growth inhibited by GHR knockdown despite their intermediate expression of GHR. Of note, MCF10A, an immortalized non-transformed mammary epithelial cell line, demonstrated high expression of GHR and significant sensitivity to GHR siRNA knockdown indicating that this may not be a cancer cell specific effect.

Because T47D cells were sensitive to GHR knockdown, and known to be hGH responsive, we stimulated these cells with hGH to determine effect on downstream signaling and cell viability. As expected, stimulation with hGH activated the STAT5 and STAT3 signaling pathways, and induced increased viability in serum-starved cells compared to control cells. Interestingly though, treatment with a GHR neutralizing antibody was unable to block STAT5 activation by hGH, similar to results published by Xu and colleagues[186]. Additionally, the authors showed heterodimerization of GHR and prolactin receptor (PRLR) in T47D cells, and further demonstrated that hGH preferentially activates PRLR to initiate downstream signaling through the JAK-STAT pathway (a pathway shared by both GHR and PRLR). Therefore, further studies are necessary to assess whether the growth induction observed in our experiment is due

to JAK-STAT signaling mainly via PRLR activation, or whether additional signaling pathways such as PI3K/Akt are activated downstream of GHR to drive this phenotype.

APPENDIX B

CHAPTER 3 SUPPLEMENTARY FIGURES

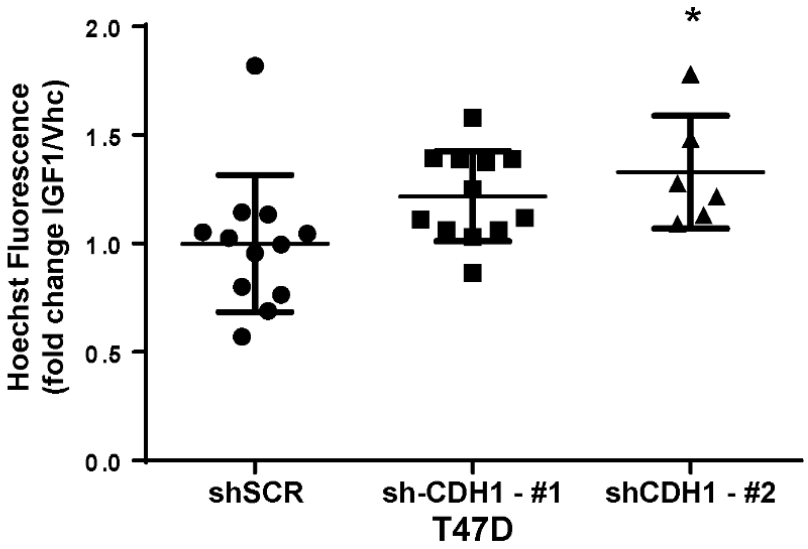

Figure 25: Knockdown of E-cadherin enhances IGF1-induced proliferation.
T47D shSCR and two clones of shCDH1 cells were plated in 96 well plates (9,000 cells per well) in serum-free media. Cells were treated with Vhc or 10nM IGF1 for 6 days and dsDNA content measured. Statistical difference in Hoechst fluorescence in IGF1 treated cells over vehicle control in each cell line was evaluated using a two-tailed student's t-test ($p<0.05$). One representative experiment shown; n=2 each with 6 biological replicates. Of note each shCDH1 clone displayed statistically significant increase in viability compared to control cells in 1 of 2 experiments, with other trending toward increased viability.

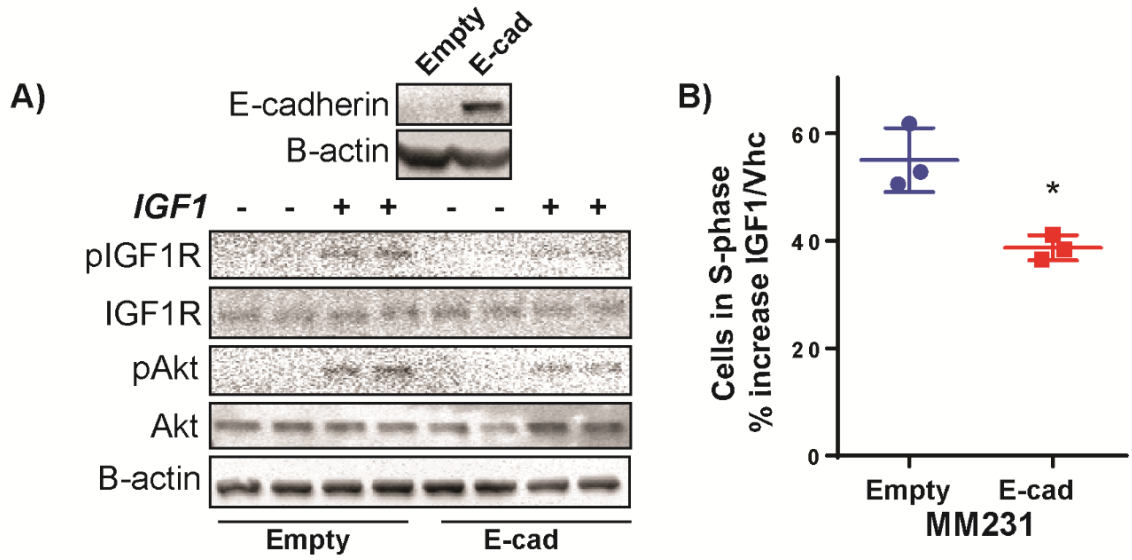

Figure 26: Overexpression of E-cadherin in MDA-MB-231 cells inhibits IGF1R mediated signaling, despite the lack of adherens junction formation.

(A-B) MDA-MB-231 (MM231) cells lacking detectable E-cadherin protein expression were stably transfected with empty of hE-cadherin-pcDNA3 vector. Cells were stimulated with Vhc or 10nM IGF1 for 10 min and IGF1R and Akt signaling assessed by immunoblot (shown in duplicate biological replicates). (C) Cells were serum-starved and stimulated with 10nM IGF1 for 17 hours and DNA stained with propidium iodide to measure cell cycle profile. The percent of cells in the IGF1/Vhc conditions in the S- and G2/M phases of the cell cycle for empty and hE-cad are shown (one independent experiment, n=3 biological replicates).

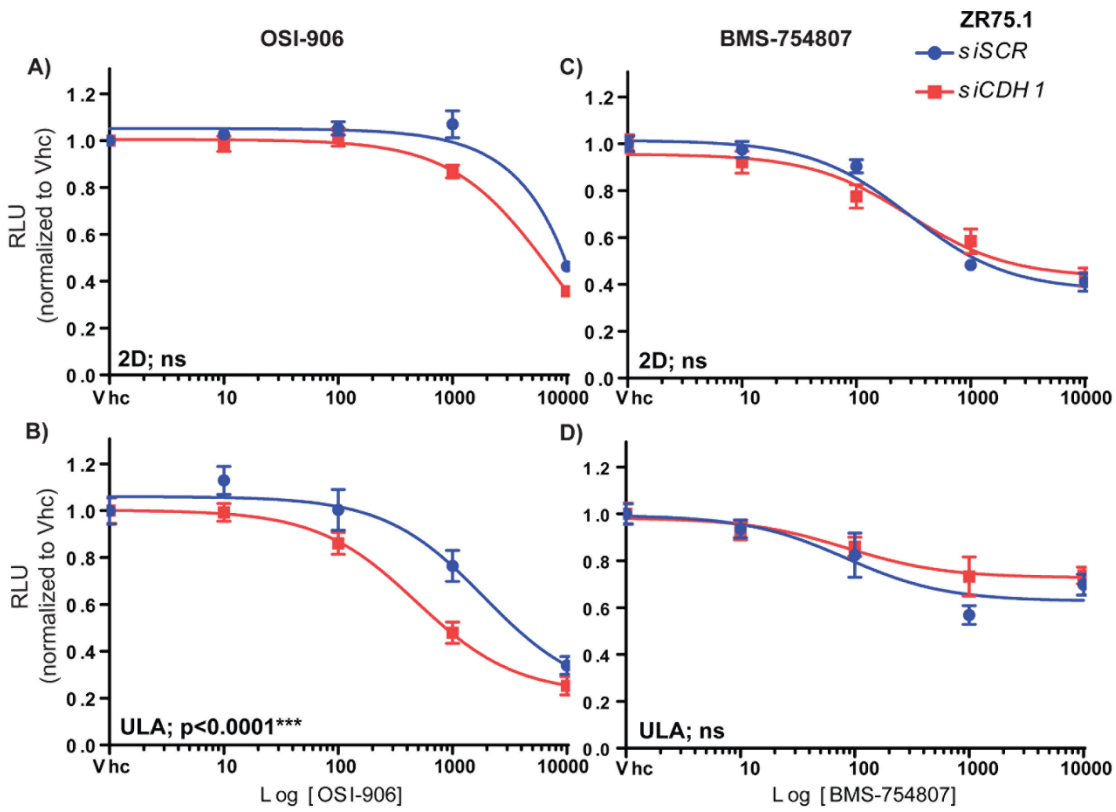

Figure 27: Knockdown of E-cadherin increases sensitivity to IGF1R inhibition in ZR75.1 cells grown in ULA.

ZR75.1 cells were reverse transfected with SCR or CDH1 siRNA and seeded into 96-well 2D or ULA plates and treated with IGF1R inhibitor (OSI-906 or BMS-754807) for 6 days. Conditions in the panels as follows: (A) OSI-906; 2D, (B) OSI-906; ULA, (C) BMS-754807; 2D, (D) BMS-754807; ULA. The CellTiter Glo assay was used to assess cell viability (relative luminescence). EC50 values for viability were calculated by non-linear regression and statistical differences evaluated using sum-of-squares Global f-test ($p<0.05$; representative experiment shown; n=3 each with 6 biological replicates).

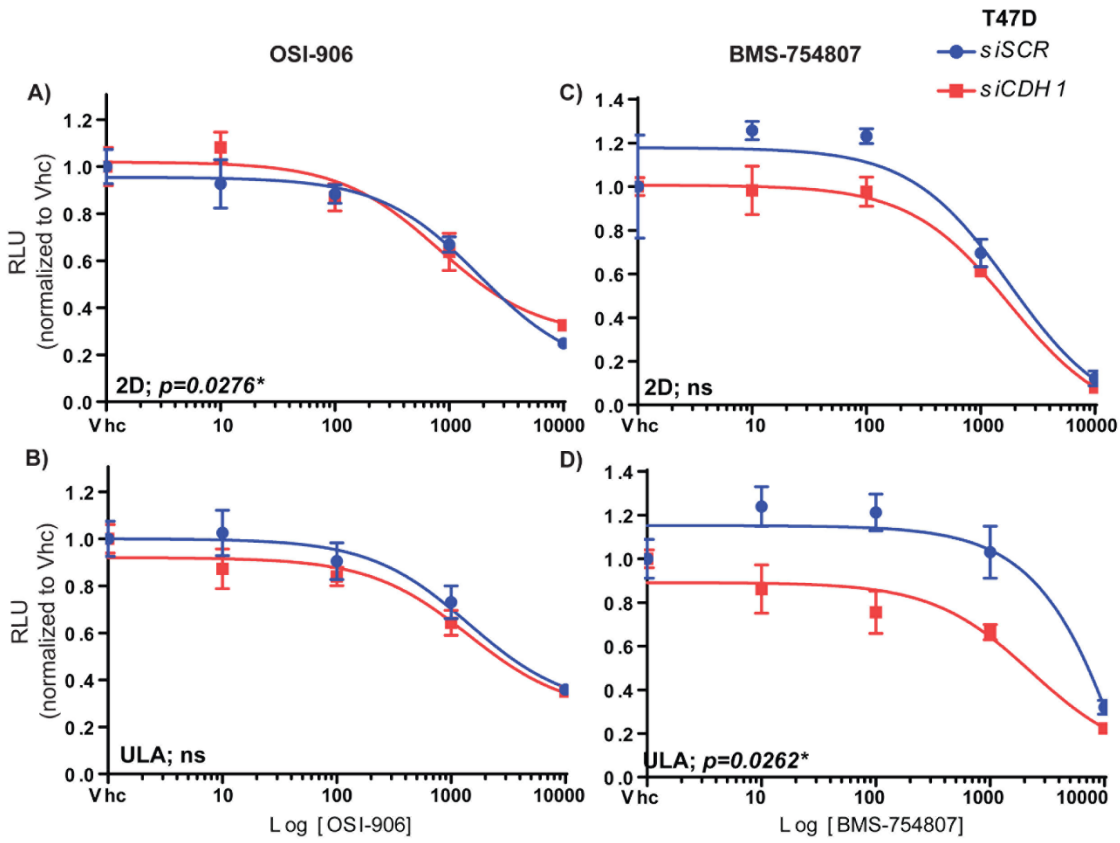

Figure 28: Loss of E-cadherin increases sensitivity to IGF1R inhibition in T47D cells grown in ULA. T47D cells were reverse transfected with SCR or CDH1 siRNA and seeded into 96-well 2D or ULA plates and treated with IGF1R inhibitor (OSI-906 or BMS-754807) for 6 days. Conditions in the panels as follows: (A) OSI-906; 2D, (B) OSI-906; ULA, (C) BMS-754807; 2D, (D) BMS-754807; ULA. The CellTiter Glo assay was used to assess cell viability (relative luminescence). EC50 values for viability were calculated by non-linear regression and statistical differences evaluated using sum-of-squares Global f-test ($p<0.05$; representative experiment shown; n=3 each with 6 biological replicates).

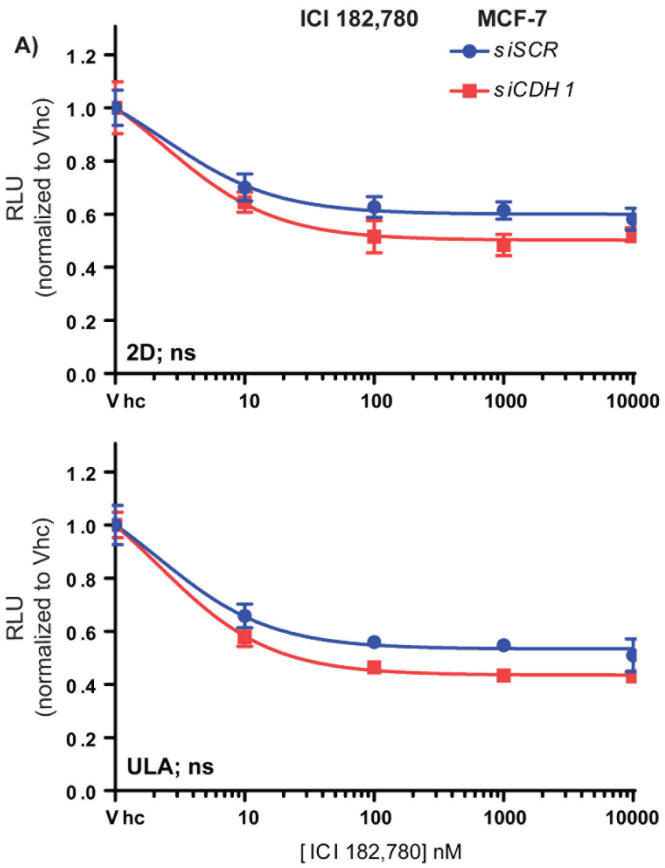

Figure 29: Loss of E-cadherin does not alter sensitivity to ICI 182,780 in breast cancer cells.
MCF-7 cells were reverse transfected with SCR or CDH1 siRNA and seeded into 96-well (A) 2D or (B) ULA plates and treated with ICI 182,780 for 6 days. CellTiter Glo assay was used to assess cell viability (relative luminescence). EC50 values for viability were calculated by non-linear regression and statistical differences evaluated using sum-of-squares Global f-test ($p<0.05$; one independent experiment, n=6 biological replicates).

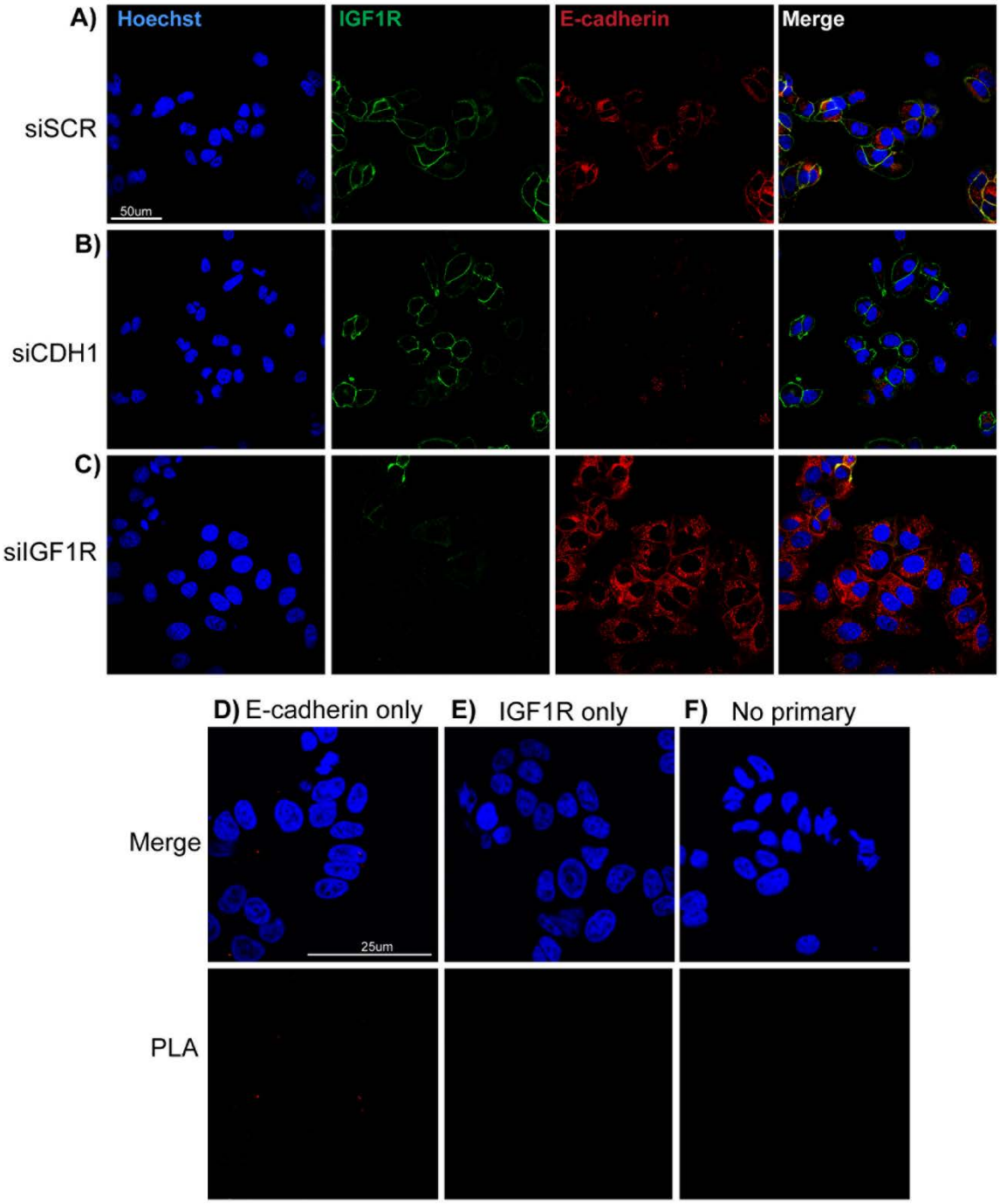

Figure 30: IGF1R and E-cadherin primary antibodies and Duolink secondary antibody probes are specific for the IGF1R-E-cadherin interaction.
MCF-7 cells were reverse transfected with SCR, CDH1, or IGF1R siRNA for 48 hours and plated on coverslips. (A) siSCR, (B) siCDH1, and (C) siIGF1R cells were fixed and immunostained for IGF1R (green) and E-cadherin (red) overnight, then imaged using confocal microscopy to demonstrate knockdown efficiency. MCF-7 cells were plated on coverslips, fixed, and stained with either (D) E-cadherin antibody alone, (E) IGF1R antibody alone, or (F) no primary antibody overnight. The Duolink (Sigma) protocol was followed and coverslips were imaged using confocal microscopy to assess non-specific interaction of Duolink secondary antibody probes.

APPENDIX C

CHAPTER 4 SUPPLEMENTARY FIGURES/TABLES

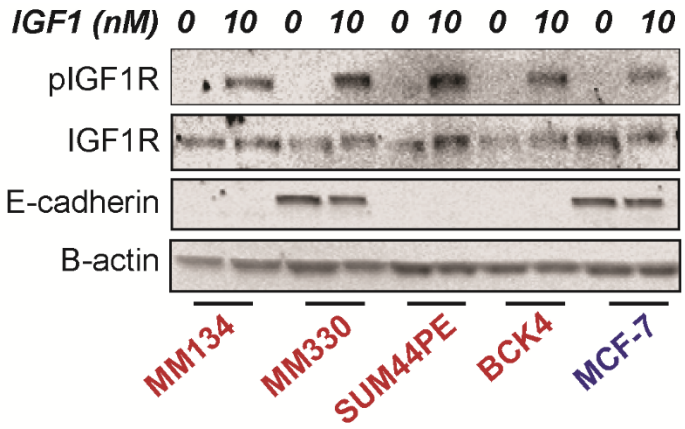

Figure 31: ILC cell lines are highly IGF1 responsive.
MM134, MM330, SUM44PE and BCK4 ILC (red) and MCF-7 (blue) cell lines were plated in 6-well plates at no more than 70% confluency. Cells were serum-starved overnight and then stimulated with IGF1 (10nM) for 10 minutes. IGF1R activation was assessed by immunoblot as measured by phosphorylation of IGF1R (pIGF1R). Of note, MM330 cells express E-cadherin protein, but harbor a mutation in α-catenin rendering their adherens junctions non-functional and therefore, classified as an ILC cell line.

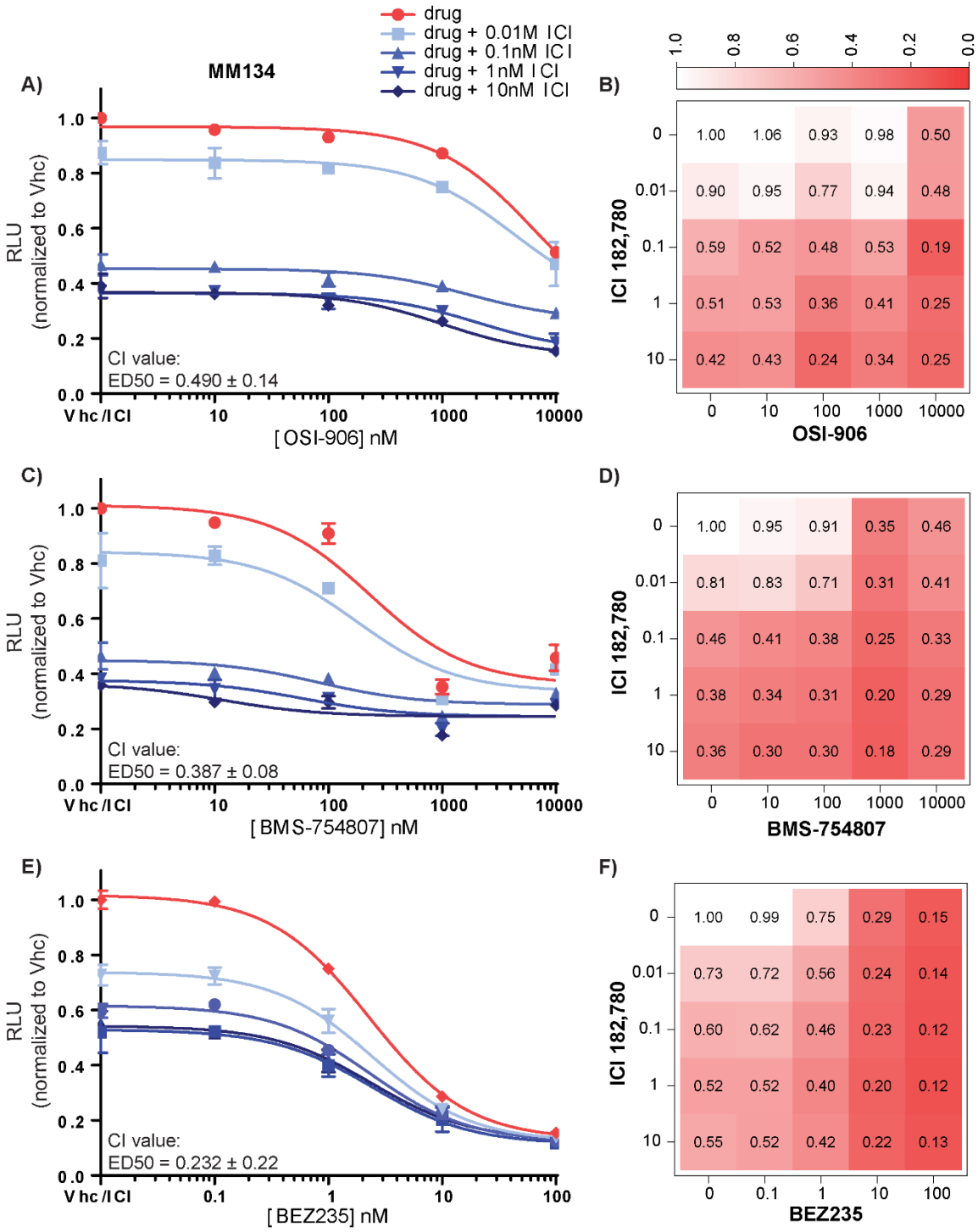

Figure 32: IGF1R pathway inhibitors and endocrine therapy synergize to inhibit cell viability in MDA-MB-134 ILC cells.

MM134 ILC cells were plated into 96-well ULA plates and treated for 6 days with increasing doses of (A, B) OSI-906, (C, D) BMS-754807, or (E, F) BEZ235 in combination with increasing doses of ICI 182,780. The dose response curves and heat maps shown indicate inhibition of cell viability (relative luminescence as measured by CellTiter Glo). Representative experiment shown; n=3 independent experiments each with 2 biological replicates per combination of doses.

Table 3: Combination index values indicating a synergist relationship between IGF1R pathway inhibitors and ICI 182, 780 to inhibit cell viability.
Synergy was measured using the Median-Effect Principle and Combination-Index Isoblogram Theorem. The table displays the E50, ED75, and ED90 values from inhibitors OSI-906, BMS-754807, or BEZ235 in combination with ICI 182,780. Values are shown +/- SEM from 3 independent experiments each with n=2 biological replicates. CI values <1 indicate a synergistic drug interaction.

Cell Line	Drug + ICI	CI: ED50	CI: ED75	CI: ED90
SUM44PE	OSI-906	0.198 ± 0.06	0.250 ± 0.10	0.398 ± 0.22
SUM44PE	BMS-754807	0.127 ± 0.06	0.081 ± 0.04	0.099 ± 0.04
SUM44PE	BEZ235	0.412 ± 0.12	0.401 ± 0.12	0.425 ± 0.12
MM134	OSI-906	0.490 ± 0.14	0.449 ± 0.18	0.808 ± 0.48
MM134	BMS-754807	0.387 ± 0.08	0.230 ± 0.04	0.667 ± 0.15
MM134	BEZ235	0.232 ± 0.22	0.547 ± 0.13	2.885 ± 1.34

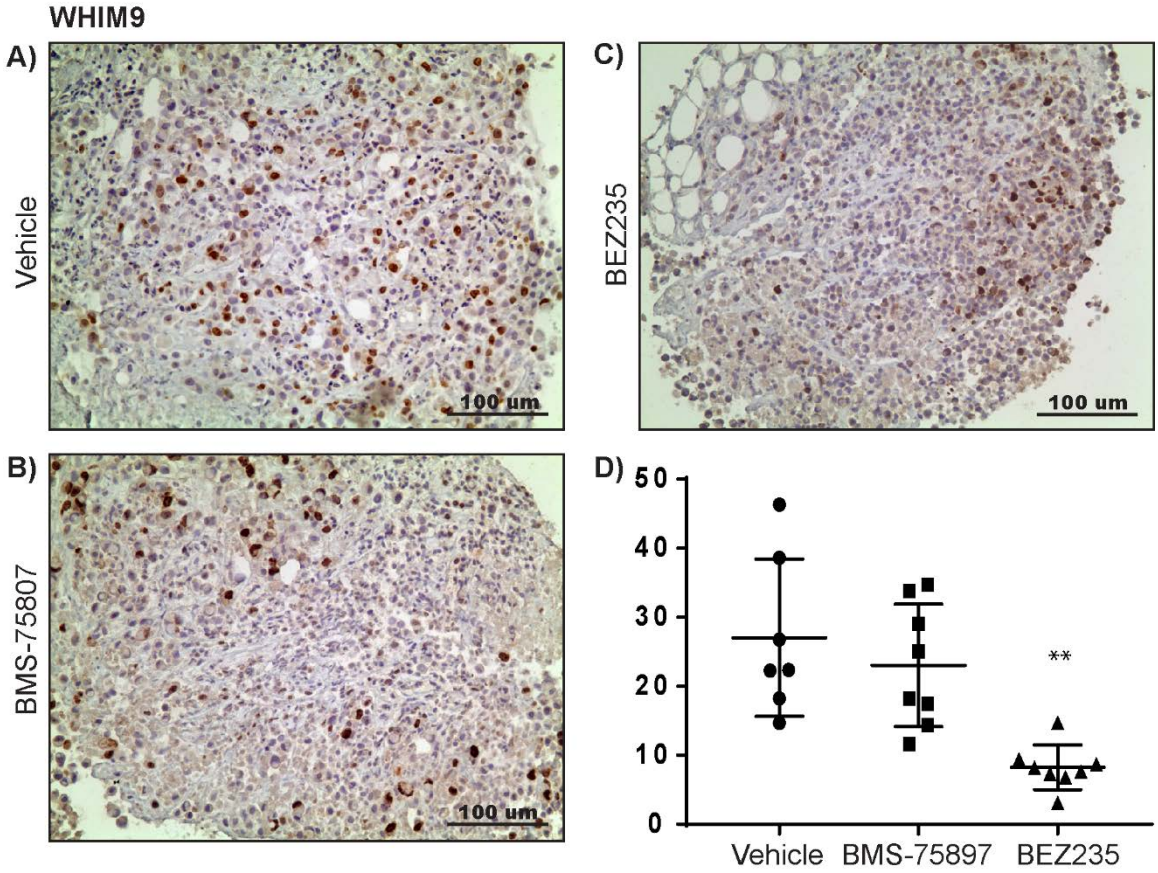

Figure 33: PI3K/mTOR inhibition reduces proliferation in an ILC tumor harboring *PIK3CA* mutation in *ex vivo* culture.

WHIM9 patient-derived xenograft tumor was harvested from immunocompromised mice, minced into 1-2mm^3 tumor chunks and then plated on gelatin sponges in 12-well plate containing 1.5ml media. Media was treated with (A) DMSO Vhc, (B) 1uM BMS-75807, or (C) 100nM BEZ235 for 72 hours. Tumor pieces were harvested by FFPE and stained for Ki67 as a marker of proliferation. (D) Staining was quantified by counting all clearly defined nuclei in 20x images. Statistical difference was assessed using a Student's t-test ($p<0.05$; n=7-8). Ki67 staining quantification was completed by Justin Kehm and Kara Burlbaugh (undergraduates; Oesterreich and Lee Labs).

BIBLIOGRAPHY

1. Siegel RL, Miller KD, Jemal A. Cancer statistics. *CA Cancer J Clin*. 2016;66(1):7-30. doi:10.3322/caac.21332.

2. Holford TR. Changing Patterns in Breast Cancer Incidence. *J Natl Cancer Inst Monogr*. 2006;8034(36):19-25. doi:10.1093/jncimonographs/lgj016.

3. Santa-Maria CA, Gradishar WJ. Changing Treatment Paradigms in Metastatic Breast Cancer. *JAMA Oncol*. 2015;1(4):528. doi:10.1001/jamaoncol.2015.1198.

4. Zardavas D, Baselga J, Piccart M. Emerging targeted agents in metastatic breast cancer. *Nat Rev Clin Oncol*. 2013;10(4):191-210. doi:10.1038/nrclinonc.2013.29.

5. Burstein HJ, Temin S, Anderson H, et al. Adjuvant Endocrine Therapy for Women With Hormone Receptor–Positive Breast Cancer: American Society of Clinical Oncology Clinical Practice Guideline Focused Update. *J Clin Oncol*. 2014;32(21):2255-2269. doi:10.1200/JCO.2013.54.2258.

6. Burstein HJ, Lacchetti C, Anderson H, et al. Adjuvant Endocrine Therapy for Women With Hormone Receptor–Positive Breast Cancer: American Society of Clinical Oncology Clinical Practice Guideline Update on Ovarian Suppression. *J Clin Oncol*. 2016;34(14):1689-1701. doi:10.1200/JCO.2015.65.9573.

7. Giordano SH, Temin S, Kirshner JJ, et al. Systemic Therapy for Patients With Advanced Human Epidermal Growth Factor Receptor 2–Positive Breast Cancer: American Society of Clinical Oncology Clinical Practice Guideline. *J Clin Oncol*. 2014;32(19):2078-2099. doi:10.1200/JCO.2013.54.0948.

8. Kümler I, Tuxen MK, Nielsen DL. A systematic review of dual targeting in HER2-positive breast cancer. *Cancer Treat Rev*. 2014;40(2):259-270. doi:10.1016/j.ctrv.2013.09.002.

9. Denduluri N, Somerfield MR, Wolff AC. Selection of Optimal Adjuvant Chemotherapy Regimens for Early Breast Cancer and Adjuvant Targeted Therapy for HER2-Positive Breast Cancers: An American Society of Clinical Oncology Guideline Adaptation of the Cancer Care Ontario Clinical Practice Guideline Summary. *J Oncol Pract*. 2016;12(5):485-488. doi:10.1200/JOP.2016.012344.

10. Lee A, Djamgoz MBA. Triple negative breast cancer: Emerging therapeutic modalities and novel combination therapies. *Cancer Treat Rev*. 2018;62:110-122. doi:10.1016/j.ctrv.2017.11.003.

11. Emens LA. Breast Cancer Immunotherapy: Facts and Hopes. *Clin Cancer Res*. 2018;24(3):511-520. doi:10.1158/1078-0432.CCR-16-3001.

12. Kamel D, Gray C, Walia JS, Kumar V. PARP Inhibitor Drugs in the Treatment of Breast, Ovarian, Prostate and Pancreatic Cancers: An Update of Clinical Trials. *Curr Drug Targets*. 2018;19(1):21-37. doi:10.2174/1389450118666170711151518.

13. First PARP Inhibitor Approved for Breast Cancer. *Cancer Discov*. 2018. doi:10.1158/2159-8290.CD-NB2018-008.

14. Barroso-Sousa R, Metzger-Filho O. Differences between invasive lobular and invasive ductal carcinoma of the breast: results and therapeutic implications. *Ther Adv Med Oncol*. 2016;8(4):261-266. doi:10.1177/1758834016644156.

15. Ciriello G, Gatza ML, Beck AH, et al. Comprehensive Molecular Portraits of Invasive Lobular Breast Cancer. *Cell*. 2015;163(2):506-519. doi:10.1016/j.cell.2015.09.033.

16. Rakha EA, Patel A, Powe DG, et al. Clinical and biological significance of E-cadherin protein expression in invasive lobular carcinoma of the breast. *Am J Surg Pathol*. 2010;34(10):1472-1479. doi:10.1097/PAS.0b013e3181f01916.

17. McCart Reed AE, Kutasovic JR, Lakhani SR, Simpson PT. Invasive lobular carcinoma of the breast: morphology, biomarkers and 'omics. *Breast Cancer Res*. 2015;17:12. doi:10.1186/s13058-015-0519-x.

18. Dabbs DJ, Schnitt SJ, Geyer FC, et al. Lobular Neoplasia of the Breast Revisited With Emphasis on the Role of E-cadherin Immunohistochemistry. *Am J Surg Pathol*. 2013;37(7):e1–e11. doi:10.1097/pas.0b013e3182918a2b.

19. Chen Z, Yang J, Li S, et al. Invasive lobular carcinoma of the breast: A special histological type compared with invasive ductal carcinoma. *PLoS One*. 2017;12(9):1-17. doi:10.1371/journal.pone.0182397.

20. Bertucci F, Orsetti B, Nègre V, et al. Lobular and ductal carcinomas of the breast have distinct genomic and expression profiles. *Oncogene*. 2008;27(40):5359-5372. doi:10.1038/onc.2008.158.

21. Rakha EA, Patel A, Powe DG, et al. Clinical and biological significance of E-cadherin protein expression in invasive lobular carcinoma of the breast. *Am J Surg Pathol*. 2010;34(10):1472-1479. doi:10.1097/PAS.0b013e3181f01916.

22. Filho OM, Giobbie-Hurder A, Mallon E, et al. Relative effectiveness of letrozole compared with tamoxifen for patients with lobular carcinoma in the BIG 1-98 Trial. *J Clin Oncol*. 2015;33(25):2772-2778. doi:10.1200/JCO.2015.60.8133.

23. Pestalozzi BC, Zahrieh D, Mallon E, et al. Distinct clinical and prognostic features of infiltrating lobular carcinoma of the breast: Combined results of 15 International Breast Cancer Study Group clinical trials. *J Clin Oncol*. 2008;26(18):3006-3014. doi:10.1200/JCO.2007.14.9336.

24. Adachi Y, Ishiguro J, Kotani H, et al. Comparison of clinical outcomes between luminal

invasive ductal carcinoma and luminal invasive lobular carcinoma. *BMC Cancer*. 2016;16(1):1-9. doi:10.1186/s12885-016-2275-4.

25. Belfiore A, Frasca F, Pandini G, Sciacca L, Vigneri R. Insulin receptor isoforms and insulin receptor/insulin-like growth factor receptor hybrids in physiology and disease. *Endocr Rev*. 2009;30(6):586-623. doi:10.1210/er.2008-0047.

26. Belardi V, Gallagher EJ, Novosyadlyy R, LeRoith D. Insulin and IGFs in Obesity-Related Breast Cancer. *J Mammary Gland Biol Neoplasia*. 2013;18(3-4):277-289. doi:10.1007/s10911-013-9303-7.

27. Engin A. Obesity-associated Breast Cancer: Analysis of risk factors. In: *Advances in Experimental Medicine and Biology*.Vol 960.; 2017:571-606. doi:10.1007/978-3-319-48382-5_25.

28. Christopoulos PF, Msaouel P, Koutsilieris M. The role of the insulin-like growth factor-1 system in breast cancer. *Mol Cancer*. 2015;14(1):1-14. doi:10.1186/s12943-015-0291-7.

29. Kleinberg DL, Wood TL, Furth P a, Lee A V. Growth hormone and insulin-like growth factor-I in the transition from normal mammary development to preneoplastic mammary lesions. *Endocr Rev*. 2009;30(1):51-74. doi:10.1210/er.2008-0022.

30. Tatar M, Bartke A, Antebi A. The endocrine regulation of aging by insulin-like signals. *Science*. 2003;299(5611):1346-1351. doi:10.1126/science.1081447.

31. Thissen J-P, Ketelslegers J-M, Underwood LE. Nutritional Regulation of the Insulin-Like Growth Factors*. *Endocr Rev*. 1994;15(1):80-101. doi:10.1210/edrv-15-1-80.

32. Kavran JM, McCabe JM, Byrne PO, et al. How IGF-1 activates its receptor. *Elife*. 2014;3:e03772. doi:10.7554/eLife.03772.

33. Boone DN, Lee A V. Targeting the Insulin-like Growth Factor Receptor: Developing Biomarkers from Gene Expression Profiling. *Crit Rev Oncog*. 2012;17(2):161-173.

34. Pollak MN. Insulin-like growth factors and neoplasia. *Nat Rev Cancer*. 2004;262(July):84-107-268. doi:10.1038/nrc1387.

35. Ekyalongo RC, Yee D. Revisiting the IGF-1R as a breast cancer target. *npj Precis Oncol*. 2017;1(1):14. doi:10.1038/s41698-017-0017-y.

36. Singh P, Alex JM, Bast F. Insulin receptor (IR) and insulin-like growth factor receptor 1 (IGF-1R) signaling systems: novel treatment strategies for cancer. *Med Oncol*. 2014;31(1):805. doi:10.1007/s12032-013-0805-3.

37. Kissau L, Stahl P, Mazitschek R, Giannis A, Waldmann H. Development of Natural Product-Derived Receptor Tyrosine Kinase Inhibitors Based on Conservation of Protein Domain Fold. *J Med Chem*. 2003;46(14):2917-2931. doi:10.1021/jm0307943.

38. Chitnis MM, Yuen JSP, Protheroe AS, Pollak M, Macaulay VM. The Type 1 Insulin-Like Growth Factor Receptor Pathway. *Clin Cancer Res*. 2008;14(20):6364-6370. doi:10.1158/1078-0432.CCR-07-4879.

39. Frasca F, Pandini G, Scalia P, et al. Insulin Receptor Isoform A, a Newly Recognized, High-Affinity Insulin-Like Growth Factor II Receptor in Fetal and Cancer Cells. *Mol Cell Biol*. 1999;19(5):3278-3288. doi:10.1128/MCB.19.5.3278.

40. Dinchuk JE, Cao C, Huang F, et al. Insulin Receptor (IR) pathway hyperactivity in IGF-IR null cells and suppression of downstream growth signaling using the dual IGF-IR/IR inhibitor, BMS-754807. *Endocrinology*. 2010;151(9):4123-4132. doi:10.1210/en.2010-0032.

41. Zhang H, Pelzer AM, Kiang DT, Yee D. Down-regulation of type I insulin-like growth factor receptor increases sensitivity of breast cancer cells to insulin. *Cancer Res*. 2007;67(1):391-397. doi:10.1158/0008-5472.CAN-06-1712.

42. Federici M, Porzio O, Zucaro L, et al. Distribution of insulin/insulin-like growth factor-I hybrid receptors in human tissues. *Mol Cell Endocrinol*. 1997;129(2):121-126. doi:10.1016/S0303-7207(97)04050-1.

43. Federici M, Zucaro L, Porzio O, et al. Increased expression of insulin/insulin-like growth factor-1 hybrid receptors in skeletal muscle of noninsulin-dependent diabetes mellitus subjects. *J Clin Invest*. 1996;98(12):2887-2893. doi:10.1172/JCI119117.

44. Menting JG, Lawrence CF, Kong GKW, Margetts MB, Ward CW, Lawrence MC. Structural Congruency of Ligand Binding to the Insulin and Insulin/Type 1 Insulin-like Growth Factor Hybrid Receptors. *Structure*. 2015;23(7):1271-1283. doi:10.1016/j.str.2015.04.016.

45. Pandini G, Vigneri R, Costantino A, et al. Insulin and Insulin-like Growth Factor-I (IGF-I) Receptor Overexpression in Breast Cancers Leads to Insulin / IGF-I Hybrid Receptor Overexpression : Evidence for a Second Mechanism of IGF-I Signaling. *Am Assoc Cancer Res J*. 1999;5(July):1935-1944. doi:10.1210/mend-5-3-452.

46. Slaaby R. Specific insulin/IGF1 hybrid receptor activation assay reveals IGF1 as a more potent ligand than insulin. *Sci Rep*. 2015;5:2-6. doi:10.1038/srep07911.

47. Benyoucef S, Surinya KH, Hadaschik D, Siddle K. Characterization of insulin/IGF hybrid receptors: contributions of the insulin receptor L2 and Fn1 domains and the alternatively spliced exon 11 sequence to ligand binding and receptor activation. *Biochem J*. 2007;403(3):603-613. doi:10.1042/BJ20061709.

48. Slaaby R, Schäffer L, Lautrup-Larsen I, et al. Hybrid receptors formed by insulin receptor (IR) and insulin-like growth factor i receptor (IGF-IR) have low insulin and high IGF-1 affinity irrespective of the IR splice variant. *J Biol Chem*. 2006;281(36):25869-25874. doi:10.1074/jbc.M605189200.

49. Pandini G, Frasca F, Mineo R, Sciacca L, Vigneri R, Belfiore A. Insulin/insulin-like growth factor I hybrid receptors have different biological characteristics depending on the insulin receptor isoform involved. *J Biol Chem*. 2002;277(42):39684-39695. doi:10.1074/jbc.M202766200.

50. Blanquart C, Gonzalez-Yanes C, Issad T. Monitoring the activation state of the insulin receptor using bioluminescence resonance energy transfer. *Mol Pharmacol*. 2001;60(4):640-645. doi:10.1124/mol.106.026989.lin.

51. Chen J, Nagle AM, Wang Y-F, Boone DN, Lee A V. Controlled dimerization of insulin-like growth factor-1 and insulin receptors reveal shared and distinct activities of holo and hybrid receptors. *J Biol Chem*. 2018:jbc.M117.789503. doi:10.1074/jbc.M117.789503.

52. Farabaugh SM, Boone DN, Lee A V. Role of IGF1R in Breast Cancer Subtypes, Stemness, and Lineage Differentiation. *Front Endocrinol (Lausanne)*. 2015;6(April):59. doi:10.3389/fendo.2015.00059.

53. Kleinberg DL, Ruan W, Catanese V, Newman CB, Feldman M. Non-lactogenic effects of growth hormone on growth and insulin-like growth factor-I messenger ribonucleic acid of rat mammary gland. *Endocrinology*. 1990;126(6):3274-3276. doi:10.1210/endo-126-6-3274.

54. Ruan W, Kleinberg DL. Insulin-like growth factor I is essential for terminal end bud formation and ductal morphogenesis during mammary development. *Endocrinology*. 1999;140(11):5075-5081. doi:10.1210/en.140.11.5075.

55. Ireland L, Santos A, Campbell F, et al. Blockade of insulin-like growth factors increases efficacy of paclitaxel in metastatic breast cancer. *Oncogene*. 2018:1. doi:10.1038/s41388-017-0115-x.

56. Richards RG, Klotz DM, Walker MP, DiAugustine RP. Mammary Gland Branching Morphogenesis Is Diminished in Mice with a Deficiency of Insulin-like Growth Factor-I (IGF-I), But Not in Mice with a Liver-Specific Deletion of IGF-I. *Endocrinology*. 2004;145(7):3106-3110. doi:10.1210/en.2003-1112.

57. Walden PD, Ruan W, Feldman M, Kleinberg DL. Evidence That the Mammary Fat Pad Mediates the Action of Growth Hormone in Mammary Gland Development. *Endocrinology*. 1998;139(2):659-662. doi:10.1210/endo.139.2.5718.

58. Ruan W, Catanese V, Wieczorek R, Feldman M, Kleinberg DL. Estradiol enhances the stimulatory effect of insulin-like growth factor-I (IGF-I) on mammary development and growth hormone-induced IGF-I messenger ribonucleic acid. *Endocrinology*. 1995;136(3):1296-1302. doi:10.1210/endo.136.3.7867584.

59. Kleinberg DL, Feldman M, Ruan W. IGF-I: an essential factor in terminal end bud formation and ductal morphogenesis. *J Mammary Gland Biol Neoplasia*. 2000;5(1):7-17. http://www.ncbi.nlm.nih.gov/pubmed/10791764. Accessed January 29, 2018.

60. Bonnette SG, Hadsell DL. Targeted Disruption of the IGF-I Receptor Gene Decreases Cellular Proliferation in Mammary Terminal End Buds. *Endocrinology*. 2001;142(11):4937-4945. doi:10.1210/endo.142.11.8500.

61. Hadsell DL, Bonnette SG, Lee AV. Genetic Manipulation of the IGF-I Axis to Regulate Mammary Gland Development and Function. *J Dairy Sci*. 2002;85(2):365-377. doi:10.3168/jds.S0022-0302(02)74083-6.

62. Lee A V., Zhang P, Ivanova M, et al. Developmental and Hormonal Signals Dramatically Alter the Localization and Abundance of Insulin Receptor Substrate Proteins in the Mammary Gland. *Endocrinology*. 2003;144(6):2683-2694. doi:10.1210/en.2002-221103.

63. Stull MA, Rowzee AM, Loladze A V., Wood TL. Growth Factor Regulation of Cell Cycle Progression in Mammary Epithelial Cells. *J Mammary Gland Biol Neoplasia*. 2004;9(1):15-26. doi:10.1023/B:JOMG.0000023585.95430.f4.

64. Kleinberg DL, Ruan W. IGF-I, GH, and Sex Steroid Effects in Normal Mammary Gland Development. *J Mammary Gland Biol Neoplasia*. 2008;13(4):353-360. doi:10.1007/s10911-008-9103-7.

65. Sternlicht MD. Key stages in mammary gland development: The cues that regulate ductal branching morphogenesis. *Breast Cancer Res*. 2005;8(1). doi:10.1186/bcr1368.

66. Laron Z, Pertzelan A, Mannheimer S. Genetic pituitary dwarfism with high serum concentation of growth hormone--a new inborn error of metabolism? *Isr J Med Sci*. 2(2):152-155. http://www.ncbi.nlm.nih.gov/pubmed/5916640. Accessed January 29, 2018.

67. Laron Z. Insulin-like growth factor 1 (IGF-1): a growth hormone. *Mol Pathol*. 2001;54(5):311-316. doi:10.1136/mp.54.5.311.

68. Lapkina-Gendler L, Rotem I, Pasmanik-Chor M, et al. Identification of signaling pathways associated with cancer protection in Laron syndrome. *Endocr Relat Cancer*. 2016;23(5):399-410. doi:10.1530/ERC-16-0054.

69. Zhou Y, Xu BC, Maheshwari HG, et al. A mammalian model for Laron syndrome produced by targeted disruption of the mouse growth hormone receptor/binding protein gene (the Laron mouse). *Proc Natl Acad Sci*. 1997;94(24):13215-13220. doi:10.1073/pnas.94.24.13215.

70. Zhang X, Mehta RG, Lantvit DD, et al. Inhibition of estrogen-independent mammary carcinogenesis by disruption of growth hormone signaling. *Carcinogenesis*. 2007;28(1):143-150. doi:10.1093/carcin/bgl138.

71. Wang Z, Prins GS, Coschigano KT, et al. Disruption of growth hormone signaling retards early stages of prostate carcinogenesis in the C3(1)/T antigen mouse. *Endocrinology*. 2005;146(12):5188-5196. doi:10.1210/en.2005-0607.

72. Livingstone C. IGF2 and cancer. *Endocr Relat Cancer*. 2013;20(6):321-339.

doi:10.1530/ERC-13-0231.

73. Rinaldi S, Peeters PHM, Berrino F, et al. IGF-I, IGFBP-3 and breast cancer risk in women: The European Prospective Investigation into Cancer and Nutrition (EPIC). *Endocr Relat Cancer*. 2006;13(2):593-605. doi:10.1677/erc.1.01150.

74. Holly J. Insulin-like growth factor-I and risk of breast cancer [letter]. *Lancet*. 1998;352(9126):490. doi:10.1016/S0140-6736(05)79226-6.

75. Chan JM, Stampfer MJ, Giovannucci E, et al. Plasma Insulin-Like Growth Factor – I and Prostate Cancer Risk : A Prospective Study. 1998;279(January):0-4.

76. Hankinson SE, Willett WC, Colditz GA, et al. Circulating concentrations of insulin-like growth factor-I and risk of breast cancer. *Lancet (London, England)*. 1998;351(9113):1393-1396. doi:10.1016/S0140-6736(97)10384-1.

77. Renehan AG, Zwahlen M, Minder C, O'Dwyer ST, Shalet SM, Egger M. Insulin-like growth factor (IGF)-I, IGF binding protein-3, and cancer risk: systematic review and meta-regression analysis. *Lancet*. 2004;363(9418):1346-1353. doi:10.1016/S0140-6736(04)16044-3.

78. de Ostrovich KK, Lambertz I, Colby JKL, et al. Paracrine overexpression of insulin-like growth factor-1 enhances mammary tumorigenesis in vivo. *Am J Pathol*. 2008;173(3):824-834. doi:10.2353/ajpath.2008.071005.

79. Digiovanni J, Bol DK, Wilker E, et al. Constitutive Expression of Insulin-like Growth Factor-1 in Epidermal Basal Cells of Transgenic Mice Leads to Spontaneous Tumor Promotion Constitutive Expression of Insulin-like Growth Factor-1 in Epidermal Basal Cells of Transgenic Mice Leads to Spontaneo. 2000;5:1561-1570.

80. Tian J, Berton TR, Shirley SH, et al. Developmental stage determines estrogen receptor alpha expression and non-genomic mechanisms that control IGF-1 signaling and mammary proliferation in mice. *J Clin Invest*. 2012;122(1):192-204. doi:10.1172/JCI42204.

81. Kim H-J, Litzenburger BC, Cui X, et al. Constitutively active type I insulin-like growth factor receptor causes transformation and xenograft growth of immortalized mammary epithelial cells and is accompanied by an epithelial-to-mesenchymal transition mediated by NF-kappaB and snail. *Mol Cell Biol*. 2007;27(8):3165-3175. doi:10.1128/MCB.01315-06.

82. Debnath J, Brugge JS. Modelling glandular epithelial cancers in three-dimensional cultures. *Nat Rev Cancer*. 2005;5(9):675-688. doi:10.1038/nrc1695.

83. Chan KK, Matchett KB, McEnhill PM, et al. Protein deregulation associated with breast cancer metastasis. *Cytokine Growth Factor Rev*. 2015;26(4):415-423. doi:10.1016/j.cytogfr.2015.05.002.

84. Cox OT, O'Shea S, Tresse E, Bustamante-Garrido M, Kiran-Deevi R, O'Connor R. IGF-1 Receptor and Adhesion Signaling: An Important Axis in Determining Cancer Cell

Phenotype and Therapy Resistance. *Front Endocrinol (Lausanne)*. 2015;6(July):106. doi:10.3389/fendo.2015.00106.

85. Taliaferro-Smith L, Oberlick E, Liu T, et al. FAK activation is required for IGF1R-mediated regulation of EMT, migration, and invasion in mesenchymal triple negative breast cancer cells. *Oncotarget*. 2015;6(7):4757-4772. doi:10.18632/oncotarget.3023.

86. Tominaga K, Shimamura T, Kimura N, et al. Addiction to the IGF2-ID1-IGF2 circuit for maintenance of the breast cancer stem-like cells. *Oncogene*. 2016;(July):1-11. doi:10.1038/onc.2016.293.

87. Litzenburger BC, Creighton CJ, Tsimelzon A, et al. High IGF-IR activity in triple-negative breast cancer cell lines and tumorgrafts correlates with sensitivity to anti-IGF-IR therapy. *Clin Cancer Res*. 2011;17(8):2314-2327. doi:10.1158/1078-0432.CCR-10-1903.

88. Litzenburger BC, Kim H, Kuiatse I, et al. BMS-536924 Reverses IGF-IR-induced Transformation of Mammary Epithelial Cells and Causes Growth Inhibition and Polarization of MCF7 Cells. *Clin Cancer Res*. 2009;15(1):1-23. doi:10.1158/1078-0432.CCR-08-0801.BMS-536924.

89. Luey BC, May FEB. Insulin-like growth factors are essential to prevent anoikis in oestrogen-responsive breast cancer cells: importance of the type I IGF receptor and PI3-kinase/Akt pathway. *Mol Cancer*. 2016;15(1):8. doi:10.1186/s12943-015-0482-2.

90. Carboni JM, Lee A V, Hadsell DL, et al. Tumor Development by Transgenic Expression of a Constitutively Active Insulin-Like Growth Factor I Receptor. 2005;(9):3781-3788.

91. Jones RA, Campbell CI, Gunther EJ, et al. Transgenic overexpression of IGF-IR disrupts mammary ductal morphogenesis and induces tumor formation. *Oncogene*. 2007;26(11):1636-1644. doi:10.1038/sj.onc.1209955.

92. Sachdev D, Hartell JS, Lee A V, Zhang X, Yee D. A Dominant Negative Type I Insulin-like Growth Factor Receptor Inhibits Metastasis of Human Cancer Cells. *J Biol Chem*. 2004;279(6):5017-5024. doi:10.1074/jbc.M305403200.

93. Lee A V, Jackson JG, Gooch JL, Hilsenbeck SG, Coronado-Heinsohn E, Osborne CK. Enhancement of insulin-like growth factor signaling in human breast cancer: estrogen regulation of insulin receptor substrate-1 expression in vitro and in vivo. *Mol Endocrinol Balt Md*. 1999;13(October):787-796.

94. Becker M a, Ibrahim YH, Cui X, Lee A V, Yee D. The IGF pathway regulates ERα through a S6K1-dependent mechanism in breast cancer cells. *Mol Endocrinol*. 2011;25(3):516-528. doi:10.1210/me.2010-0373.

95. Sachdev D, Yee D. The IGF system and breast cancer. *Endocr Relat Cancer*. 2001;8(3):197-209. doi:10.1677/erc.0.0080197.

96. Gelsomino L, Gu G, Rechoum Y, et al. ESR1 mutations affect anti-proliferative responses

to tamoxifen through enhanced cross-talk with IGF signaling. *Breast Cancer Res Treat*. 2016. doi:10.1007/s10549-016-3829-5.

97. Li Z, Levine KM, Bahreini A, et al. Upregulation of IRS1 enhances IGF1 response in Y537S and D538G ESR1 mutant breast cancer cells. *Endocrinology*. 2017;159(1):285-296. doi:10.1210/en.2017-00693.

98. Lu Y, Zi X, Zhao Y, Mascarenhas D, Pollak M. Insulin-like growth factor-I receptor signaling and resistance to trastuzumab (Herceptin). *J Natl Cancer Inst*. 2001;93(24):1852-1857. http://www.ncbi.nlm.nih.gov/pubmed/11752009. Accessed January 18, 2018.

99. Casa AJ, Dearth RK, Litzenburger BC, Lee A V, Cui X. The type I insulin-like growth factor receptor pathway: a key player in cancer therapeutic resistance. *Front Biosci*. 2008;13:3273-3287. http://www.ncbi.nlm.nih.gov/pubmed/18508432. Accessed January 18, 2018.

100. Guha M. Anticancer IGF1R classes take more knocks. *Nat Rev Drug Discov*. 2013;12(4):250-250. doi:10.1038/nrd3992.

101. Puzanov I, Lindsay CR, Goff L, et al. A phase I study of continuous oral dosing of OSI-906, a dual inhibitor of insulin-like growth factor-1 and insulin receptors, in patients with advanced solid tumors. *Clin Cancer Res*. 2015;21(4):701-711. doi:10.1158/1078-0432.CCR-14-0303.

102. Jones RL, Kim ES, Nava-Parada P, et al. Phase I Study of Intermittent Oral Dosing of the Insulin-like Growth Factor-1 and Insulin Receptors Inhibitor OSI-906 in Patients With Advanced Solid Tumors. *Clin Cancer Res*. 2015;21(4):693-700. doi:10.1158/1078-0432.CCR-14-0265.

103. Mulvihill MJ, Cooke A, Rosenfeld-Franklin M, et al. Discovery of OSI-906: a selective and orally efficacious dual inhibitor of the IGF-1 receptor and insulin receptor. *Future Med Chem*. 2009;1(6):1153-1171. doi:10.4155/fmc.09.89.

104. Carboni JM, Wittman M, Yang Z, et al. BMS-754807, a small molecule inhibitor of insulin-like growth factor-1R/IR. *Mol Cancer Ther*. 2009;8(12):3341-3349. doi:10.1158/1535-7163.MCT-09-0499.

105. Friedbichler K, Hofmann MH, Kroez M, et al. Pharmacodynamic and antineoplastic activity of BI 836845, a fully human IGF ligand-neutralizing antibody, and mechanistic rationale for combination with rapamycin. *Mol Cancer Ther*. 2014;13(2):399-409. doi:10.1158/1535-7163.MCT-13-0598.

106. Mireuta M, Birman E, Barmash M, Pollak M. Quantification of binding of IGF-1 to BI 836845, a candidate therapeutic antibody against IGF-1 and IGF-2, and effects of this antibody on IGF-1:IGFBP-3 complexes in vitro and in male C57BL/6 mice. *Endocrinology*. 2014;155(3):703-715. doi:10.1210/en.2013-1791.

107. Zha J, O'Brien C, Savage H, et al. Molecular predictors of response to a humanized anti-

insulin-like growth factor-I receptor monoclonal antibody in breast and colorectal cancer. *Mol Cancer Ther*. 2009;8(8):2110-2121. doi:10.1158/1535-7163.MCT-09-0381.

108. Huang F, Greer A, Hurlburt W, et al. The mechanisms of differential sensitivity to an insulin-like growth factor-1 receptor inhibitor (BMS-536924) and rationale for combining with EGFR/HER2 inhibitors. *Cancer Res*. 2009;69(1):161-170. doi:10.1158/0008-5472.CAN-08-0835.

109. Byron SA, Horwitz KB, Richer JK, Lange CA, Zhang X, Yee D. Insulin receptor substrates mediate distinct biological responses to insulin-like growth factor receptor activation in breast cancer cells. *Br J Cancer*. 2006;95(9):1220-1228. doi:10.1038/sj.bjc.6603354.

110. Oh JS, Kucab JE, Bushel PR, et al. Insulin-like growth factor-1 inscribes a gene expression profile for angiogenic factors and cancer progression in breast epithelial cells. *Neoplasia*. 2002;4(3):204-217. doi:10.1038/sj/neo/7900229.

111. Pacher M, Seewald MJ, Mikula M, et al. Impact of constitutive IGF1/IGF2 stimulation on the transcriptional program of human breast cancer cells. *Carcinogenesis*. 2007;28(1):49-59. doi:10.1093/carcin/bgl091.

112. Creighton CJ, Casa A, Lazard Z, et al. Insulin-like growth factor-I activates gene transcription programs strongly associated with poor breast cancer prognosis. *J Clin Oncol*. 2008;26(25):4078-4085. doi:10.1200/JCO.2007.13.4429.

113. Lorincz a M, Sukumar S. Molecular links between obesity and breast cancer. *Endocr Relat Cancer*. 2006;13(2):279-292. doi:10.1677/erc.1.00729.

114. Law JH, Habibi G, Hu K, et al. Phosphorylated insulin-like growth factor-I/insulin receptor is present in all breast cancer subtypes and is related to poor survival. *Cancer Res*. 2008;68(24):10238-10246. doi:10.1158/0008-5472.CAN-08-2755.

115. Buck E, Gokhale PC, Koujak S, et al. Compensatory insulin receptor (IR) activation on inhibition of insulin-like growth factor-1 receptor (IGF-1R): rationale for cotargeting IGF-1R and IR in cancer. *Mol Cancer Ther*. 2010;9(10):2652-2664. doi:10.1158/1535-7163.MCT-10-0318.

116. Krüger M, Kratchmarova I, Blagoev B, Tseng Y-H, Kahn CR, Mann M. Dissection of the insulin signaling pathway via quantitative phosphoproteomics. *Proc Natl Acad Sci U S A*. 2008;105(7):2451-2456. doi:10.1073/pnas.0711713105.

117. Senutovitch N, Vernetti L, Boltz R, DeBiasio R, Gough A, Taylor DL. Fluorescent protein biosensors applied to microphysiological systems. *Exp Biol Med (Maywood)*. 2015;240(6):795-808. doi:10.1177/1535370215584934.

118. Tibes R, Qiu Y, Lu Y, et al. Reverse phase protein array: validation of a novel proteomic technology and utility for analysis of primary leukemia specimens and hematopoietic stem cells. *Mol Cancer Ther*. 2006;5(10):2512-2521. doi:10.1158/1535-7163.MCT-06-0334.

119. Daemen A, Griffith OL, Heiser LM, et al. Modeling precision treatment of breast cancer. *Genome Biol*. 2013;14(10):R110. doi:10.1186/gb-2013-14-10-r110.

120. Toettcher JE, Weiner OD, Lim WA. Using optogenetics to interrogate the dynamic control of signal transmission by the Ras/Erk module. *Cell*. 2013;155(6):1422-1434. doi:10.1016/j.cell.2013.11.004.

121. Iadevaia S, Lu Y, Morales FC, Mills GB, Ram PT. Identification of optimal drug combinations targeting cellular networks: Integrating phospho-proteomics and computational network analysis. *Cancer Res*. 2010;70(17):6704-6714. doi:10.1158/0008-5472.CAN-10-0460.

122. Neve RM, Chin K, Fridlyand J, et al. A collection of breast cancer cell lines for the study of functionally distinct cancer subtypes. *Cancer Cell*. 2006;10(6):515-527. doi:10.1016/j.ccr.2006.10.008.

123. Hu J, He X, Baggerly KA, Coombes KR, Hennessy BTJ, Mills GB. Non-parametric quantification of protein lysate arrays. 2018;23(15):1986-1994. doi:10.1093/bioinformatics/btm283.

124. Erdem C, Nagle AM, Casa AJ, et al. Proteomic Screening and Lasso Regression Reveal Differential Signaling in Insulin and Insulin-like Growth Factor I (IGF1) Pathways. *Mol Cell Proteomics*. 2016;15(9):3045-3057. doi:10.1074/mcp.M115.057729.

125. Cheung KJ, Ewald AJ. Illuminating breast cancer invasion: Diverse roles for cell-cell interactions. *Curr Opin Cell Biol*. 2014;30:99-111. doi:10.1016/j.ceb.2014.07.003.

126. Friedl P, Alexander S. Cancer invasion and the microenvironment: Plasticity and reciprocity. *Cell*. 2011;147(5):992-1009. doi:10.1016/j.cell.2011.11.016.

127. Lau M-T, Klausen C, Leung PCK. E-cadherin inhibits tumor cell growth by suppressing PI3K/Akt signaling via β-catenin-Egr1-mediated PTEN expression. *Oncogene*. 2011;30(24):2753-2766. doi:10.1038/onc.2011.6.

128. Gottardi CJ, Wong E, Gumbiner BM. E-cadherin suppresses cellular transformation by inhibiting β-catenin signaling in an adhesion-independent manner. *J Cell Biol*. 2001;153(5):1049-1059. doi:10.1083/jcb.153.5.1049.

129. de-Freitas-Junior JCM, Carvalho S, Dias AM, et al. Insulin/IGF-I Signaling Pathways Enhances Tumor Cell Invasion through Bisecting GlcNAc N-glycans Modulation. An Interplay with E-Cadherin. *PLoS One*. 2013;8(11):e81579. doi:10.1371/journal.pone.0081579.

130. Qian X, Karpova T, Sheppard AM, McNally J, Lowy DR. E-cadherin-mediated adhesion inhibits ligand-dependent activation of diverse receptor tyrosine kinases. *EMBO J*. 2004;23(8):1739-1784. doi:10.1038/sj.emboj.7600136.

131. Flaveny CA, Griffett K, El-gendy BEM, et al. Broad Anti-tumor Activity of a Small

Molecule that Selectively Targets the Warburg Effect and Article Broad Anti-tumor Activity of a Small Molecule that Selectively Targets the Warburg Effect and Lipogenesis. *Cancer Cell*. 2015;28(1):42-56. doi:10.1016/j.ccell.2015.05.007.

132. Fullerton MD, Galic S, Marcinko K, et al. Single phosphorylation sites in Acc1 and Acc2 regulate lipid homeostasis and the insulin-sensitizing effects of metformin. *Nat Med*. 2013;19(12):1649-1654. doi:10.1038/nm.3372.

133. Becker M a, Ibrahim YH, Cui X, Lee A V, Yee D. The IGF pathway regulates ERα through a S6K1-dependent mechanism in breast cancer cells. *Mol Endocrinol*. 2011;25(3):516-528. doi:10.1210/me.2010-0373.

134. Hawsawi Y, El-Gendy R, Twelves C, Speirs V, Beattie J. Insulin-like growth factor - oestradiol crosstalk and mammary gland tumourigenesis. *Biochim Biophys Acta*. 2013;1836(2):345-353. doi:10.1016/j.bbcan.2013.10.005.

135. Yee D, Lee A V. Crosstalk between the insulin-like growth factors and estrogens in breast cancer. *J Mammary Gland Biol Neoplasia*. 2000;5(1):107-115. http://www.ncbi.nlm.nih.gov/pubmed/10791773. Accessed November 28, 2015.

136. Baserga R, Peruzzi F, Reiss K. The IGF-1 receptor in cancer biology. *Int J Cancer*. 2003;107(6):873-877. doi:10.1002/ijc.11487.

137. Crudden C, Girnita A, Girnita L. Targeting the IGF-1R: The Tale of the Tortoise and the Hare. *Front Endocrinol (Lausanne)*. 2015;6(April):64. doi:10.3389/fendo.2015.00064.

138. Onder TT, Gupta PB, Mani SA, Yang J, Lander ES, Weinberg RA. Loss of E-cadherin promotes metastasis via multiple downstream transcriptional pathways. *Cancer Res*. 2008;68(10):3645-3654. doi:10.1158/0008-5472.CAN-07-2938.

139. Hanahan D, Weinberg RA. Hallmarks of cancer: The next generation. *Cell*. 2011;144(5):646-674. doi:10.1016/j.cell.2011.02.013.

140. Mauro L, Salerno M, Morelli C, Boterberg T, Bracke ME, Surmacz E. Role of the IGF-I receptor in the regulation of cell-cell adhesion: Implications in cancer development and progression. *J Cell Physiol*. 2003;194(2):108-116. doi:10.1002/jcp.10207.

141. Roxanis I. Occurrence and significance of epithelial-mesenchymal transition in breast cancer. *J Clin Pathol*. 2013;66:517-521. doi:10.1136/jclinpath-2012-201348.

142. Derksen PWB, Liu X, Saridin F, et al. Somatic inactivation of E-cadherin and p53 in mice leads to metastatic lobular mammary carcinoma through induction of anoikis resistance and angiogenesis. *Cancer Cell*. 2006;10(5):437-449. doi:10.1016/j.ccr.2006.09.013.

143. Gualberto a, Pollak M. Emerging role of insulin-like growth factor receptor inhibitors in oncology: early clinical trial results and future directions. *Oncogene*. 2009;28(34):3009-3021. doi:10.1038/onc.2009.172.

144. Guvakova M a, Surmacz E. Overexpressed IGF-I receptors reduce estrogen growth requirements, enhance survival, and promote E-cadherin-mediated cell-cell adhesion in human breast cancer cells. *Exp Cell Res*. 1997;231(1):149-162. doi:10.1006/excr.1996.3457.

145. Robertson DM, Zhu M, Wu Y-C. Cellular distribution of the IGF-1R in corneal epithelial cells. *Exp Eye Res*. 2012;94(1):179-186. doi:10.1016/j.exer.2011.12.006.

146. Curto M, Cole BK, Lallemand D, Liu CH, McClatchey AI. Contact-dependent inhibition of EGFR signaling by Nf2/Merlin. *J Cell Biol*. 2007;177(5):893-903. doi:10.1083/jcb.200703010.

147. Burstein MD, Tsimelzon A, Poage GM, et al. Comprehensive genomic analysis identifies novel subtypes and targets of triple-negative breast cancer. *Clin Cancer Res*. 2015;21(7):1688-1698. doi:10.1158/1078-0432.CCR-14-0432.

148. Jambal P, Badtke MM, Harrell JC, et al. Estrogen switches pure mucinous breast cancer to invasive lobular carcinoma with mucinous features. *Breast Cancer Res Treat*. 2013;137(2):431-448. doi:10.1007/s10549-012-2377-x.

149. Chou TC, Talalay P. Quantitative analysis of dose-effect relationships: the combined effects of multiple drugs or enzyme inhibitors. *Adv Enzyme Regul*. 1984;22(C):27-55. doi:10.1016/0065-2571(84)90007-4.

150. Li S, Shen D, Shao J, et al. Endocrine-Therapy-Resistant ESR1 Variants Revealed by Genomic Characterization of Breast-Cancer-Derived Xenografts. *Cell Rep*. 2013;4(6):1116-1130. doi:10.1016/j.celrep.2013.08.022.

151. Sikora MJ, Cooper KL, Bahreini A, et al. Invasive lobular carcinoma cell lines are characterized by unique estrogen-mediated gene expression patterns and altered tamoxifen response. *Cancer Res*. 2014;74(5):1463-1474. doi:10.1158/0008-5472.CAN-13-2779.

152. Andersen CL, Sikora MJ, Boisen MM, et al. Active estrogen receptor-alpha signaling in ovarian cancer models and clinical specimens. *Clin Cancer Res*. 2017:clincanres.1501.2016. doi:10.1158/1078-0432.CCR-16-1501.

153. Centenera MM, Raj G V, Knudsen KE, Tilley WD, Butler LM. Ex vivo culture of human prostate tissue and drug development. *Nat Rev Urol*. 2013;10(8):483-487. doi:10.1038/nrurol.2013.126.

154. Dean JL, McClendon a. K, Hickey TE, et al. Therapeutic response to CDK4/6 inhibition in breast cancer defined by ex vivo analyses of human tumors. *Cell Cycle*. 2012;11(14):2756-2761. doi:10.4161/cc.21195.

155. Majumder B, Baraneedharan U, Thiyagarajan S, et al. Predicting clinical response to anticancer drugs using an ex vivo platform that captures tumour heterogeneity. *Nat Commun*. 2015;6:6169. doi:10.1038/ncomms7169.

156. Nakagawa S, Miki Y, Miyashita M, et al. Tumor microenvironment in invasive lobular carcinoma: possible therapeutic targets. *Breast Cancer Res Treat*. 2016;155(1):65-75. doi:10.1007/s10549-015-3668-9.

157. Wang L, Zhang Q, Zhang J, et al. PI3K pathway activation results in low efficacy of both trastuzumab and lapatinib. *BMC Cancer*. 2011;11(1):11:248. doi:10.1186/1471-2407-11-248.

158. Lewis Cantley. PI 3-kinase links obesity, insulin resistance, and cancer. In: Philadelphia, PA: AACR-NCI-EORTC Molecular Targets and Cancer Therapeutics Meeting; 2017.

159. Mohibi S, Mirza S, Band H, Band V. Mouse models of estrogen receptor-positive breast cancer. *J Carcinog*. 2011;10(1):35. doi:10.4103/1477-3163.91116.

160. Holen I, Speirs V, Morrissey B, Blyth K. *In vivo* models in breast cancer research: progress, challenges and future directions. *Dis Model Mech*. 2017;10(4):359-371. doi:10.1242/dmm.028274.

161. Derksen PWB, Braumuller TM, van der Burg E, et al. Mammary-specific inactivation of E-cadherin and p53 impairs functional gland development and leads to pleomorphic invasive lobular carcinoma in mice. *Dis Model Mech*. 2011;4(3):347-358. doi:10.1242/dmm.006395.

162. Annunziato S, Kas SM, Nethe M, et al. Modeling invasive lobular breast carcinoma by CRISPR / Cas9-mediated somatic genome editing of the mammary gland. 2016:1470-1480. doi:10.1101/gad.279190.116.6.

163. Boelens MC, Nethe M, Klarenbeek S, Ruiter JR De, Schut E, Bonzanni N. PTEN Loss in E-Cadherin-Deficient Mouse Mammary Epithelial Cells Rescues Apoptosis and Results in Development of Classical Invasive Lobular Carcinoma. *Cell Rep*. 2016;16:1-15. doi:10.1016/j.celrep.2016.07.059.

164. Boussadia O, Kutsch S, Hierholzer A, Delmas V, Kemler R. E-cadherin is a survival factor for the lactating mouse mammary gland. *Mech Dev*. 2002;115(1-2):53-62. doi:10.1016/S0925-4773(02)00090-4.

165. Wagner KU, Wall RJ, St-Onge L, et al. Cre-mediated gene deletion in the mammary gland. *Nucleic Acids Res*. 1997;25(21):4323-4330. doi:10.1093/nar/25.21.4323.

166. Rowse GJ, Ritland SR, Gendler SJ. Genetic modulation of neu proto-oncogene-induced mammary tumorigenesis. *Cancer Res*. 1998;58(12):2675-2679.

167. Rose-Hellekant TA, Gilchrist K, Sandgren EP. Strain background alters mammary gland lesion phenotype in transforming growth factor-α transgenic mice. *Am J Pathol*. 2002;161(4):1439-1447. doi:10.1016/S0002-9440(10)64419-7.

168. Lehmann BDB, Bauer J a J, Chen X, et al. Identification of human triple-negative breast cancer subtypes and preclinical models for selection of targeted therapies. *J Clin Invest*. 2011;121(7):2750-2767. doi:10.1172/JCI45014DS1.

169. Jassem J, Langer CJ, Karp DD, et al. Randomized, open label, phase III trial of figitumumab in combination with paclitaxel and carboplatin versus paclitaxel and carboplatin in patients with non-small cell lung cancer (NSCLC). *J Clin Oncol*. 2010;28(15_suppl):7500-7500. doi:10.1200/jco.2010.28.15_suppl.7500.

170. Lee A V, Yee D. Targeting IGF-1R: at a Crossroads. https://www.ncbi.nlm.nih.gov/pmc/articles/PMC3925073/pdf/nihms550749.pdf. Accessed February 25, 2018.

171. Perry JK, Liu D-X, Wu Z-S, Zhu T, Lobie PE. Growth hormone and cancer: an update on progress. *Curr Opin Endocrinol Diabetes Obes*. 2013;20(4):307-313. doi:10.1097/MED.0b013e328363183a.

172. Brooks AJ, Waters MJ. The growth hormone receptor: mechanism of activation and clinical implications. *Nat Rev Endocrinol*. 2010;6(9):515-525. doi:10.1038/nrendo.2010.123.

173. Mertani HC, Raccurt M, Abbate A, et al. Nuclear translocation and retention of growth hormone. *Endocrinology*. 2003;144(7):3182-3195. doi:10.1210/en.2002-221121.

174. Malaguarnera R, Belfiore A. The emerging role of insulin and insulin-like growth factor signaling in cancer stem cells. *Front Endocrinol (Lausanne)*. 2014;5(FEB):10. doi:10.3389/fendo.2014.00010.

175. Chhabra Y, Waters MJ, Brooks AJ. Role of the growth hormone-IGF-1 axis in cancer. *Expert Rev Endocrinol Metab*. 2011;6(1):71-84. doi:10.1586/eem.10.73.

176. Lombardi S, Honeth G, Ginestier C, et al. Growth hormone is secreted by normal breast epithelium upon progesterone stimulation and increases proliferation of stem/progenitor cells. *Stem Cell Reports*. 2014;2(6):780-793. doi:10.1016/j.stemcr.2014.05.005.

177. Swanson SM, Unterman TG. The growth hormone-deficient Spontaneous Dwarf rat is resistant to chemically induced mammary carcinogenesis growth hormone (GH)/ insulin-like growth factor I axis Spontaneous Dwarf rat (SDR) arose from the Sprague –. 2002;23(6):977-982.

178. Shen Q, Lantvit DD, Lin Q, et al. Advanced rat mammary cancers are growth hormone dependent. *Endocrinology*. 2007;148(10):4536-4544. doi:10.1210/en.2007-0513.

179. Divisova J, Kuiatse I, Lazard Z, et al. The growth hormone receptor antagonist pegvisomant blocks both mammary gland development and MCF-7 breast cancer xenograft growth. *Breast Cancer Res Treat*. 2006;98(3):315-327. doi:10.1007/s10549-006-9168-1.

180. Perry JK, Mohankumar KM, Emerald BS, Mertani HC, Lobie PE. The contribution of growth hormone to mammary neoplasia. *J Mammary Gland Biol Neoplasia*. 2008;13(1):131-145. doi:10.1007/s10911-008-9070-z.

181. Chiesa J, Ferrer C, Arnould C, et al. Autocrine proliferative effects of hGH are maintained in primary cultures of human mammary carcinoma cells. *J Clin Endocrinol Metab*.

2011;96(9):E1418-26. doi:10.1210/jc.2011-0473.

182. Zhu T, Starling-Emerald B, Zhang X, et al. Oncogenic Transformation of Human Mammary Epithelial Cells by Autocrine Human Growth Hormone. *Cancer Res*. 2005;65(1):317-324.

183. Bougen NM, Steiner M, Pertziger M, et al. Autocrine human GH promotes radioresistance in mammary and endometrial carcinoma cells. *Endocr Relat Cancer*. 2012;19(5):625-644. doi:10.1530/ERC-12-0042.

184. Chen Y-J, Zhang X, Wu Z-S, et al. Autocrine human growth hormone stimulates the tumor initiating capacity and metastasis of estrogen receptor-negative mammary carcinoma cells. *Cancer Lett*. 2015;365(2):182-189. doi:10.1016/j.canlet.2015.05.031.

185. Zhang W, Qian P, Zhang X, et al. Autocrine/Paracrine Human Growth Hormone-stimulated MicroRNA 96-182-183 Cluster Promotes Epithelial-Mesenchymal Transition and Invasion in Breast Cancer. *J Biol Chem*. 2015;290(22):13812-13829. doi:10.1074/jbc.M115.653261.

186. Xu J, Zhang Y, Berry P a, et al. Growth hormone signaling in human T47D breast cancer cells: potential role for a growth hormone receptor-prolactin receptor complex. *Mol Endocrinol*. 2011;25(4):597-610. doi:10.1210/me.2010-0255.

187. Xu J, Sun D, Jiang J, et al. The role of prolactin receptor in GH signaling in breast cancer cells. *Mol Endocrinol*. 2013;27(February 2013):266-279. doi:10.1210/me.2012-1297.